



ENVIRONMENTAL
MONITORING

M-871 | 2017

Monitoring of greenhouse gases and aerosols at Svalbard and Birkenes in 2016

Annual report



COLOPHON

Executive institution

NILU - Norsk institutt for luftforskning
P.O. Box 100, 2027 Kjeller

ISBN: 978-82-425-2913-8 (electronic)
ISSN: 2464-3327

Project manager for the contractor

Cathrine Lund Myhre

Contact person in the Norwegian Environment Agency

Camilla Fossum Pettersen

M-no

871

Year

2017

Pages

143

Contract number

16078043

Publisher

NILU - Norsk institutt for luftforskning
NILU report 39/2017
NILU project no. O-99093/O-105020/O-113007

The project is funded by

Norwegian Environment Agency and
NILU - Norwegian Institute for Air Research.

Author(s)

C.L. Myhre, T. Svendby, O. Hermansen, C. Lunder, M. Fiebig, A.M. Fjæraa, G. Hansen, N. Schmidbauer, T. Krognest

Title - Norwegian and English

Monitoring of greenhouse gases and aerosols at Svalbard and Birkenes in 2016 - Annual report
Overvåking av klimagasser og partikler på Svalbard og Birkenes i 2016: Årsrapport

Summary - sammendrag

The report summaries the activities and results of the greenhouse gas monitoring at the Zeppelin Observatory situated on Svalbard in Arctic Norway during the period 2001-2016, and the greenhouse gas monitoring and aerosol observations from Birkenes for 2009-2016.

Rapporten presenterer aktiviteter og måleresultater fra klimagassovertvåkingen ved Zeppelin observatoriet på Svalbard for årene 2001-2016 og klimagassmålinger og klimarelevante partikkelmålinger fra Birkenes for 2009-2016.

4 emneord

Drivhusgasser, partikler, Arktis, halokarboner

4 subject words

Greenhouse gases, aerosols, Arctic, halocarbons

Front page photo

Kjetil Tørseth, NILU

Preface

This report presents the 2016 annual results from the national monitoring of greenhouse gas concentrations and climate-relevant aerosol (particle) properties. The observations are done at two atmospheric supersites; one regional background site in southern Norway and one Arctic site. The observations made are part of the national monitoring programme conducted by NILU on behalf of The Norwegian Environment Agency. Additionally, the report includes results from Trollhaugen observatory in Antarctica. These measurements are not a part of the national monitoring programme, but receive direct support from Ministry of Climate and Environment.

The national monitoring programme includes measurements of 46 greenhouse gases at the Zeppelin Observatory in the Arctic; and this includes a long list of halocarbons, which are not only greenhouse gases but also most of them are also ozone depleting substances. The number of measured species has increased by 23 since the report in 2014. In 2009, NILU upgraded and extended the observational activity at the Birkenes Observatory in Aust-Agder and from 2010, the national monitoring programme was extended to also include aerosol properties (size, number, scattering and absorption properties) relevant for understanding the effects of aerosols on radiation.

The present report is the third of a series of annual reports for 2017, which cover the national monitoring of atmospheric composition in the Norwegian rural background environment. The other three reports focuses on the atmospheric composition and deposition of air pollution of particulate and gas phase of inorganic constituents, particulate carbonaceous matter, ground level ozone and particulate matter, the second presents the monitoring of the ozone layer and UV.

Data and results from the national monitoring programme supports various international programmes, including EMEP (European Monitoring and Evaluation Programme) under the CLTRAP (Convention on Long-range Transboundary Air Pollution), and AGAGE (Advanced Global Atmospheric Gases Experiment). Data from this report are also contributing to European Research Infrastructure network ACTRIS (Aerosols, Clouds, and Trace gases Research InfraStructure Network) and ICOS (*Integrated Carbon Observation System*). Participation in these international programmes is crucial for quality assurance and quality control of the Norwegian measurement data and instruments.

All measurement data presented in the current report are public and can be received by contacting NILU, or they can be downloaded directly from the database: <http://ebas.nilu.no>.

A large number of persons at NILU have contributed to the current report, including those responsible for sampling, technical maintenance, chemical analysis and quality control and data management. In particular, Tove Svendby, Ove Hermansen, Chris Lunder, Markus Fiebig, Georg Hanssen, Terje Krognæs, Ann Mari Fjæraa and Norbert Schmidbauer.

NILU, Kjeller, 15 November 2017

Cathrine Lund Myhre
Senior Scientist, Dep. Atmospheric and Climate Research

Content

Preface	2
Sammendrag (Norwegian)	5
Summary.....	7
1. Introduction to monitoring of greenhouse gases and aerosols.....	12
1.1 The monitoring programme in 2016	12
1.2 The measurements in relation to research and policy agreements	13
1.3 The ongoing monitoring programme and the link to networks and research infrastructures	14
1.4 Greenhouse gases, aerosols and their climate effects.....	19
1.4.1 Revisions of forcing estimates of carbon dioxide, methane, and nitrous oxide.	23
2. Observations of climate gases.....	25
2.1 Climate gases with natural and anthropogenic sources	28
2.1.1 Carbon dioxide (CO ₂).....	28
2.1.2 Methane (CH ₄).....	31
2.1.3 Nitrous Oxide (N ₂ O)	37
2.1.4 Volatile organic compounds (VOC)	39
2.1.5 Carbon monoxide (CO)	43
2.1.6 Methyl Chloride at the Zeppelin Observatory	47
2.1.7 Methyl bromide - CH ₃ Br at the Zeppelin Observatory.....	48
2.2 Greenhouse gases with solely anthropogenic sources	51
2.2.1 Chlorofluorocarbons (CFCs) at Zeppelin Observatory.....	51
2.2.2 Hydrochlorofluorocarbons (HCFCs) at Zeppelin Observatory	54
2.2.3 Hydrofluorocarbons (HFCs) at Zeppelin Observatory	56

2.2.4	Halons measured at Zeppelin Observatory.....	61
2.2.5	Other chlorinated hydrocarbons at Zeppelin Observatory	62
2.2.6	Perfluorinated compounds at Zeppelin Observatory	66
2.3	Summary of measurements of climate gases.....	70
3.	Aerosols and climate.....	73
3.1	Observed optical properties of aerosols.....	77
3.1.1	Optical aerosol properties measured at the Birkenes Observatory.....	77
3.1.2	Optical aerosol properties measured the Zeppelin Observatory.....	81
3.1.3	Optical aerosol properties measured at the Trollhaugen Observatory	83
3.2	Measurements of aerosol number and size	86
3.2.1	Physical aerosol properties measured at the Birkenes Observatory.....	86
3.2.2	Physical aerosol properties measured in situ at the Zeppelin Observatory	88
3.2.3	Physical aerosol properties measured in situ at the Trollhaugen Observatory ..	90
3.3	Summary of physical and optical aerosol properties.....	93
3.4	Column optical aerosol properties measured by ground-based remote sensing	97
3.4.1	Column optical aerosol properties measured by ground-based remote sensing at Birkenes Observatory.....	97
3.4.2	Column optical aerosol properties measured by ground-based remote sensing at Ny-Ålesund	101
4.	References	105
	APPENDIX I: Data Tables.....	110
	APPENDIX II Description of instruments and methodologies.....	122
	APPENDIX III: Abbreviations.....	138

Sammendrag (Norwegian)

Denne årsrapporten beskriver aktivitetene i og hovedresultatene fra delprogrammet "Overvåking av klimagasser og aerosoler på Zeppelin-observatoriet på Svalbard og Birkenes-observatoriet i Aust-Agder, Norge". Rapporten omfatter målinger av 46 klimagasser fram til og med år 2016 og inkluderer de viktigste naturlig forekommende drivhusgassene, syntetiske klimagasser og ulike partikkelegenskaper som har høy relevans for stråling og klimaet. Mange av gassene har også sterke ozonreducerende effekter. For de fleste klimagassene er utvikling og trender for perioden 2001-2016 rapportert, i tillegg til daglige og årlige gjennomsnittsmålinger. Programmet er utvidet med 16 nye gasser i 2015, og videre med seks nye gasser i 2016. For de nye komponentene er tidligere innhentede data tilbake til 2010 tatt med i analysene. Utviklingen av alle gassene som inngår i programmet er vist i tabell 1 på side 9. Ytterligere detaljer om klimagasser presenteres i kapittel 2 av rapporten.

Målingene på Zeppelin-observatoriet gir informasjon om utviklingen i bakgrunnsnivåkonsentrasjonene av klimagasser i Arktis. Birkenes-observatoriet ligger i det området i Sør-Norge som er mest berørt av langtransportert luftforurensning, og et omfattende program for målinger av klima-relevante egenskaper til aerosoler (partikler) utføres der. Observasjoner av karbondioksid (CO₂) og metan (CH₄) foretas på begge steder. Påvirkning fra lokal vegetasjon er også særlig viktig for CO₂-målingene ved Birkenes.

Observasjonene fra 2016 viser nye rekordhøye nivåer for de fleste av de målte klimagassene. Spesielt er det viktig å være oppmerksom på de nye rekordnivåene av CO₂ og CH₄. CO₂ passerte 400 ppm (parts per million) på Zeppelin, Birkenes og globalt i 2015, og fortsatte å øke betydelig i 2016. Totalt har den atmosfæriske konsentrasjonen av alle de viktigste klimagassene vært økende siden 2001. Unntakene er ozonnedbrytende KFK-er og noen få halogenerte gasser, som reguleres gjennom den vellykkede Montrealprotokollen.

Siden starten av målingene på Zeppelin har CO₂-konsentrasjonen gått opp hvert eneste år, i samsvar med økningen av menneskeskapte utslipp. De nye rekordnivåene for 2016 er 404,3 ppm på Zeppelin og 409,9 ppm på Birkenes. Økningen fra 2015 er på henholdsvis 3,1 ppm og 4,7 ppm. Dette gjør 2016 til det året med sterkest CO₂-vekst siden målestart på Birkenes, og siden NILU startet målinger på Zeppelin. Globalt så vi en rekordøkning i CO₂ på 3,3 ppm fra 2015 til 2016. El Niño-fenomenet i 2015/2016 bidro til økt vekst gjennom komplekse vekselvirkninger mellom klimaendringer og karbonsyklusen.

I 2016 nådde konsentrasjonen av metan et nytt rekordnivå, med en økning fra 2015 på så mye som 12 ppb (0,62 %) (parts per billion) på Zeppelin og så ekstremt som 16 ppb (0,83 %) på Birkenes. Endringene i løpet av de siste ti årene er store i forhold til utviklingen av metannivået i perioden 1998-2005, da var endringen nær null både på Zeppelin og globalt. Den globale økningen i metan fra 2015 til 2016 var 9 ppb, noe mindre enn det vi ser på våre stasjoner.

Også dinitrogenoksid (lystgass, N₂O) nådde nytt rekordnivå i 2016, og fortsatte stigningen i samme takt som tidligere.

De syntetiske menneskeskapte klimagassene som inngår i overvåkingsprogrammet på Zeppelin er fire klorfluorkarboner (KFK-er), tre hydroklorfluorkarboner (HKFK-er), og 11 hydrofluorkarboner (HFK-er), de to sistnevnte gruppene er KFK-erstatninger. I tillegg inngår

tre haloner, og en gruppe med åtte andre halogenerte klimagasser. For andre gang rapporteres også fire perfluorerte karboner (PFK-er) med svært høyt globalt oppvarmingspotensial. Videre rapporteres sulfurylfluorid og nitrogentrifluorid for første gang i 2016. Begge er ekstremt sterke drivhusgasser.

Utviklingen for KFK-gassene gir grunn til optimisme, fordi konsentrasjonen for de fleste av disse gassene er synkende. Men konsentrasjonene av KFK-erstatningsstoffene HKFKer og HFKer økte i perioden 2001-2016 - for HKFKer dog med en litt avtagende økning det siste året. HFK-gassene øker kraftig fra 2001, og det gjelder også for 2016. Konsentrasjonene av HFKer er fortsatt svært lave, noe som betyr at disse menneskeskaptene gassenes bidrag til den globale oppvarmingen per i dag er lite. Men, gitt den ekstremt raske økningen i bruk og atmosfæriske konsentrasjoner vi har observert, er det viktig å følge utviklingen nøye i fremtiden. Konsentrasjonene av PFKer og svovelfluorider (SF_6 og SO_2F_2) er fortsatt lave, men konsentrasjonen av SF_6 har økt så mye som 70% siden 2001. PFK-ene er nye i overvåkningsprogrammet og viser en stigning siden starten av datainnsamling i 2010.

Aerosoler er små partikler i atmosfæren. Partiklenes klimapåvirkning avhenger av mengden partikler og absorpsjonsegenskapene til enkeltpartiklene. Tilførselen av partikler til målestasjonen ved Birkenes bestemmes i hovedsak av den langtransporterte luftforurensningen fra det kontinentale Europa og renere luft fra Atlanterhavet og Arktis, i tillegg til regionale og lokale biogene kilder. Siden oppstarten av målingene ser vi ingen trend i de undersøkte partikkelegenskapene (antall, absorpsjons og strålingsspredningsegenskaper) på Birkenes, noe som er i samsvar med andre nordiske stasjoner, men tidsseriene er foreløpig korte og trendberegningen er usikker. På Zeppelin har vi i år inkludert nye målinger av klimaeffekten av absorberende partikler. Ved å sammenstille våre målinger med deres målinger, ser vi at det er en nedadgående trend i aerosol-absorpsjonen, noe som viser at konsentrasjonen av sot eller såkalt «*black carbon*» går ned. Observasjoner av den totale mengden av aerosolpartikler i atmosfæren over Ny-Ålesund (aerosol optisk dybde) viser økte konsentrasjonsnivåer i løpet av våren sammenlignet med resten av året. Dette fenomenet, som kalles arktisk dis (*Arctic haze*), skyldes transport av forurensning fra lavere breddegrader, hovedsakelig Europa og Russland, i løpet av vinteren/våren.

Summary

This annual report describes the activities and main results of the program “*Monitoring of greenhouse gases and aerosols at the Zeppelin Observatory, Svalbard, and Birkenes Observatory, Aust-Agder, Norway*”. The report comprises the measurements of 46 climate gases up to the year 2016; including the most important naturally occurring well-mixed greenhouse gases, synthetic greenhouse gases, and various particle properties with high relevance to climate. Many of the gases also have strong ozone depleting effects. For the climate gases, the development and trends for the period 2001-2016 are reported for most gases, in addition to daily and annual mean observations. In 2015, the program was extended with 16 new gases, all with measurements analysed back to 2010. In 2016 the programme was further extended with six more (three hydrofluorocarbons (HFCs), sulphuryl fluoride (SO₂F₂), and the halon H-2402) and nitrogen trifluoride (NF₃) after modification of the instrument at Zeppelin. Data for these compounds is reported for the first time. The trends of all gases included in the programme are shown in Table 1, and further details on all climate gases are presented in section 2 of the report.

The measurements at Zeppelin Observatory provide the trend in background level concentrations of greenhouse gases in the Arctic. Birkenes Observatory is located in the area in southern Norway most affected by long-range transport of pollutants. The influence of local vegetation/terrestrial interactions is also important at Birkenes. A comprehensive aerosol measurement program is undertaken at Birkenes, and in addition, new measurements (optical properties) are included at Zeppelin. Observations of carbon dioxide (CO₂) and methane (CH₄) are available at both sites.

The observations from 2016 show new record high levels for most of the greenhouse gases measured. In particular, it is important to note the new record levels of CO₂ and CH₄. CO₂ passed 400 ppm (parts per million) at Zeppelin, Birkenes and globally in 2015, and continued to increase significantly in 2016. In total, the concentration of all main greenhouse gases have been increasing since 2001, except for the ozone-depleting chlorofluorocarbons (CFCs) and a few halogenated gases, regulated through the successful Montreal protocol.

CO₂ concentration has increased every year since the start of the measurements at Zeppelin, in accordance with the increase in anthropogenic emissions. The annual average for 2016 are 404.3 ppm at Zeppelin and 409.9 ppm at Birkenes. The increases from 2015 are 3.1 ppm and 4.7 ppm, respectively. This makes 2016 the year with the strongest CO₂ increase since the start of the measurements at Birkenes, and the start of NILU's measurements at Zeppelin. Globally, we saw a record increase of 3.3 ppm in CO₂ from 2015 to 2016. The El Niño phenomenon in 2015/2016 contributed to increased growth through complex interactions between climate change and the carbon cycle.

The concentration of CH₄ reached a new record level with an increase since 2015 of as much as 12 ppb (0.62 %) (parts per billion) and as extreme as 16 ppb (0.88 %) at Zeppelin and Birkenes, respectively. The changes over the last 10 years are large compared to the evolution of the methane levels in the period 1998-2005, when the change was close to zero both at Zeppelin and globally. The global increase in methane from 2015 to 2016 was 9 ppb, somewhat less than what we see at the Norwegian stations.

N₂O also reached a new record level in 2015. This was as expected and follows last year's development and growth rate.

The synthetic manmade greenhouse gases included in the monitoring programme at Zeppelin are 4 chlorofluorocarbons (CFCs), 3 hydrochlorofluorocarbons (HCFCs), and 11 HFCs - the last two being CFC substitutes. In addition comes three halons, and a group of 8 other halogenated gases. For the second time 4 perfluorinated carbons (PFCs) with very high global warming potentials are reported. Furthermore, sulphuryl fluoride and nitrogen trifluoride are reported for the first time in 2016. Both are extremely strong greenhouse gases.

In total, the development of the CFC gases is positive as the concentration of most observed CFCs are declining. However, the CFC substitutes HCFCs and HFCs increased over the period 2001-2016. For the HCFCs, a relaxation in the upward trend was observed last year. The HFCs have increased strongly since 2001, and this trend is continuing. The contribution from these manmade gases to global warming is small today, as the concentrations of HFCs are still very low. But given the extremely rapid increase in the use of these gases, it is crucial to follow their development in the future.

Concentrations PFCs and sulphur hexafluoride (SF₆) are still low, but the concentration of SF₆ has increased as much as 70% since 2001. The PFCs are new and reported for first time this year, and they show a slight increase since 2010.

Aerosols are small particles in the atmosphere, and their anthropogenic sources include combustion of fossil fuel, coal and biomass, including waste from agriculture and forest fires. Aerosol can have warming or cooling effects on climate, depending on their properties. Aerosol loads and properties at Birkenes are mainly caused by long-range transport of air pollution from continental Europe, combined with regional sources like biogenic particle formation. Since starting the measurements at Birkenes, no trends in the aerosol physical properties can be detected. This is in agreement with results from other Nordic stations, but the time series are too short for firm conclusions. For Zeppelin the situation is different. At Zeppelin, we have included observations of aerosol absorption as of this year. By comparing our aerosol absorption data collected at Zeppelin with data from collaborating institutes, a decreasing trend is observed, indicating a decrease of "black carbon" in the aerosol at Zeppelin. Observations of the total amount of aerosol particles in the atmosphere above Ny-Ålesund (aerosol optical depth) show high concentration levels during springtime compared to the rest of the year. This phenomenon, called Arctic haze, is due to transport of pollution from lower latitudes (mainly Europe and Russia) accumulating in the arctic atmosphere during winter/spring.

Table 1a: Key findings; Greenhouse gases measured at Zeppelin, Ny-Ålesund; lifetimes in years¹, global warming potential (GWP over 100 years, when available), annual mean concentrations for 2016 and their long term trends per year over the period 2001-2016. The compounds marked in green are new and fully implemented in 2016, with measurements back to 2010, and the trend is for 2010 - 2016. Those in bold are reported for the first time this year. Concentrations are in ppm (parts per million) for CO₂, ppb (part per billion) for CH₄, and ppt (parts per trillion) for the other gases. Trend method are described in the appendix.

Component		Life-time	GWP	Annual mean 2016	Absolute change last year	Long term trend /yr
Carbon dioxide - Zeppelin	CO ₂	-	1	404.3	3.1	2.5
Carbon dioxide - Birkenes				409.9	4.7	2.3
Methane - Zeppelin	CH ₄	12.4	28	1932.2	11.9	5.6
Methane - Birkenes				1942.2	16.0	7.6
Carbon monoxide	CO	few months	-	113.0	-0.3	-1.3
Nitrous oxide	N ₂ O	121	265	329.0	0.3	0.9
Chlorofluorocarbons						
CFC-11*	CCl ₃ F	45	4 660	231.6	-1.04	-1.92
CFC-12*	CF ₂ Cl ₂	640	10 200	516.6	-2.88	-2.21
CFC-113*	CF ₂ ClCFCl ₂	85	13 900	71.7	-0.60	-0.65
CFC-115*	CF ₃ CF ₂ Cl	1 020	7 670	8.5	0.03	0.02
Hydrochlorofluorocarbons						
HCFC-22	CHClF ₂	11.9	1 760	247.8	2.84	6.36
HCFC-141b	C ₂ H ₃ FCl ₂	9.2	782	26.2	0.37	0.61
HCFC-142b*	CH ₃ CF ₂ Cl	17.2	1 980	23.3	-0.09	0.61
Hydrofluorocarbons						
HFC-125	CHF ₂ CF ₃	28.2	3 170	22.9	2.61	1.36
HFC-134a	CH ₂ FCF ₃	13.4	1 300	96.5	6.44	4.93
HFC-152a	CH ₃ CHF ₂	1.5	506	10.1	0.05	0.53
HFC-23	CHF ₃	228	12 400	29.6	0.79	0.99
HFC-365mfc	CH ₃ CF ₂ CH ₂ CF ₃	8.7	804	1.20	0.10	0.08
HFC-227ea	CF ₃ CHFCF ₃	38.9	3 350	1.34	0.13	0.10
HFC-236fa	CF ₃ CH ₂ CF ₃	242	8 060	0.16	0.01	0.01
HFC-245fa	CHF ₂ CH ₂ CF ₃	7.7	858	2.78	0.22	0.20
HFC-32	CH ₂ F ₂	5.2	677	14.98	2.29	1.59
HFC-4310mee	C ₅ H ₂ F ₁₀	16.1	1 650	0.28	0.01	0.01
HFC-143a	CH ₃ CF ₃	47.1	4 800	20.67	1.63	1.47
Fluorinated compounds						
PFC-14	CF ₄	50 000	6 630	83.24	0.85	-
PFC-116	C ₂ F ₆	10 000	11 100	4.63	0.09	0.09
PFC-218	C ₃ F ₈	2600	8 900	0.64	0.02	0.01
PFC-318	c-C ₄ F ₈	3200	9 540	1.59	0.06	0.05
Sulphurhexafluoride*	SF ₆	3 200	23 500	9.08	0.34	0.28

* The measurements of these components have higher uncertainty. See Appendix I for more details.

¹ From Scientific Assessment of Ozone Depletion: 2010 (WMO, 2011b) and the 4th Assessment Report of the IPCC

Component		Life-time	GWP	Annual mean 2016	Absolute change last year	Long term trend /yr
Nitrogen trifluoride	NF ₃	500	16 100	1.61	-	-
Sulphuryl fluoride	SO ₂ F ₂	36	4 090	2.35	0.12	0.10
Halons						
H-1211*	CBrClF ₂	16	1 750	3.65	-0.12	-0.05
H-1301	CBrF ₃	65	7 800	3.40	-0.002	0.02
H-2402	CBrF ₂ CBrF ₂	20	1 470	0.42	-0.006	-0.01
Halogenated compounds						
Methylchloride	CH ₃ Cl	1	12	523.12	9.59	-0.16
Methylbromide	CH ₃ Br	0.8	2	6.76	0.09	-0.19
Dichloromethane	CH ₂ Cl ₂	0.4	9	56.57	2.57	1.85
Chloroform	CHCl ₃	0.4	16	14.35	0.63	0.24
Carbon tetrachloride	CCl ₄	26	1730	80.68	-1.35	-0.99
Methylchloroform	CH ₃ CCl ₃	5	160	2.73	-0.52	-2.19
Trichloroethylene	CHClCCl ₂	-	-	0.38	-0.03	-0.01
Perchloroethylene	CCl ₂ CCl ₂	-	-	2.54	-0.04	-0.13
Volatile Organic Compounds (VOC)						
Ethane	C ₂ H ₆	Ca 78 days*		1581.74	-64.14	32.11
Propane	C ₃ H ₈	Ca 18 days*		562.85	21.73	9.07
Butane	C ₄ H ₁₀	Ca 8 days*		163.31	-15.51	-0.98
Pentane	C ₅ H ₁₂	Ca 5 days*		58.05	-4.32	0.37
Benzene	C ₆ H ₆	Ca 17 days*		68.97	-0.48	-2.34
Toluene	C ₆ H ₅ CH ₃	Ca 2 days*		27.52	0.53	-1.12

Table 1b: Annual average values and changes from last year for atmospheric aerosol properties measured at Birkenes, Zeppelin, and Trollhaugen. Long term trends cannot be calculated yet due to insufficient length of the time series. The atmospheric lifetime for aerosol particles varies over several orders of magnitude depending on particle size and meteorological conditions. An approximate range is therefore given. Changes from last year are not calculated for particle concentrations at Trollhaugen, due to an instrument upgrade, and for absorption coefficient at Zeppelin due to upstart of the time series in summer 2015. Annual mean particle concentrations at Zeppelin are not stated due to start in 2016.

Component		Life-time	Annual mean 2016, and standard deviation	Absolute change last year
Particle number conc., ultrafine - Birkenes, cm^{-3}	N_{ait}	2.5 h - 1.5 d	1063 ± 1015	-263 ± 1599
Particle number conc., accum. range - Birkenes, cm^{-3}	N_{acc}	1 - 10 d	357 ± 366	-33 ± 531
Particle number conc., coarse - Birkenes, cm^{-3}	N_{coa}	1 - 10 d	0.392 ± 1.568	0.052 ± 1.831
Particle number conc., total - Birkenes, cm^{-3}	N_{tot}	2.5 h - 10 d	1421 ± 1178	-296 ± 1811
Particle number conc., ultrafine - Zeppelin, cm^{-3}	N_{ait}	2.5 h - 1.5 d	n.a.	n.a.
Particle number conc., accum. range - Zeppelin, cm^{-3}	N_{acc}	1 - 10 d	n.a.	n.a.
Particle number conc., ultrafine - Trollhaugen, cm^{-3}	N_{ait}	2.5 h - 1.5 d	231 ± 271	n.a.
Particle number conc., accum range - Trollh., cm^{-3}	N_{acc}	1 - 10 d	37 ± 31	n.a.
Particle scattering coefficient, 550 nm, Birkenes, Mm^{-1}	σ_{sp}	2.5 h - 10 d	12.26 ± 14.91	-2.1 ± 29.39
Particle absorption coeff., 550 nm, Birkenes, Mm^{-1}	σ_{ap}	2.5 h - 10 d	1.12 ± 1.27	-0.44 ± 2.95
Particle scattering coefficient, 550 nm, Zeppelin, Mm^{-1}	σ_{sp}	2.5 h - 10 d	n.a.	n.a.
Particle absorption coeff., 550 nm, Zeppelin, Mm^{-1}	σ_{ap}	2.5 h - 10 d	0.24 ± 0.40	n.a.
Particle scattering coefficient, 550 nm, Trollhaugen, Mm^{-1}	σ_{sp}	2.5 h - 10 d	1.31 ± 1.74	-0.01 ± 3.33
Particle absorption coeff., 550 nm, Trollhaugen, Mm^{-1}	σ_{ap}	2.5 h - 10 d	0.06 ± 3.02	0.02 ± 3.02

1. Introduction to monitoring of greenhouse gases and aerosols

1.1 The monitoring programme in 2016

The purpose of the monitoring programme is to study the long-term development of climate gases and aerosols (particles). Measurements are performed at three sites and the results are used as input to European and global observation networks.

The atmospheric monitoring programme presented in this report focuses on the concentrations of atmospheric greenhouse gases and on selected aerosol physical and optical properties relevant for the understanding of climate change. Sampling sites are at Svalbard in the Norwegian Arctic (Zeppelin Observatory), where observations are considered to be representative for well-mixed background concentration levels. A second site is in southern Norway (Birkenes Observatory), where observations are more influenced by regional and local sources. A third site is in the Antarctic (Troll station).

The main objectives are to quantify the levels of greenhouse gases including ozone depleting substances, describe the relevant optical and physical properties of aerosols, and document the development over time. Measurements of the greenhouse gas concentrations and aerosol properties are core data for studies and assessments of climate change, and also crucial in order to evaluate mitigation strategies and their effectiveness. The Norwegian monitoring sites are located in areas where the influence of local sources are minimal, hence the sites are representative for a wider region and allows detection of long-term changes in atmospheric composition.



Figure 1: Location of NILU's atmospheric supersites measuring greenhouse gases and aerosol properties.

1.2 The measurements in relation to research and policy agreements

The Norwegian greenhouse gas and aerosol monitoring programme is set up to meet national and international needs for greenhouse gas and aerosol measurement data, both for the scientific community, national environmental authorities and global policy making.

Greenhouse gases: The targets set by the Kyoto protocol for its first and second commitment periods are to reduce the total emissions of greenhouse gases by the industrialized countries. Later, the Paris Agreement was negotiated and adopted by consensus at the 21st Conference of the Parties of the UNFCCC in Paris on 12 December 2015. The Paris Agreement entered into force on 4 November 2016. October 2017, and currently 169 of the 197 Parties to the Convention, have ratified the Protocol.

The central aim of the Paris agreement is to keep the increase in the global average temperature well below 2 °C increase compared to pre-industrial levels and to pursue efforts to limit the temperature increase to 1.5 °C. The EU Heads of State and Governments agreed in October 2014 on the headline targets and the architecture for the EU framework on climate and energy for 2030. The agreed targets include a cut in greenhouse gas emissions by at least 40% by 2030 compared to 1990 levels².

Ozone depleting substances and their replacement gases: In 1987 the Montreal Protocol was signed and entered into force in 1989 in order to reduce the production, use and eventually emission of the ozone-depleting substances (ODS). The amount of most ODS in the troposphere is now declining slowly and is expected to be back to pre-1980 levels around year 2050. It is central to follow the development of the concentration of these ozone depleting gases in order to verify that the Montreal Protocol and its amendments work as expected. The development of the ozone layer above Norway is monitored closely, and the results of the national monitoring of ozone and UV is presented in “*Monitoring of the atmospheric ozone layer and natural ultraviolet radiation: Annual report 2016*” (Svendby et al. 2017). The ozone depleting gases and their replacement gases are also strong greenhouse gases making it even more important to follow the development of their concentrations.

To control the new replacement gases, a historical agreement was signed on 15 October 2016 when negotiators from 197 countries agreed on a deal reducing emissions of hydrofluorocarbons (HFCs). The agreement was finalized at the United Nations meeting in Kigali, Rwanda, aiming to reduce the projected emissions of HFCs by more than 80% over the course of the twenty-first century. The agreement in Kigali represents an expansion of the 1987 Montreal Protocol. The HFCs can be up to 10000 times as effective at trapping heat compared to carbon dioxide. Today HFCs account for a small fraction of the greenhouse-gas emissions and have had limited influence on the global warming up to know. However, the use of HFCs is growing rapidly and the projected HFC emission could contribute up to 0.5 °C of global warming by the end of this century if not regulated (Xu et al., 2013). Because the

² Details here: <http://ec.europa.eu/clima/policies/strategies/2030/> and here http://www.consilium.europa.eu/uedocs/cms_data/docs/pressdata/en/ec/145397.pdf

³ *Norwegian Environment Agency monitoring reports

agreement in Kigali is an expansion of the Montreal Protocol, which was ratified back in the 1990s, this new agreement is legally binding.

1.3 The ongoing monitoring programme and the link to networks and research infrastructures

As a response to the need for monitoring of greenhouse gases and ozone depleting substances, the *Norwegian Environment Agency* and *NILU - Norwegian Institute for Air Research* signed a contract commissioning NILU to run a programme for monitoring greenhouse gases at the Zeppelin Observatory, close to Ny-Ålesund in Svalbard in 1999. This national programme includes now monitoring of 46 greenhouse gases and trace gases at the Zeppelin Observatory in the Arctic, many of them also ozone depleting substances. In 2009, NILU upgraded and extended the observational activity at the Birkenes Observatory in Aust-Agder. From 2010, the Norwegian Environment Agency/NILU monitoring programme was extended to also include the new observations from Birkenes of the greenhouse gases CO₂ and CH₄ and selected aerosol observations particularly relevant for the understanding of climate change. Relevant components are also reported in “*Monitoring of long-range transported air pollutants in Norway, annual report 2016*”⁴(Aas et al. 2017), this includes particulate and gaseous inorganic constituents, particulate carbonaceous matter, ground level ozone and particulate matter for 2016. This report also includes a description of the weather in Norway in 2016 in Chap. 2, which is relevant for the observed concentrations of greenhouse gases and aerosols.

The location of both sites are shown in Figure 1, and pictures of the sites are shown in Figure 2. The unique location of the Zeppelin Observatory at Svalbard, together with the infrastructure of the scientific research community in Ny-Ålesund, makes it ideal for monitoring the global changes of concentrations of greenhouse gases and aerosols in the atmosphere. There are few local sources of emissions, and the Arctic location is also important as the Arctic is a particularly vulnerable region. The observations at the Birkenes Observatory complement the Arctic site. Birkenes Observatory is located in a forest area with few local sources. However, the Observatory often receives long-range transported pollution from Europe and the site is ideal to analyse the contribution of long range transported greenhouse gases and aerosol properties.

⁴ *Norwegian Environment Agency monitoring reports



Figure 2: The two atmospheric supersites included in this programme, Zeppelin above and Birkenes to the left

Data and results from the national monitoring programme are also included in various international programmes. Both sites are contributing to EMEP (European Monitoring and Evaluation Programme) under the CLTRAP (Convention on Long-range Transboundary Air Pollution). Data from the sites are also reported to CAMP (Comprehensive Atmospheric Monitoring Programme) under OSPAR (the Convention for the Protection of the marine Environment of the North-East Atlantic, <http://www.ospar.org>), AMAP (Arctic Monitoring and Assessment Programme <http://www.amap.no>), WMO/GAW (The World Meteorological Organization, Global Atmosphere Watch programme, <http://www.wmo.int>) and AGAGE (Advanced Global Atmospheric Gases Experiment).

Zeppelin and Birkenes are both included into two central European environmental research infrastructures (RI) focusing on climate forcers and air quality. This ensure high quality data with harmonised methods and measurements across Europe and also with a global link through GAW, to have comparable data and results. This is essential to reduce the uncertainty on trends and in the observed levels of the wide range of climate forcers. International collaboration and harmonisation of these types of observations are crucial for improved processes understanding and satisfactory quality to assess trends. The two central RIs are ICOS (Integrated Carbon Observation System, <https://www.icos-ri.eu>) focusing on the understanding of carbon cycle, and ACTRIS (Aerosols, Clouds, and Trace gases Research InfraStructure, www.actris.eu) focusing on short-lived aerosol climate forcers and related reactive gases, and clouds. The networks EMEP and AGAGE, and the research infrastructures ACTRIS and ICOS are crucial for quality assurance and quality control of the Norwegian measurement data and instruments. All measurements included in this report follow the protocols, methodology and recommendations of these frameworks. This is a prerequisite for

harmonised and comparable data on both European and global scale, see Table 2 at page 17. Implementation of Norwegian measurements in ICOS through the ICOS-Norway⁵ project is described in the appendix II.

NILU host the data centres of the European Monitoring and Evaluation Programme (EMEP), ACTRIS (Aerosols, Clouds, and Trace gases Research InfraStructure) and the WMO Global Atmosphere Watch (GAW) World Data Centre for Aerosol (WDCA) and GAW- World Data Centre for Reactive Gases (WDCRG) (from 2015), and numerous other projects and programs (e.g. AMAP, HELCOM) and all data reported are accessible in the EBAS data base:

<http://ebas.nilu.no>. All data from the national monitoring programme and from these frameworks are reported to this data base. It is important to highlight that NILUs work in ACTRIS and also hosting the WMO GAW World Data Centres for Aerosol, among many other synergy effects, ensures efficient dissemination of the data on atmospheric aerosol properties collected within the Norwegian climate monitoring programme, to the scientific community. Among others, ACTRIS will develop a primary standard for calibrating instruments measuring aerosol absorption, one of the properties of atmospheric black carbon, and develop quality standards for measuring the aerosol particle size distribution in order to further improve assessments of aerosol climate forcing. Another project relevant in this context is *Environmental Research Infrastructures Providing Shared Solutions for Science and Society* (ENVRI^{plus})⁶ project. ENVRI^{plus} is an umbrella project for all environmental research infrastructures funded or supported by the EU. One of its objectives will be to put data from the atmospheric, marine, tectonic, and biosphere domains into a common context by making the data interoperable, i.e. visible in common services. The efforts started with achieving this goal first within the atmospheric domain.

Compiled key information on the national monitoring programme is listed in Table 2. From 2015 the programme was extended with 16 new greenhouse gases and reactive trace gases, mainly HFCs and non-methane hydrocarbons. From 2016 also NF₃ and 5 PFCs and SO₂F₂ was added. More detailed information on the monitoring program and measurement frequencies are provided in Appendix II. For the measurements of aerosol properties more details are presented in chapter 4.

⁵ <https://no.icos-cp.eu>

⁶ <http://www.envriplus.eu>

Table 2: Summary of the ongoing relevant measurement program run under NILU responsibility at Birkenes and Zeppelin Observatory 2016. The compounds marked in green are new, and implemented in 2016 and this year with measurements back to 2010. Those in bold are reported for first time this year.

Component	Birkenes Start	Zeppelin Start	International network, QA program in bold	Comment
Trace gases				
CO ₂	2009	2012	ICOS	Measured at Zeppelin since 1988 by Univ. Stockholm. By NILU at Zeppelin since 2012, now included in the programme. Qualified as ICOS class 1 site, and passed first step in September, 2016. ICOS labelling scheduled in 2018 for Birkenes
CH ₄	2009	2001	ICOS, EMEP	ICOS labelling and implementation in 2017 for Zeppelin, 2018 for Birkenes
N ₂ O	-	2009	ICOS	ICOS labelling and implementation in 2017
CO	-	2001	ICOS	ICOS labelling and implementation in 2017
Ozone (surface)	1985	1989	EMEP	Reported in Aas et al. 2017; M-780/2017.
CFCs		2001/ 2010 and later	AGAGE	<p>*The measurements of “*” these components are not within the required precision of AGAGE, but a part of the AGAGE quality assurance program.</p> <p>New compounds marked in green are included in the national monitoring program from 2015, with harmonised time series and measurements back to 2010 when the Medusa instrument was installed at Zeppelin.</p>
CFC-11*				
CFC-12*				
CFC-113*				
CFC-115*				
HCFCs				
HCFC-22				
HCFC-141b				
HCFC-142b				
HFC-125				
HFC-134a				
HFC-152a				
HFCs				
HFC-125				
HFC-134a				
HFC-152a				
HFC-23				
HFC-227ea				
HFC-236fa				
HFC-245fa				
HFC-365mfc				
HFC-32				
HFC-4310mee				
HFC-143a				
PFCs				
PFC-14				
PFC-116				
PFC-218				
PFC-318				
Halons				
H-1211				
H-1301				
H-2402				
Other chlorinated				
CH ₃ Cl				
CH ₃ Br				
CH ₂ Cl ₂				
CHCl ₃				
CCl ₄				
CH ₃ CCl ₃				
CHClCCl ₂				
CCl ₂ CCl ₂				
Other fluorinated				
SF ₆				
NF ₃		2016		
SO ₂ F ₂		2010		

Component	Birkenes Start	Zeppelin Start	International network, QA program in bold	Comment
VOCs				
C ₂ H ₆ - ethane				VOCs are included in the national monitoring program from 2015, but the measurements are harmonised back to 2010.
C ₃ H ₈ - propane				
C ₄ H ₁₀ - butane		2010	ACTRIS , EMEP	
C ₅ H ₁₂ - pentane				
C ₆ H ₆ - benzene				
C ₆ H ₅ CH ₃ - toluene				
Aerosol measurements				
Absorption properties	2009	2015	ACTRIS , EMEP	Measured by Univ. of Stockholm at Zeppelin, New from late 2015
Scattering properties	2009	-	ACTRIS , EMEP	Measured by Univ. of Stockholm at Zeppelin
Number Size Distribution	2009	2010	ACTRIS , EMEP	Reported in Aas et al. 2017; M-780/2017.
Cloud Condensation Nuclei	2012	-	ACTRIS	Zeppelin: In collaboration with Korean Polar Research Institute
Aerosol Optical depth	2010	2007	AERONET , GAW-PFR	Birkenes: AERONET, Ny-Ålesund: GAW-PFR
PM ₁₀	2001		EMEP	Reported in Aas et al. 2017; M-780/2017.
PM _{2.5}	2001		EMEP	
Chemical composition -inorganic	1978	1979	EMEP	
Chemical composition - carbonaceous matter	2001		EMEP	

1.4 Greenhouse gases, aerosols and their climate effects

The IPCC's Fifth Assessment Report (IPCC AR5) and the contribution from Working Group I “*Climate Change 2013: The Physical Science Basis*” was published in September 2013. This substantial climate assessment report presents new evidence of past and projected future climate change from numerous independent scientific studies ranging from observations of the climate system, paleoclimate archives, theoretical studies on climate processes and simulations using climate models. Their main conclusion was:

“Warming of the climate system is unequivocal, and since the 1950s, many of the observed changes are unprecedented over decades to millennia. The atmosphere and ocean have warmed, the amounts of snow and ice have diminished, sea level has risen, and the concentrations of greenhouse gases have increased”

(IPCC, Summary for policy makers, WG I, 2013)

Their conclusions are based on a variety of independent indicators, some of them are observations of atmospheric compositional change. The overall conclusion with respect to the development of the concentrations of the main greenhouse gases is:

“The atmospheric concentrations of carbon dioxide, methane, and nitrous oxide have increased to levels unprecedented in at least the last 800,000 years. Carbon dioxide concentrations have increased by 40% since pre-industrial times, primarily from fossil fuel emissions and secondarily from net land use change emissions. The ocean has absorbed about 30% of the emitted anthropogenic carbon dioxide, causing ocean acidification”

(IPCC, Summary for policy makers, 2013)

In particular chapter 2, “*Observations: Atmosphere and Surface*”, presents all types of atmospheric and surface observations, including observations of greenhouse gases since the start of the observations in mid-1950s and changes in aerosols since the 1980s. The IPCC AR5 report was the first time long term changes of aerosols were included in the report, based on global and regional measurement networks and satellite observations. The main conclusion with respect to development of the aerosol levels is that “*It is very likely that aerosol column amounts have declined over Europe and the eastern USA since the mid-1990s and increased over eastern and southern Asia since 2000*” (Hartmann et al, 2013). This is important since the total effect of aerosols is atmospheric cooling, counteracting the effect of greenhouse gases. The changes in Europe and USA is mainly due to mitigation strategies of e.g. sulphur, while the emissions are increasing rapidly in Asia, including increasing emissions of the warming component black carbon.

The basic metric to compare the effect of the various climate change drivers is radiative forcing (RF). RF is the net change in the energy balance of the Earth system due to some

imposed change. RF provides a quantitative basis for comparing potential climate response to different changes. Forcing is often presented as the radiative change from one time-period to another, such as pre-industrial to present-day. For many forcing agents the RF is an appropriate way to compare the relative importance of their potential climate effect. However, rapid adjustments in the troposphere can either enhance or reduce the perturbations, leading to large differences in the forcing driving the long-term climate change. In the last IPCC report it was also introduced a new concept, the effective radiative forcing (ERF). The ERF concept aims to take rapid adjustments into account, and is the change in net TOA (Top Of Atmosphere) downward radiative flux after allowing for atmospheric temperatures, water vapour and clouds to adjust, but with surface temperature or a portion of surface conditions unchanged (Myhre et al, 2013b). Figure 3 shows the RF and ERF of the main components referring to a change in the atmospheric level since 1750, pre-industrial time.

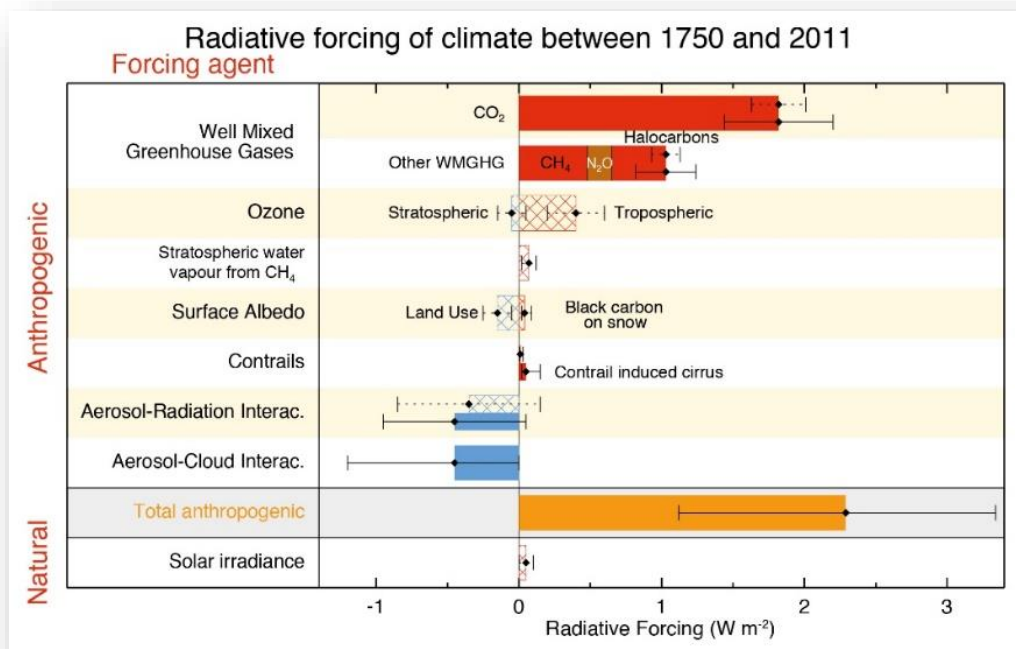


Figure 3: Bar chart for RF (hatched) and ERF (solid) for the period 1750-2011. Uncertainties (5 to 95% confidence range) are given for RF (dotted lines) and ERF (solid lines). (Taken from Myhre et al, 2013b).

Total adjusted anthropogenic forcing is 2.29 W m^{-2} , [1.13 to 3.33], and the main anthropogenic component driving this is CO₂ with a total RF of 1.82 W m^{-2} . The direct and indirect effect of aerosols are cooling and calculated to -0.9 W m^{-2} . The diagram in Figure 4 shows a comparison in percent % of the various contribution from the long-lived greenhouse gases to the total forcing of the well-mixed greenhouse gases, based on 2011 levels.

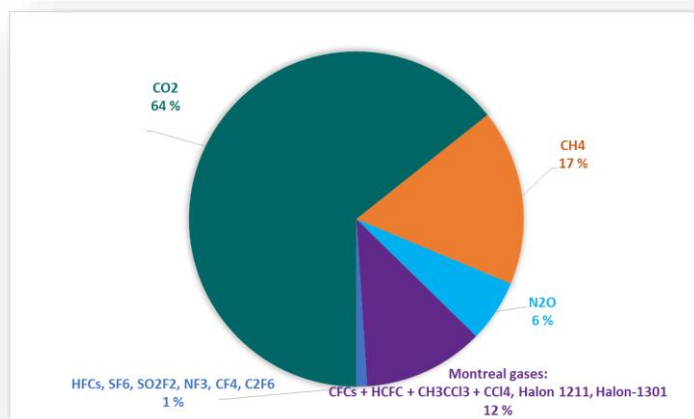


Figure 4: The contribution in % of the well-mixed greenhouse gases to the total forcing of the well-mixed greenhouse gases for the period 1750-2011 based on estimates in Table 8.2 in Chap 8, of IPCC (Myhre et al, 2013b).

An interesting and more detailed picture of the influence of various emissions on the RF is illustrated in Figure 5. This Figure shows the forcing since 1750 by emitted compounds, to better illustrate the effects of emissions and potential impact of mitigations.

As seen, the number of emitted compounds and changes leading to RF is larger than the number of compounds causing RF directly. This is due to indirect effects, in particular components involved in atmospheric chemistry that affects e.g. CH₄ and ozone. Emissions of CH₄, CO, and NMVOC all lead to excess CO₂ as one end product if the carbon is of fossil origin, and this is the reason why the RF of direct CO₂ emissions is slightly lower than the RF of abundance change of CO₂ in Figure 3. Note also that for CH₄, the contribution from emission is estimated to be almost twice as large as that from the CH₄ concentration change, 0.97 W m⁻² versus 0.48 W m⁻² shown in Figure 3 and Figure 5 respectively. This is because emission of CH₄ leads to ozone production (shown in green colour in the CH₄ bar in Figure 5), stratospheric water vapour, CO₂ (as mentioned above), and importantly affects its own lifetime. As seen from the Figure, there is also a particularly complex picture of the effects of aerosols. Black carbon heats the atmosphere, originating from both fossil fuel, biofuel and biomass burning. The direct effect of black carbon from fossil and biofuel is +0.4 W m⁻², while black carbon from biomass burning is 0 in total due to co-emitted effects of organic carbon, cooling the atmosphere and cancelling out the heating effect.

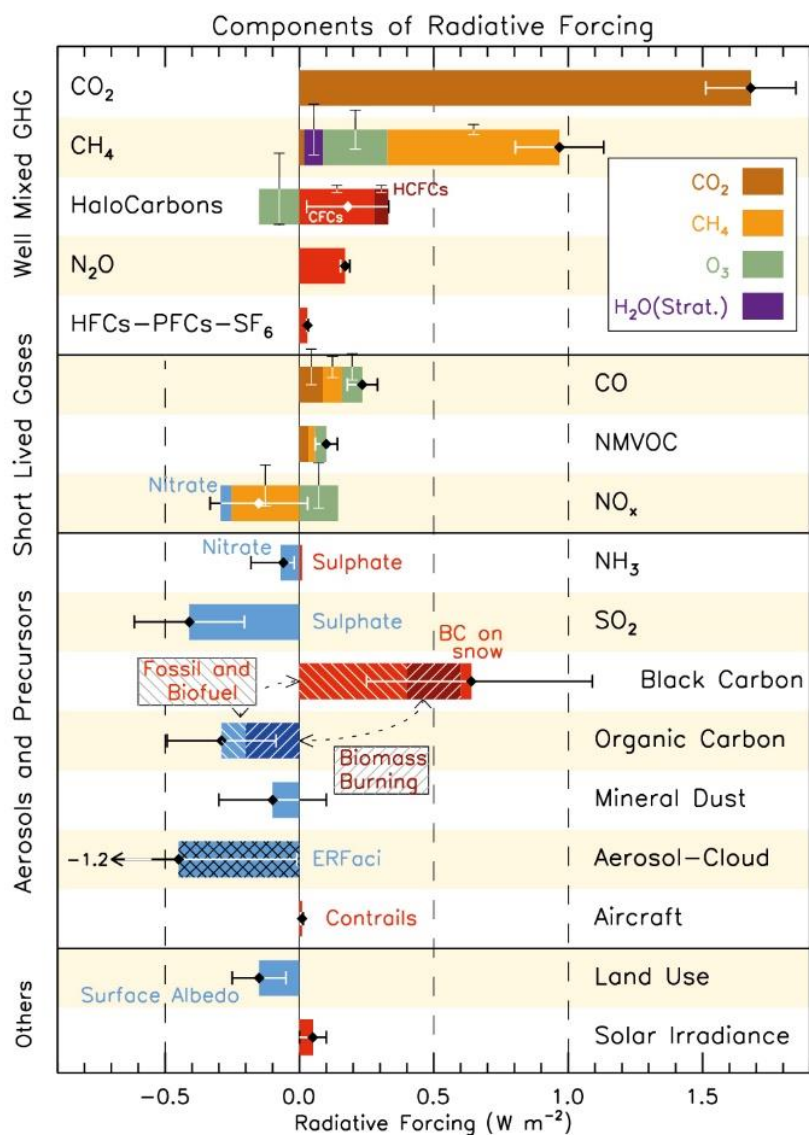


Figure 5: RF bar chart for the period 1750-2011 based on emitted compounds (gases, aerosols or aerosol precursors) or other changes. Red (positive RF) and blue (negative forcing) are used for emitted components which affect few forcing agents, whereas for emitted components affecting many compounds several colours are used as indicated in the inset at the upper part the figure. The vertical bars indicate the relative uncertainty of the RF induced by each component. Their length is proportional to the thickness of the bar, that is, the full length is equal to the bar thickness for a $\pm 50\%$ uncertainty. The net impact of the individual contributions is shown by a diamond symbol and its uncertainty (5 to 95% confidence range) is given by the horizontal error bar. ERFaci is ERF due to aerosol-cloud interaction. BC and OC are co-emitted, especially for biomass burning emissions (given as Biomass Burning in the figure) and to a large extent also for fossil and biofuel emissions (given as Fossil and Biofuel in the figure where biofuel refers to solid biomass fuels) (The Figure is taken from Myhre et al, 2013b).

In addition there is a small heating effect of black carbon on snow (0.04 W m^{-2} since 1750). The effect of black carbon on snow since 1750 is currently in the order of one year increase of CO_2 concentration in the atmosphere (around 2 ppm).

1.4.1 Revisions of forcing estimates of carbon dioxide, methane, and nitrous oxide

In 2016 there was an important study publishing revised radiative forcing of carbon dioxide, methane, and nitrous oxide. This resulted in a significant revision of the methane radiative forcing, and minor changes in the others. To reduce uncertainty of the forcing, there were performed more accurate forcing estimates and revised the global warming potential with consistent methodology used within IPCC and earlier estimates. For CH₄ this resulted in **25% stronger forcing than given in the last IPCC report**, due to inclusion of the shortwave and near-infrared bands of CH₄, improved knowledge about water vapour absorption, more detailed models (Etminan *et al.*, 2016). Figure 6 is taken from Etminan *et al.* (2016) and show the revised estimates, compared to the old as included in IPCC AR5. The estimates are based on concentration development as in representative concentration pathway (RCP⁷) RCP8.5 from IPCC AR5.

To put this in perspective, a recent paper in Nature Geoscience is using data from Zeppelin and the monitoring programme, together with other data to calculate radiative forcing due to CO₂ and all greenhouse gases, presently and up till 2016 (Myhre *et al.*, 2017) with comparison to future RCP pathways. The paper shows that we are now halfway to doubling of CO₂ in terms for radiative forcing but not in concentrations. According to the observed concentrations, we are now following path between RCP8.5 and other RCP scenarios.

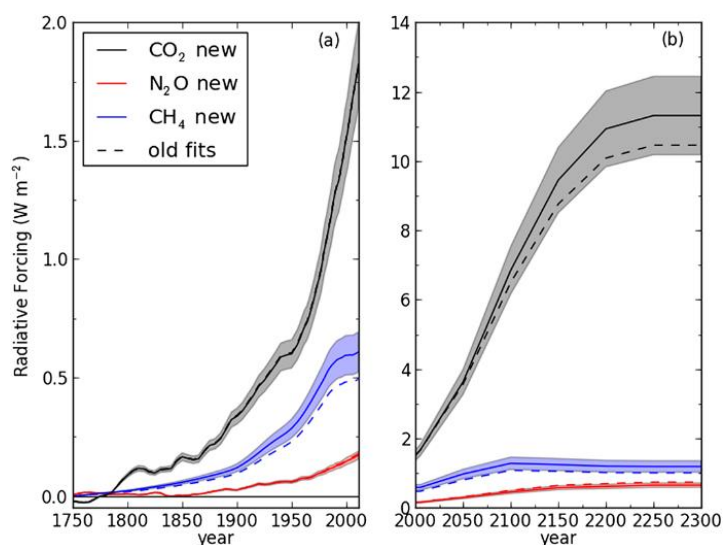


Figure 6: Radiative forcing of CO₂, N₂O, and CH₄ concentration change: (a) from 1755 to 2011 and (b) from 2000 to 2300 (using RCP8.5 concentrations from IPCC AR5 relative to preindustrial value (280 ppm of CO₂, 275 ppb of N₂O, and 750 ppb of CH₄) using old and new expressions. Shading for the new expressions indicates the estimated radiative uncertainty in the forcing (Etminan *et al.*, 2016).

⁷ https://en.wikipedia.org/wiki/Representative_Concentration_Pathways

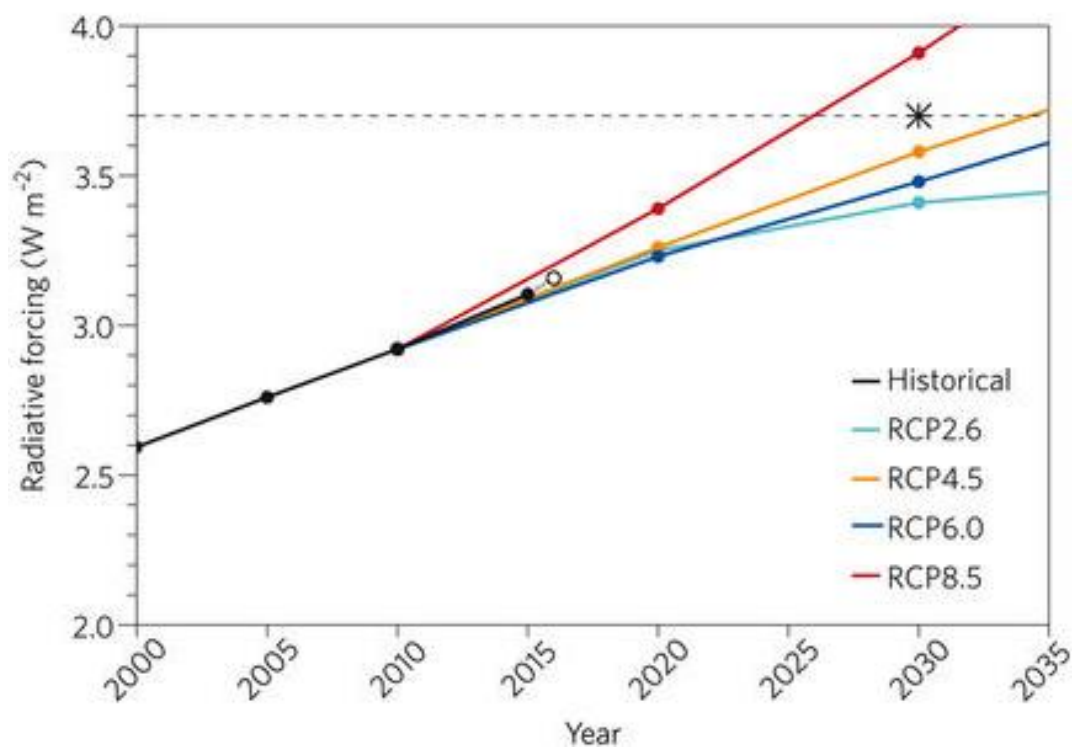


Figure 7: Radiative forcing for all WMGHGs calculated. Historical values are based on observed concentrations. CH₄ concentrations are also from the IPCC. For 2015 the global annual mean concentrations of CO₂, CH₄ and N₂O are from the National Oceanic and Atmospheric Administration, and for halocarbons the relative increase since 2010 are from the Arctic Zeppelin observatory. Preliminary data for 2016 is included, which may be subject to small changes, taken from (Myhre et al, 2017) Figure 8

2. Observations of climate gases

NILU measures 46 climate gases at the Zeppelin Observatory at Svalbard and 2 at Birkenes, in addition to surface ozone reported in Aas et al. 2017. The results from these measurements, and analysis are presented in this chapter. Also observations of CO₂ for the time period 1988-2012 at Zeppelin performed by the Stockholm University - Department of Environmental Science and Analytical Chemistry (ACES), are included in the report.

Table 3 summarizes the main results for 2016 and the trends over the period 2001-2016. Also a comparison between the main greenhouse gas concentrations at Zeppelin and Birkenes to annual mean values given in BAMS (2017) and WMO (2017) is included.

Table 3: Greenhouse gases measured at Zeppelin and Birkenes; lifetimes in years, global warming potential (GWP) for 100 year horizon and annual mean for 2016, change last year, the trends per year over the period 2001-2016 for is included. Red is increasing, and blue is decreasing trends. Additionally, global mean for 2016 taken from BAMS (Hall et al., 2017) and WMO (WMO 2017) for comparison. The values taken for WMO is indicated with a *. All concentrations are mixing ratios in ppt, except for methane, nitrous oxide and carbon monoxide (ppb) and carbon dioxide (ppm). The components marked in green are implemented in the programme in 2015 and 2016, with measurements back to 2010, and several are reported for the first time, in bold.

Component		Life-time	GWP	Global mean BAMS/WMO * 2016	Annual mean 2016	Absolute change last year	Trend /yr
Carbon dioxide - Zeppelin	CO ₂	-	1	403.3*	404.3	3.1	2.5
Carbon dioxide - Birkenes					409.9	4.7	2.3
Methane - Zeppelin	CH ₄	12.4	28	1853 ± 2*	1932.2	11.9	5.6
Methane - Birkenes					1942.2	16.0	7.6
Carbon monoxide	CO	few months	-	-	113.0	-0.3	-1.3
Nitrous oxide	N ₂ O	121	265	324 ± 0.1*	329.0	0.3	0.9
Chlorofluorocarbons							
CFC-11*	CCl ₃ F	45	4 660	230.1	231.6	-1.04	-1.92
CFC-12*	CF ₂ Cl ₂	640	10 200	512.5	516.6	-2.88	-2.21
CFC-113*	CF ₂ ClCFCl ₂	85	13 900	71.6	71.7	-0.60	-0.65
CFC-115*	CF ₃ CF ₂ Cl	1 020	7 670		8.5	0.03	0.02
Hydrochlorofluorocarbons							
HCFC-22	CHClF ₂	11.9	1 760	237.2	247.8	2.84	6.36
HCFC-141b	C ₂ H ₃ FCl ₂	9.2	782	24.5	26.2	0.37	0.61
HCFC-142b*	CH ₃ CF ₂ Cl	17.2	1 980	22	23.3	-0.09	0.61
Hydrofluorocarbons							
HFC-125	CHF ₂ CF ₃	28.2	3 170	18.9	22.9	2.61	1.36
HFC-134a	CH ₂ FCF ₃	13.4	1 300	89.1	96.5	6.44	4.93
HFC-152a	CH ₃ CHF ₂	1.5	506	6.6	10.1	0.05	0.53
Hydrofluorocarbons cont.							
HFC-23	CHF ₃	228	12 400	28.9	29.6	0.79	0.99
HFC-365mfc	CH ₃ CF ₂ CH ₂ CF ₃	8.7	804	0.89	1.20	0.10	0.08

Component		Life-time	GWP	Global mean BAMS/WMO * 2016	Annual mean 2016	Absolute change last year	Trend /yr
HFC-227ea	CF ₃ CHFCF ₃	38.9	3 350	1.2	1.34	0.13	0.10
HFC-236fa	CF ₃ CH ₂ CF ₃	242	8 060	-	0.16	0.01	0.01
HFC-245fa	CHF ₂ CH ₂ CF ₃	7.7	858	-	2.78	0.22	0.20
HFC-32	CH ₂ F ₂	5.2	677	11.5	14.98	2.29	1.59
HFC-4310mee	C ₅ H ₂ F ₁₀	16.1	1 650	-	0.28	0.01	0.01
HFC-143a	CH ₃ CF ₃	47.1	4 800	17.5	20.67	1.63	1.47
Perfluorinated compounds							
PFC-14	CF ₄	50 000	6 630	82.7	83.24	0.85	-
PFC-116	C ₂ F ₆	10 000	11 100	4.56	4.63	0.09	0.09
PFC-218	C ₃ F ₈	2600	8 900	-	0.64	0.02	0.01
PFC-318	c-C ₄ F ₈	3200	9 540	-	1.59	0.06	0.05
Sulphurhexafluoride*	SF ₆	3 200	23 500	8.88	9.08	0.34	0.28
Nitrogen trifluoride	NF ₃	500	16 100	-	1.61	-	-
Sulphuryl fluoride	SO ₂ F ₂	36	4 090	-	2.35	0.12	0.10
Halons							
H-1211*	CBrClF ₂	16	1 750	3.5	3.65	-0.12	-0.05
H-1301	CBrF ₃	65	7 800	3.3	3.40	-0.002	0.02
H-2402	CBrF ₂ CBrF ₂	20	1 470	0.4	0.42	-0.006	-0.01
Halogenated compounds							
Methylchloride	CH ₃ Cl	1	12	563.0	523.12	9.59	-0.16
Methylbromide	CH ₃ Br	0.8	2	6.90	6.76	0.09	-0.19
Dichloromethane	CH ₂ Cl ₂	0.4	9	-	56.57	2.57	1.85
Chloroform	CHCl ₃	0.4	16	-	14.35	0.63	0.24
Carbon tetrachloride	CCl ₄	26	1730	81.3	80.68	-1.35	-0.99
Methylchloroform	CH ₃ CCl ₃	5	160	2.6	2.73	-0.52	-2.19
Trichloroethylene	CHClCCl ₂	-	-	-	0.38	-0.03	-0.01
Perchloroethylene	CCl ₂ CCl ₂	-	-	-	2.54	-0.04	-0.13
Volatile Organic Compounds (VOC)							
Ethane	C ₂ H ₆	Ca 78 days [#]	-	-	1581.74	-64.14	32.11
Propane	C ₃ H ₈	Ca 18 days [#]	-	-	562.85	21.73	9.07
Butane	C ₄ H ₁₀	Ca 8 days [#]	-	-	163.31	-15.51	-0.98
Pentane	C ₅ H ₁₂	Ca 5 days [#]	-	-	58.05	-4.32	0.37
Benzene	C ₆ H ₆	Ca 17 days [#]	-	-	68.97	-0.48	-2.34
Toluene	C ₆ H ₅ CH ₃	Ca 2 days [#]	-	-	27.52	0.53	-1.12

[#]The lifetimes of VOC are strongly dependant on season, sunlight, other components etc. The estimates are global averages given in C. Nicholas Hewitt (ed.): *Reactive Hydrocarbons in the Atmosphere*, Academic Press, 1999, p. 313. The times series for these are short and the trend is very uncertain.

Greenhouse gases and other climate gases have numerous sources, both anthropogenic and natural. Trends and future changes in concentrations are determined by their sources and the sinks, and in section 2.1 are observations and trends of the monitored greenhouse gases with both natural and anthropogenic sources presented in more detail. In section 2.2 are the detailed results of the ozone depleting substances with purely anthropogenic sources presented.

We have used the method described in Appendix II in the calculation of the annual trends, and also include a description of the measurements at Zeppelin at Svalbard and Birkenes Observatory in southern Norway in more details. Generally, Zeppelin Observatory is a unique site for observations of changes in the background level of atmospheric components. All peak concentrations of the measured gases are significantly lower here than at other sites at the Northern hemisphere, due to the station's remote location. Birkenes is closer to the main source areas. Further, the regional vegetation is important for regulating the carbon cycle, resulting in much larger variability in the concentration level compared to the Arctic region.

2.1 Climate gases with natural and anthropogenic sources

The annual mean concentrations for all gases included in the program for all years are given in Appendix I, Table A 1 at page 112. All the trends, uncertainties and regression coefficients are found in Table A 2 at page 115. Section 2.1 focuses on the measured greenhouse gases that have both natural and anthropogenic sources.

2.1.1 Carbon dioxide (CO₂)

Carbon dioxide (CO₂) is the most important anthropogenic greenhouse gas with a radiative forcing of 1.82 W m⁻² since the year 1750, and an increase since the previous IPCC report (AR4, 2007) of 0.16 Wm⁻² (Myhre et al., 2013b). Etminan et al. (2016) presented revised forcing estimates for all main greenhouse gases (see section 1.4.1 at page 23), and confirmed the forcing estimates for CO₂, with only minor changes.

The increase in forcing is due to the increase in concentrations over these last years. CO₂ is the end product in the atmosphere of the oxidation of all main organic compounds, and it has shown an increase of as much as 40 % since the pre industrial time (Hartmann et al, 2013). This is mainly due to emissions from combustion of fossil fuels and land use change. CO₂ emissions from fossil fuel burning and cement production increased by 2.3% in 2013 since 2012, with a total of 9.9±0.5 GtC (billion tonnes of carbon) equal to 36 GtCO₂ emitted to the atmosphere, 61% above 1990 emissions (the Kyoto Protocol reference year). Emissions are projected to decrease slightly (-0.6%) in 2015 according to Global Carbon Project estimates <http://www.globalcarbonproject.org>, it is still too early to assess and evaluate this.

NILU started CO₂ measurements at the Zeppelin Observatory in 2012 and the results are presented in Figure 9, together with the time series provided by ITM, University of Stockholm, back to 1988. ITM provides all data up till 2012 and we acknowledge the effort they have been doing in monitoring CO₂ at the site. After upgrading Birkenes in 2009, there are continuous measurements of CO₂ and CH₄ from mid May 2009 also at this site.

The atmospheric daily mean CO₂ concentration measured at Zeppelin Observatory for the period mid 1988-2016 is presented in Figure 9 upper panel, together with the shorter time series for Birkenes in the lower panel.

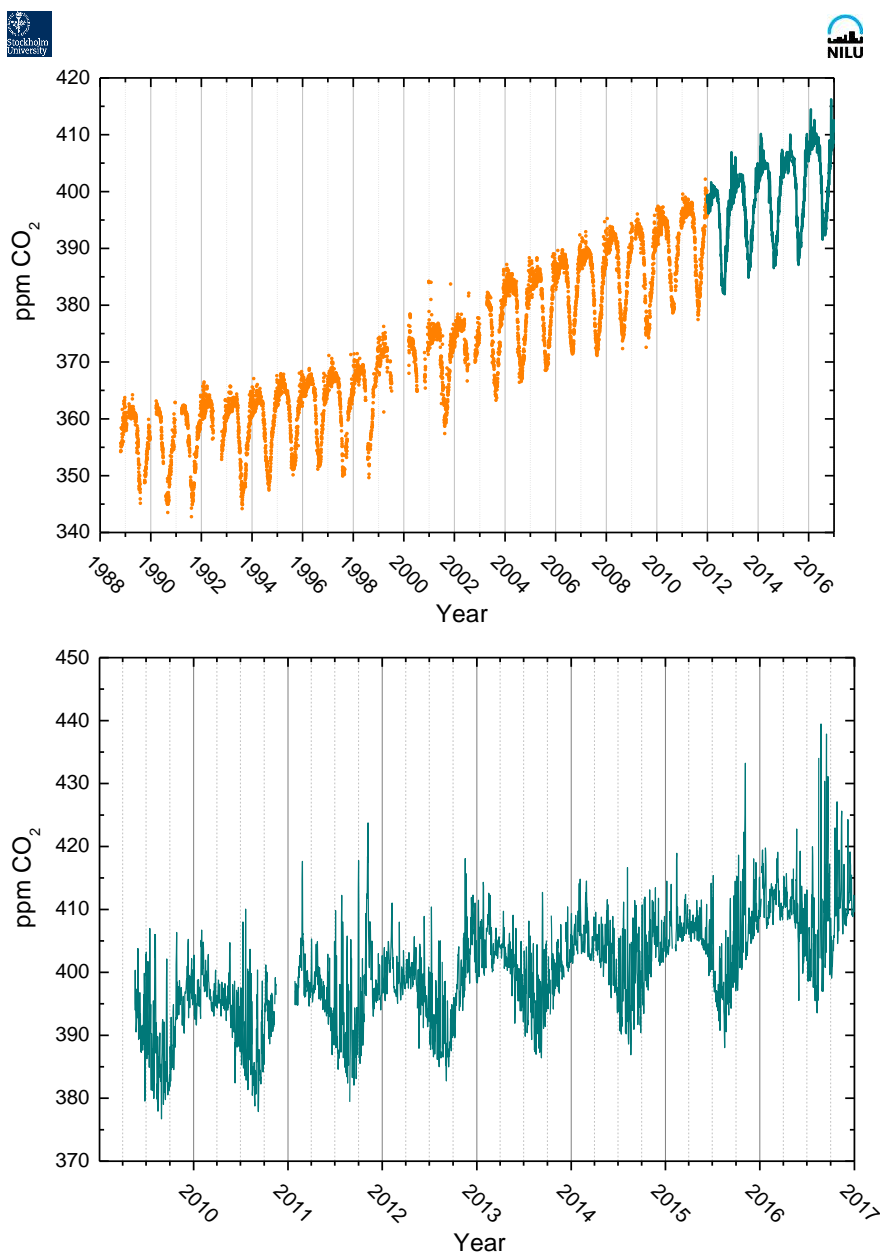


Figure 9: The atmospheric daily mean CO₂ concentration measured at Zeppelin Observatory for the period mid 1988-2016 is presented in the upper panel. Prior to 2012, ITM University of Stockholm provides all data, shown as orange dots and the green solid line is from the Picarro instrument installed by NILU in 2012. The measurements for Birkenes are shown in the lower panel, the green line is the daily mean concentration.

The results show continuous increase since the start of the observations at both sites. As can be seen there are much stronger variability at Birkenes than Zeppelin. At Zeppelin the largest variability is during winter/spring. For Birkenes it is high variability all year around. In summer there is also a clear diurnal variation with high values during the night and lower values during daytime (not shown). This is mainly due to changes between plant photosynthesis and respiration, but also the general larger meteorological variability and diurnal change in planetary boundary layer, particularly during summer contributes to larger variations in the concentrations. In addition to the diurnal variations, there are also episodes with higher levels at both sites due to transport of pollution from various regions. In general,

there are high levels when the meteorological situation results in transport from Central Europe or United Kingdom at Birkenes, and central Europe or Russia at Zeppelin.

The maximum daily mean value for CO₂ in 2016 was 439.5 ppm at Birkenes 25th August. In this period there was transport of air from central Europe. At Zeppelin the highest daily mean value was 416 ppm at 20th November 2016, and the air was transported from Kola Peninsula and western Siberia with the large oil and gas installations.

Figure 10 shows the development of the annual mean concentrations of CO₂ measured at Zeppelin Observatory for the period 1988-2016 in orange together with the values from Birkenes in green since 2010. The global mean values as given by WMO (WMO, 2017) in black. The yearly annual change is shown in the lower panel.

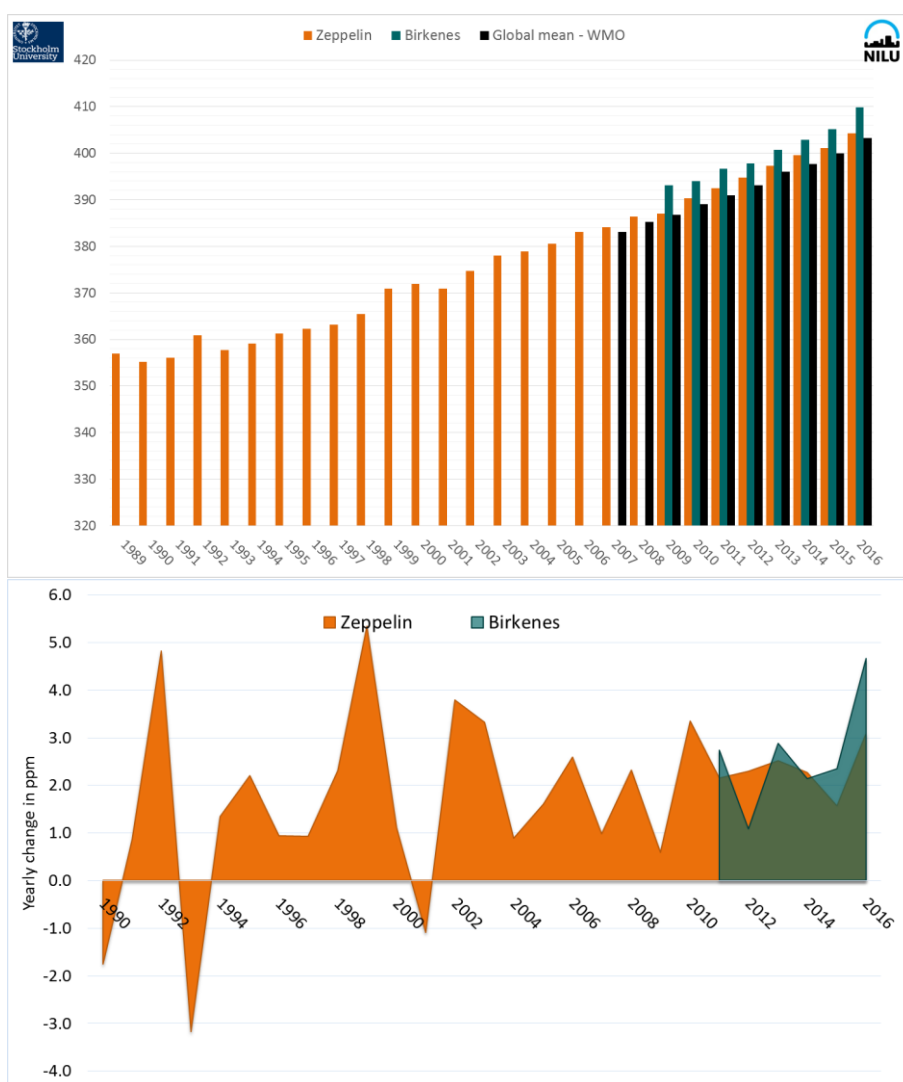


Figure 10: Upper panel: the annual mean concentrations of CO₂ measured at Zeppelin Observatory for the period 1988-2016 shown in orange. Prior to 2012, ITM University of Stockholm provides all data. The annual mean values from Birkenes are shown as green bars. The global mean values as given by WMO (2017) are included in black. The yearly annual change is shown in the lower panel, orange for Zeppelin, green for Birkenes.

The global mean increase for CO₂ from 2015 to 2016 was 3.3 ppm (WMO, 2017), the largest annual increase ever reported by WMO. The annual mean values for Birkenes and Zeppelin are higher than the global mean as there are more anthropogenic sources and pollution at the Northern hemisphere. The mixing to the southern hemisphere takes time, ca 2-3 years. The annual change shown in the lower panel shows an increase of only 1.6 ppm at Zeppelin from 2014 to 2015 which is remarkably low compared to global mean increase and the reason for this would need an in depth analysis. The change from 2015 to 2016 was more as expected with 3.1 ppm compared to 3.3 ppm in the global mean increase. At Birkenes, the increase from 2015 to 2016 was higher; 4,7 ppm in one year. This is higher than the global increase, and also the strongest yearly growth we have detected since the start in 2009. The time series for CO₂ at Birkenes is short and the reported trends should be used with caution. In short time series the end years will have relatively high impact on the trends.

A recent paper in Nature Geoscience (Myhre et al, 2017) is commenting on the relation between forcing of CO₂ and the CO₂ concentrations. Halfway to a doubling in the CO₂ concentration is 417 ppm, which will be reached before 2025 with current CO₂ growth rates. However, with a global mean CO₂ abundance in 2016 at 403 ppm the halfway point to a doubling of CO₂, in terms of radiative forcing, has been reached. Hence, at CO₂ concentrations between 393 ppm and 417 ppm we are more than a halfway to a doubling of CO₂ in terms of radiative forcing, but not in concentration (see also see section 1.4.1).

Key findings for CO₂: CO₂ concentrations have increased all years subsequently, in accordance with accumulation of gas in the atmosphere and the global development and increase in anthropogenic emissions. **The new record levels in 2016 are 404.3 ppm at Zeppelin and 409.8 ppm at Birkenes.** The increase from 2015 to 2016 is 3.1 ppm and 4.7 ppm, respectively, compared to global mean which was 3.3 ppm increase. Generally, the increase is now very high, and higher than previous years both globally, at Zeppelin, and at Birkenes in particular. It is urgent to understand the reasons more in detail, also the impact of natural sources and sinks on the annual variations. It is assumed that El Niño phenomenon in 2015/2016 contributed to increased growth through complex interactions between climate change and the carbon cycle.

2.1.2 Methane (CH₄)

Our measurements from 2016 reveal a pronounced new record in the observed CH₄ level, both at Zeppelin and Birkenes. Methane (CH₄) is the second most important greenhouse gas from human activity after CO₂. IPCC reported a radiative forcing is 0.48 W m⁻² since 1750 and up to 2011 (Myhre et al., 2013b), but as high as 0.97 W m⁻² for the emission based radiative forcing (Figure 5, page 22) due to complex atmospheric effects. Etminan et al. (2016) presented revised forcing estimates for all main greenhouse gases (see section see section 1.4.1 at page 23), and for CH₄ this resulted in 25% stronger forcing than given in the last IPCC report, increasing from 0.48 W m⁻² to 0.61 W m⁻². This emphasize the importance of CH₄ as greenhouse gas even further, and stressing the needs for understanding the recent changes.

In addition to being a dominant greenhouse gas, methane also plays central role in the atmospheric chemistry. The atmospheric lifetime of methane is approx. 12 years, when indirect effects are included, as explained in section 1.4.

The main sources of methane include boreal and tropical wetlands, rice paddies, emission from ruminant animals, biomass burning, and extraction and combustion of fossil fuels. Further, methane is the principal component of natural gas and e.g. leakage from pipelines; off-shore and on-shore installations are a known source of atmospheric methane. The distribution between natural and anthropogenic sources is approximately 40% natural sources, and 60% of the sources are direct result of anthropogenic emissions. Of natural sources there is a large unknown potential methane source under the ocean floor, so called methane hydrates and seeps. Further, a large unknown amount of carbon is captured in the permafrost layer in Siberia and North America and this might be released as methane if the permafrost layer thaws as a feedback to climate change.

The average CH₄ concentration in the atmosphere is determined by a balance between emission from the various sources and reaction and removal by free hydroxyl radicals (OH) to produce water and CO₂. A small fraction is also removed by surface deposition. Since the reaction with OH also represents a significant loss path for the oxidant OH, additional CH₄ emission will consume additional OH and thereby increasing the CH₄ lifetime, implying further increases in atmospheric CH₄ concentrations (Isaksen and Hov, 1987; Prather et al., 2001). The OH radical has a crucial role in the tropospheric chemistry by reactions with many emitted components and is responsible for the cleaning of the atmosphere (e.g. removal of CO, hydrocarbons, HFCs, and others). A stratospheric impact of CH₄ is due to the fact that CH₄ contributes to water vapour build up in this part of the atmosphere, influencing and reducing stratospheric ozone.

The concentration of CH₄ was, after a strong increase during the 20th century, relatively stable over the period 1998-2006. The global average change was close to zero for this period, also at Zeppelin. Recently an increase in the CH₄ levels is evident from our observations both at Zeppelin and Birkenes as well as observations at other sites, and in the global mean (see e.g. section 2.2.1.1.2 in Hartmann et al, 2013).

Figure 11 depicts the daily mean observations of CH₄ at Zeppelin since the start in 2001 in the upper panel and Birkenes since start in 2009 in the lower panel.

As can be seen from the figures there has been an increase in the concentrations of CH₄ observed at both sites the last years, and in general the concentrations are much higher at Birkenes than at Zeppelin. The highest ever ambient background CH₄ concentration detected at Zeppelin was on the 20th November 2016. The same day with the maximum level in CO₂ as well. The CH₄ concentration was 1996.1 ppb, and the transport pattern of that day shows strong influence from Russian industrial pollution from Kola Peninsula and western Siberia. Fugitive emission from Russian gas installations is a possible source of this CH₄ however, on this particular day, both CO and CO₂ levels were also very high, indicative of an industrial pollution episode as well.

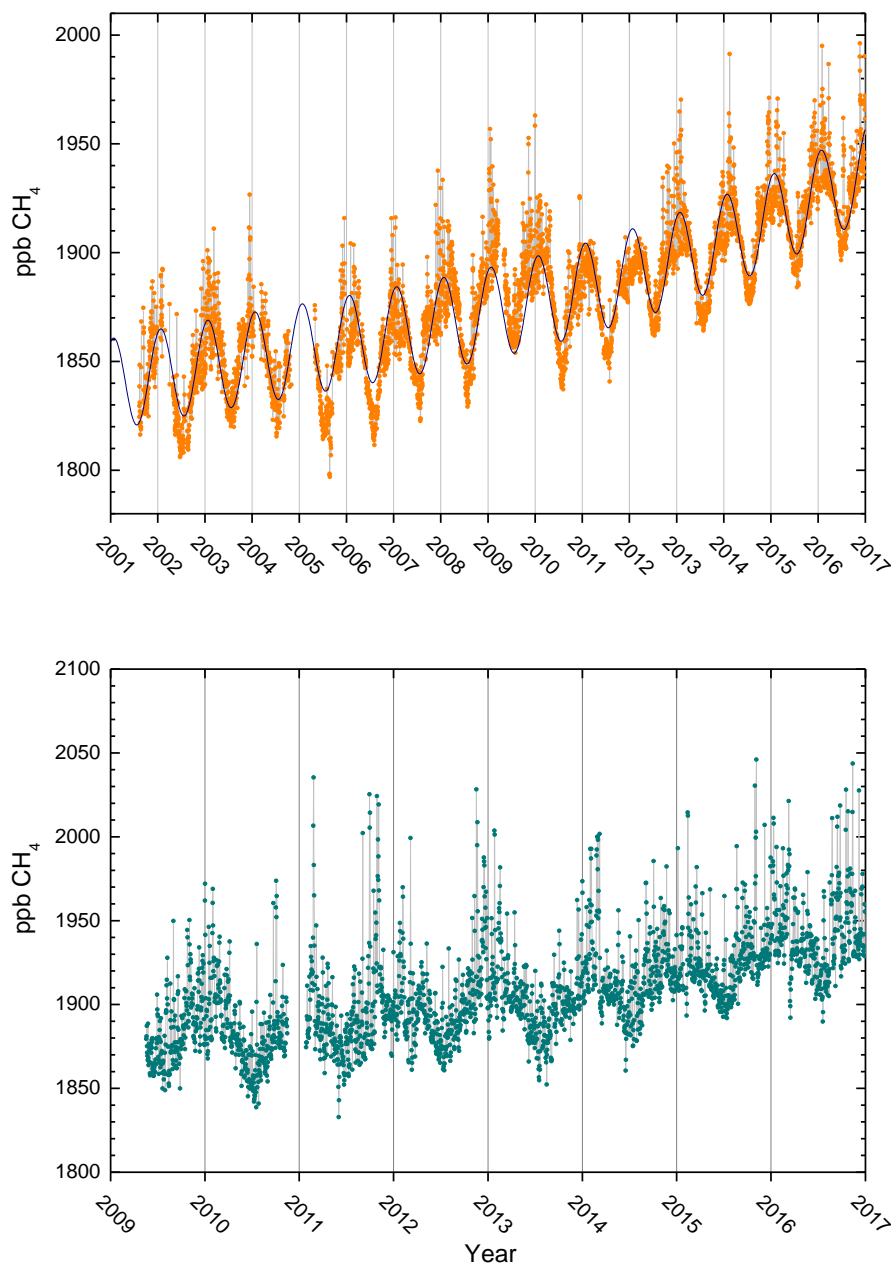


Figure 11: Observations of daily averaged methane mixing ratio for the period 2001-2016 at the Zeppelin Observatory in the upper panel. The black solid line is empirical fitted background methane mixing ratio. The lower panel shows the Daily mean observations for Birkenes are shown as green dots.

For both Zeppelin and Birkenes, the seasonal variations are clearly visible, although stronger at Birkenes than Zeppelin. This is due longer distance to the sources at Zeppelin, and thus the sink through reaction with OH dominates the variation. The larger variations at Birkenes are explained by both the regional sources in Norway, as well as a stronger impact of pollution episodes from long transport of pollution from central Europe or UK. For the daily mean in Figure 11, the measurements show very special characteristics in 2010 and 2011 at Zeppelin. As shown, there is remarkably lower variability in the daily mean in 2011 with fewer episodes than the typical situation in previous and subsequent years (e.g. summer/autumn 2012). The reason for this has been intensively investigated as part of various national and international

research programmes, also at NILU (e.g. Thompson *et al*, 2016) and seem to be due to less impact of episodes from Northern Russia, and not e.g. instrumental problems.

At Zeppelin there are now 15 years of data, for which the trend has been calculated. To retrieve the annual trend in the methane for the entire period, the observations have been fitted by an empirical equation. The fit to the observed methane values are shown as the black solid line in Figure 11. This corresponds to a trend of 5.62 ppb per year, or ca 0.5-0.6% per year, the last years. The pronounced increase started in November/December 2005 and continued throughout the years 2007 - 2009, and is particularly evident in the late summer-winter 2007, and summer-autumn 2009.

For Birkenes shown in the lower panel, the time series is too short for accurate trend calculations (as described for CO₂), but a yearly increase is evident since the start 2009. There are also episodes with higher levels due to transport of pollution from various regions. In general, there are high levels when the meteorological situation results in transport from Central Europe.

The CH₄ global annual mean of year 2016 was higher than ever measured before, at a level of 1853 ppb (WMO, 2017), and Zeppelin and Birkenes experienced new record levels at both sites. The annual mean increase in the CH₄ levels the last years is visualised in Figure 12 showing the CH₄ annual mean concentration for the period 2001-2016 from Zeppelin (orange) and for Birkenes (green) from 2010-2016. The global mean values given by WMO (WMO, 2017) are included for comparison.

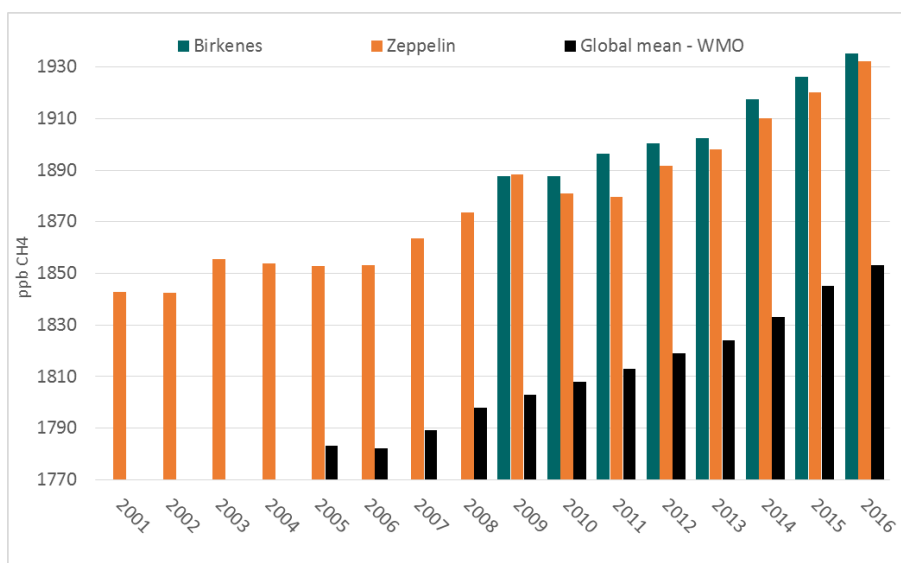


Figure 12: Development of the annual mean mixing ratio of methane in ppb measured at the Zeppelin Observatory (orange bars) for the period 2001-2016, Birkenes for the period 2010-2016 in green bars, compared to global mean provided by WMO as black bars (WMO, 2017).

The annual means are based on the measured methane values. Modelled empirical background values are used, when data is lacking in the calculation of the annual mean. The diagram in Figure 12 clearly illustrates the increase in the concentrations of methane at Zeppelin since 2005 a small decrease from 2010 to 2011, and then a new record level in 2016. The annual mean mixing ratio for 2016 was 1932 ppb, an increase of 12 ppb, from 2015 to 2016. The annual mean value for 2016 confirms that there is still a strong increase from year

to year in Arctic methane. The global mean for 2016 was 1953 ppb, with an increase of 9.0 ppb since the previous year. The increase since 2005 at Zeppelin is 79 ppb (approx. 4.3 %) which is high compared to the development of the methane mixing ratio in the period from 1999-2005 at Zeppelin, Svalbard and globally. It is also slightly higher than the global mean increase since 2005 which was 70 ppb, as published in the yearly bulletins by WMO (WMO, 2011, 2012, 2013, 2014, 2015, 2016, 2017). The global mean shows an increase since 2006, which over the years 2009-2013 was e.g. 5-6 ppb per year but as high as 12 ppb from 2014-2015, and 9 ppb from 2015 to 2016. For comparison, during the 1980s when the methane mixing ratio showed the strongest increase, the annual global mean change was around 15 ppb per year. A strong increase is also evident for Birkenes, with a growth of as high as 16 ppb since 2015. This is the strongest yearly increase we have observed, with particularly high values during the autumn months.

Larger fluctuations are evident at Zeppelin, than in the global mean both throughout the year, and from year to year. This is explained by the distribution of the sources; there are more sources in the northern hemisphere, and thus more inter-annual variations. The global mean is lower as this includes all areas of the globe, e.g. remote locations such as Antarctica and is therefore lower than the values at Zeppelin and Birkenes, located closer to the sources. Hence, there is a time lag in the development.

Currently, the observed increase over the last years is not fully explained. The recent observed increase in the atmospheric methane concentrations has led to enhanced focus and intensified research to improve the understanding of the methane sources and changes particularly in responses to global and regional climate change. Leaks from gas installations, world-wide, both onshore and offshore might be an increasing source. Hence, it is essential to find out if the increase since 2005 is due to high emissions from point sources, or if it is caused by newly initiated processes releasing methane to the atmosphere e.g. the thawing of the permafrost layer or processes in the ocean, both related to permafrost and others. Recent and ongoing scientific discussions point in the direction of increased emissions from wetlands located both in the tropical region and in the Arctic region. This is also investigated in a collaboration between NILU and Cicero (Dalsøren et al., 2016). Gas hydrates at the sea floor are widespread in thick sediments in this area between Spitsbergen and Greenland. If the sea bottom warms, this might initiate further emissions from this source. This is the core of the large polar research project *MOCA - Methane Emissions from the Arctic Ocean to the Atmosphere: Present and Future Climate Effects*⁸, which started at NILU in October 2013, and was finalized spring 2017. A few results from this is included in the next section.

There is a combination of causes explaining the increase in methane the last years, and the dominating reason is not clear. A probable explanation is increased methane emissions from wetlands, both in the tropics as well as in the Arctic region, in addition to increases in emission from the fossil fuel industry. Ethane and methane are emitted together from fossile oil and gas sources, and the decrease in ethane support the hypothesis that wetland changes is a large contributor to the change in CH₄. A study exploring isotopic data of CH₄ is under reviews in a scientific journal, to try to bring better answer the open questions. The isotopic signatures of CH₄ from wetlands is very different from natural gas. Thawing of permafrost,

⁸ <http://moca.nilu.no/>

both in terrestrial regions and in marine region, might introduce new possible methane emission sources initiated by the temperature increase the last years in the Arctic region.

Key findings for Methane - CH₄: In 2016 the mixing ratios of methane increased to a **new record level both at Zeppelin, Birkenes and globally**. At Zeppelin the annual mean value reached 1932 ppb with an increase of as much as 12 ppb since 2015. The changes at Zeppelin the last 10 years are large compared to the evolution of the methane levels in the period 1998-2005, when the change was close to zero both at Zeppelin and globally, after a strong increase during the mid 20th Century. The methane increase at the Zeppelin observatory from 2005 to 2016, (79 ppb, or around 4.3%) was larger than the global increase in the same period (approx. 70 ppb). The measurements of CH₄ at Birkenes showed an annual mean value for 2016 of 1942 ppb, which is 16 ppb more than the year before. This is a dramatic increase and needs attention to understand the reasons.

2.1.2.1 Methane from Arctic Ocean to the atmosphere?

A comprehensive research project “**MOCA - Methane Emissions from the Arctic Ocean to the Atmosphere: Present and Future Climate Effects**” has just ended which focused on methane from Arctic Ocean to the atmosphere. This was a collaboration with CAGE (The Centre for Arctic Gas Hydrate, Environment and Climate, at UiT The Arctic University of Norway) and Cicero, but lead by NILU. The driving questions for MOCA were:

- I. What is the status and current release of methane from marine seep sites and methane hydrates in the Arctic Ocean, and specifically around Svalbard?
- II. How are these processes depending on trends in sea temperature and annual variations?
- III. Where are the most important areas in the Arctic Ocean which could constitute a possible source of atmospheric methane, now and in the future?
- IV. What is the present CH₄ emission from the seabed to the atmosphere?
- V. What is the most likely change in flux, the next 50 and 100 years under realistic climate scenarios? And what is the global effect of this?
- VI. What is the ocean temperature threshold for large changes in emission of methane from hydrates?

In this project we used integrated approaches to answer these questions. Figure 13 shows the exploratory platforms involved. Comprehensive measurement campaigns involving ship, aircrafts and Zeppelin have been performed. Additionally we use models both atmospheric chemistry, methane hydrates modelling at sea floor, and climate models.

What are gas hydrates?

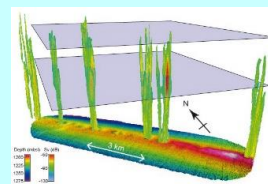
Large amounts of natural gas, mainly methane, are stored in the form of hydrates in continental margins worldwide, particularly, in the Arctic. Gas hydrate consists of ice-like crystalline solids of water molecules



encaging gas molecules, and is often referred to as ‘the ice that burns’.

What are seeps?

Cold seeps are locations where hydrocarbons are emitted from sub-seabed gas reservoirs into the ocean. This can be both from petroleum reservoirs and methane hydrates. The illustration is gas bubbles rising 800 m up from Vestnesa Ridge, offshore Svalbard (Smith et al. 2014).



<http://cage.uit.no>

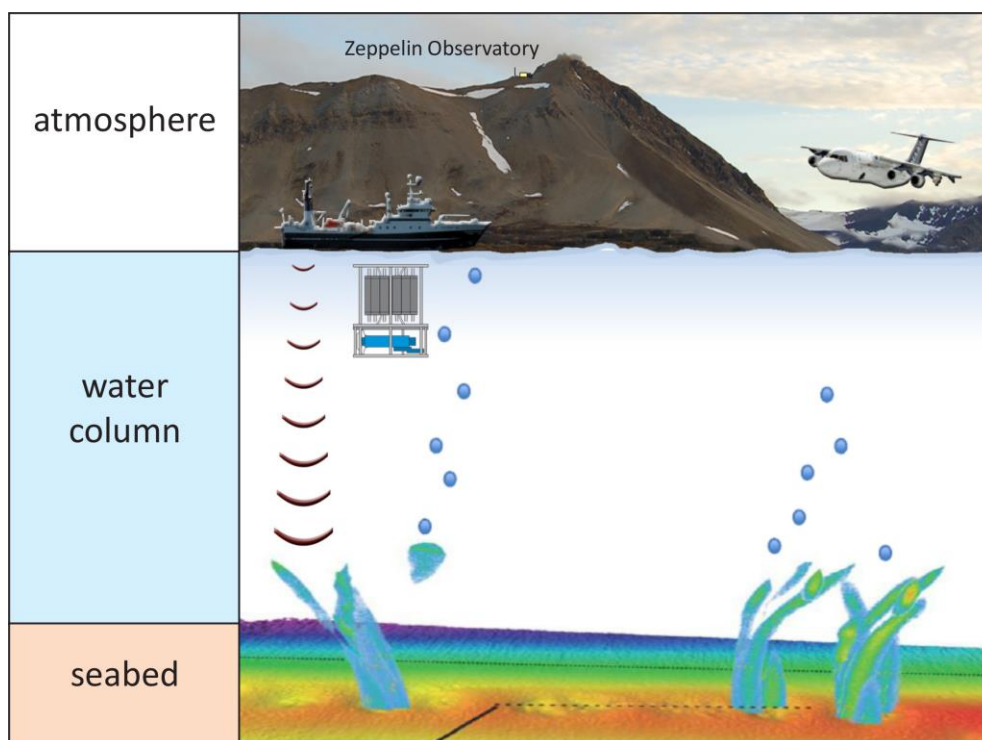


Figure 13: Field campaign and measurement platforms at the sea floor, in the water column, and in the atmosphere west of Svalbard in June-July 2014. Seeps on the seafloor, represented here by swath bathymetry, release gas bubbles that rise through the water column. The Research Vessel Helmer Hanssen detected gas bubbles and collected water samples at various depths, and provided online atmospheric CH₄, CO and CO₂ mixing ratios and discrete sampling of complementary trace gases and isotopic ratios. The Facility of Airborne Atmospheric Measurements (FAAM) aircraft measured numerous gases in the atmosphere, and an extended measurement program was performed at the Zeppelin Observatory close to Ny-Ålesund. Data from Zeppelin was used for comparison to detect possible oceanic sources.

We have used different state-of-the-art models to assess and understand the variation in Arctic methane, to investigate potential oceanic sources in various regions, in particular methane hydrates and cold seeps. First, results are presented in Myhre et al (2016), Pisso et al (2016), Thompson et al (2016), and some information can be found here: <http://forskning.no/havforskning-klima-arktis/2016/05/metan-slipper-ikke-ut-av-polhavet-om-sommeren>.

Several papers are in the finale stage, and will add important information to the understanding of CH₄ and ethane and the interaction between ocean and atmosphere both now and in the future, when published.

2.1.3 Nitrous Oxide (N₂O)

Nitrous Oxide (N₂O) is a greenhouse gas with both natural and anthropogenic sources. The sources include oceans, tropical forests, soil, biomass burning, cultivated soil and use of particular synthetic fertilizer, and various industrial processes. There are high uncertainties in the major soil, agricultural, combustion and oceanic sources of N₂O. Also frozen peat soils in Arctic tundra is reported as a potential source (Repo et al., 2009), but studies identify tropical and sub-tropical regions as the largest source regions (Thompson et al, 2013). N₂O is

an important greenhouse gas with a radiative forcing of 0.17 W m^{-2} since 1750 contributing around 6 % to the overall well-mixed greenhouse gas forcing over the industrial era. N_2O is also the major source of the ozone-depleting nitric oxide (NO) and nitrogen dioxide (NO_2) in the stratosphere, thus the component is also influencing the stratospheric ozone layer. The Assessment of the ozone depletion (WMO, 2011) suggests that current emissions of N_2O are presently the most significant substance that depletes ozone.

N_2O has increased from around 270 ppb prior to industrialization and up to an average global mean of 328.0 ppb in 2015 (WMO, 2016). In 2009, NILU installed a new instrument at Zeppelin measuring N_2O with high time resolution of 15 minutes. The instrument was in full operation in April 2010 and the results for 2010 -2016 are presented in Figure 14.

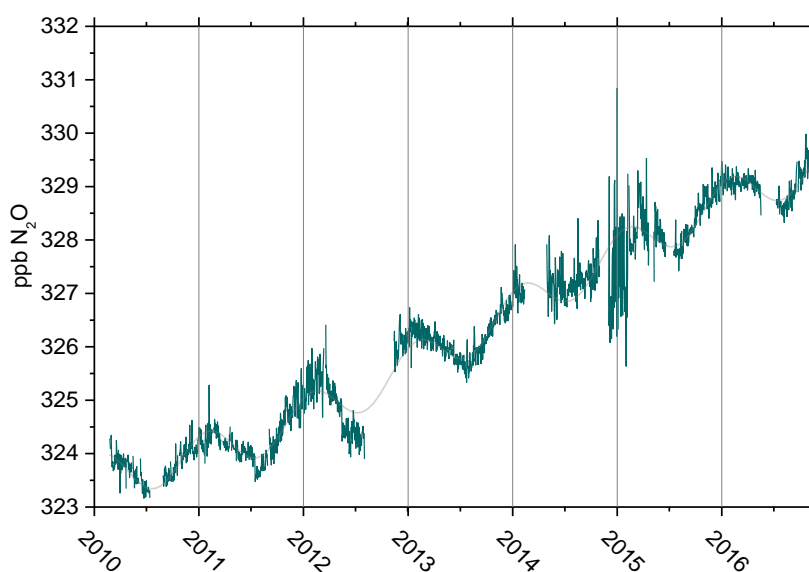


Figure 14: Measurements of N_2O at the Zeppelin Observatory for 2010-2016. The grey line is empirical modelled N_2O mixing ratio.

The time series is short for trend calculations, and also connected to uncertainty due to instrument problems.

According to WMO (WMO, 2017) there is a global mean increase of 1 ppb since 2015. Annual mean for Zeppelin in 2016 was 328.1 with a standard deviation of 0.66 ppb. Due to instrumental problems there was a higher uncertainty this year, compared to earlier periods. As can be seen a high variability in 2015 is evident. As a part of ICOS-Norway a Norwegian infrastructure project funded by Norwegian Research Council, a new instrument is purchased and installed in 2017. The two instruments will run in parallel to ensure overlap and consistent long time series.

Figure 15 shows annual average concentrations of N_2O measured at Zeppelin for the periods 2011-2016. The global annual means of N_2O in 2016 (WMO, 2017) is included as a black bar for comparison. The concentrations at Zeppelin are slightly higher than the global means.

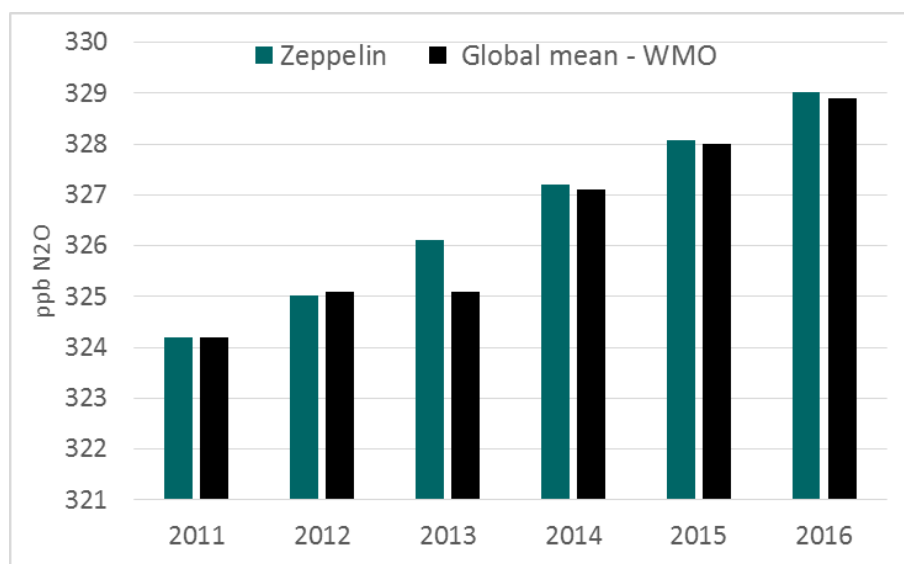


Figure 15: Annual mean concentration of N₂O at the Zeppelin Observatory for 2010-2016.

Key findings Nitrous Oxide -N₂O: The global mean level of N₂O has increased from around 270 ppb prior to industrialization and up to an average global mean of 328.9 ppb in 2016. This is slightly lower than at Zeppelin, where the annual mean is 329.0 ppb. The difference is not significant, taking the uncertainty of the Zeppelin data into account.

2.1.4 Volatile organic compounds (VOC)

Volatile Organic Compounds (VOCs) are a large group of carbon-based compounds that have a high vapor pressure and easily evaporate at room temperature. VOCs oxidation contributes to the production of tropospheric ozone and influences photochemical processing, both impacting climate and air quality. Sources of VOCs (here ethane, propane, butane, pentane, benzene and toluene) include natural (mostly geological but also from wild fires) and anthropogenic (fossil fuels) ones. CH₄ and VOCs are co-emitted from oil and natural gas sources, for CH₄ to ethane the mass ratio varies from 7 to 14 (Helmig et al, 2016). The atmospheric ethane budget is not well understood and state-of-the-art atmospheric models underestimate ethane-mixing ratios, implying that current emission inventories require additional sources to balance the global atmospheric ethane budget.

Helmig *et al.* (2016) showed, from long-term observations of ethane from a global network that concentrations are increasing (since circa 2010), and that there is a strong latitudinal gradient, with the highest abundances observed in the Arctic, and a steep decline towards the south. They concluded that emissions from North American oil and natural gas development are the primary cause of increasing concentrations in recent years. However, there might be other factors. A recent study by Nicewonger *et al.* (2016) used analysis of polar ice cores to estimate the pre-industrial emissions and concluded that natural ethane emissions from geologic seeps contributed significantly to the preindustrial ethane budget. Etiope and Ciccioli (2009) suggested that a substantial part of the missing ethane source can be attributed to gas seepage, but they did not include the Arctic in their study.

Figure 16 shows the daily mean observations of the four non-methane hydrocarbons included in the programme, ethane, propane, butane and pentane, at Zeppelin since the start in September 2010.

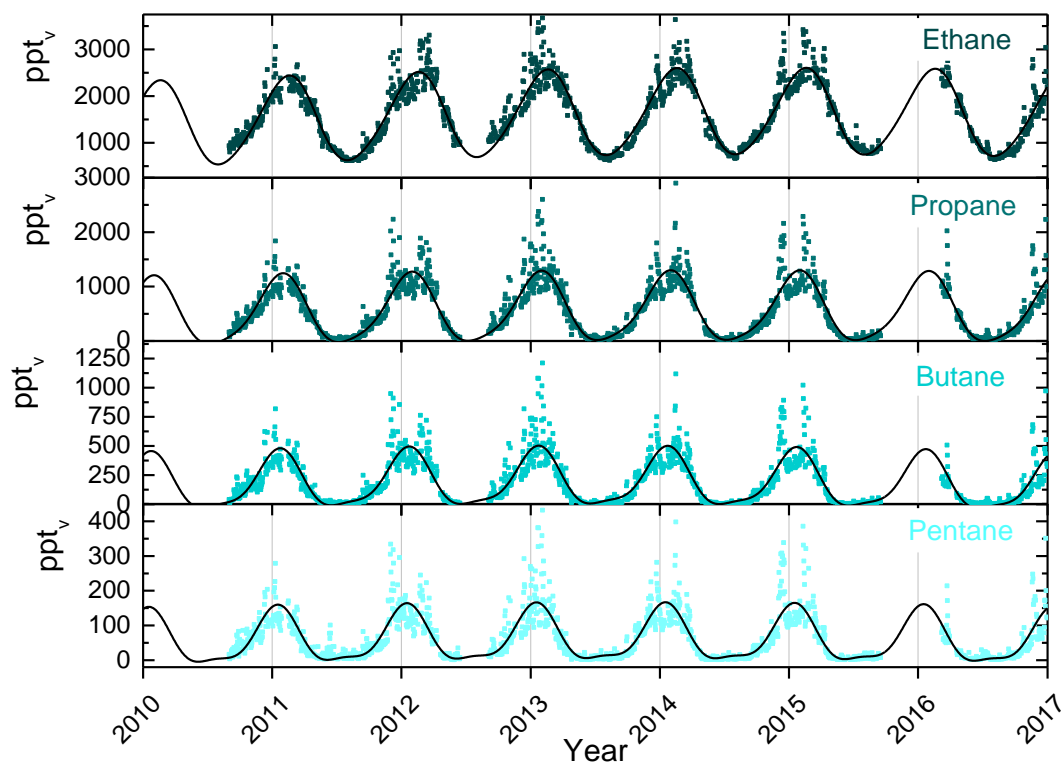


Figure 16: Observations of daily averaged mixing ratio of benzene (upper panel) and toluene (lower panel) for the period September 2010 - 2016 at the Zeppelin Observatory.

Due to the short lifetimes ranging from a few days for pentane to 2-3 months for ethane, the annual cycles are very strong, regulated by OH. The annual mean developments are given in Figure 17.

The data coverage of the compounds are relatively low over the last period. Still, it seems that the development of the annual means since 2011 demonstrates that ethane has increased and have a different development than the more heavy non-methane hydrocarbons in the lower panels, although many of the sources are considered as the same. Hence, this can indicate that some of dominating ethane sources, with less content of the heavier non-methane hydrocarbons is increasing, compared to the others.

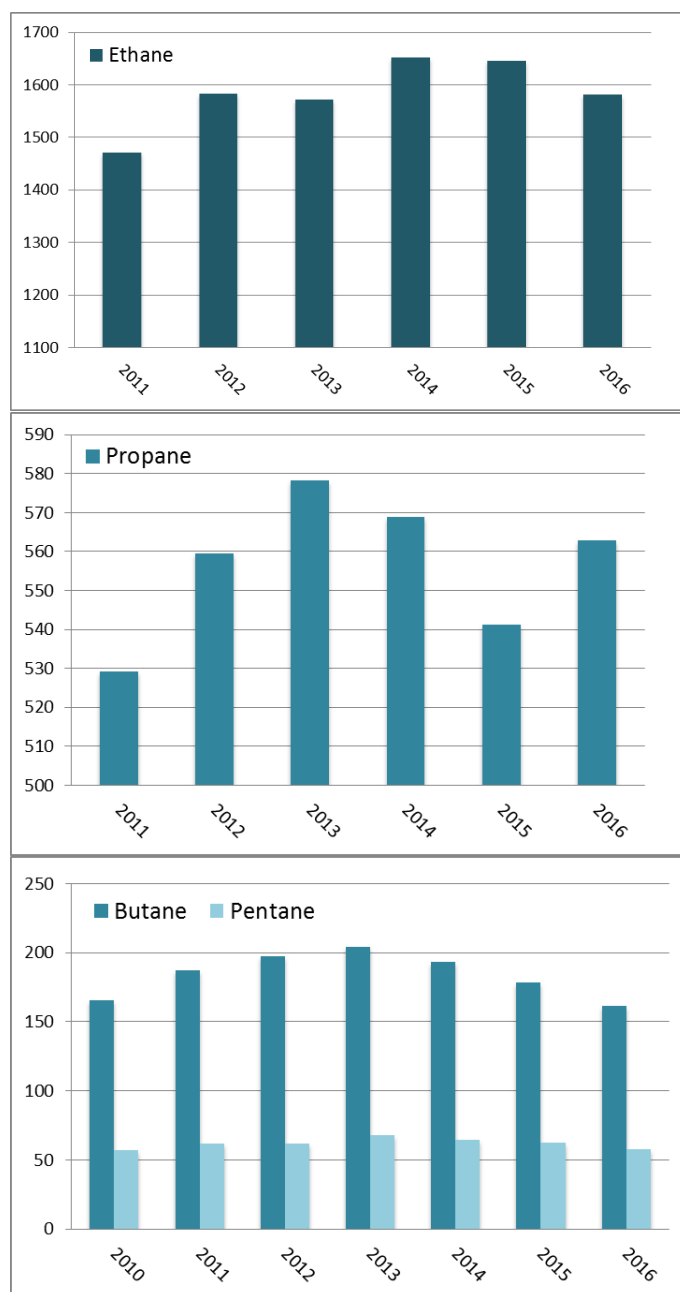


Figure 17: Development of the annual means of the measured non-methane hydrocarbons at the Zeppelin Observatory for the period 2011-2016. Upper panel in dark green: ethane, mid-panel propane, and lower panel Butane and Pentane. All concentrations are in ppt.

At Zeppelin 2 cyclic more heavy VOCs are measured, *benzene and toluene*, which belong to a group of VOCs found in petroleum hydrocarbons, such as gasoline. The compounds have attracted much attention since they are considered a strong carcinogen (especially benzene), but they are also relevant for climate. The VOCs have relatively short atmospheric lifetimes and small direct impact on radiative forcing. However, anthropogenic secondary organic aerosols (SOA) are formed from photo oxidation of benzene and toluene (Ng et al., 2007), which indirectly impacts the climate. The SOA formation from these VOCs is most effective under low-NO_x conditions and when ambient concentration of organic aerosols is high. Thus, benzene and toluene influence climate through their production of secondary organic

aerosols and their involvement in photochemistry, i.e., production of O_3 in the presence of light.

Figure 18 depicts the daily mean observations of benzene and toluene at Zeppelin since the start in September 2010.

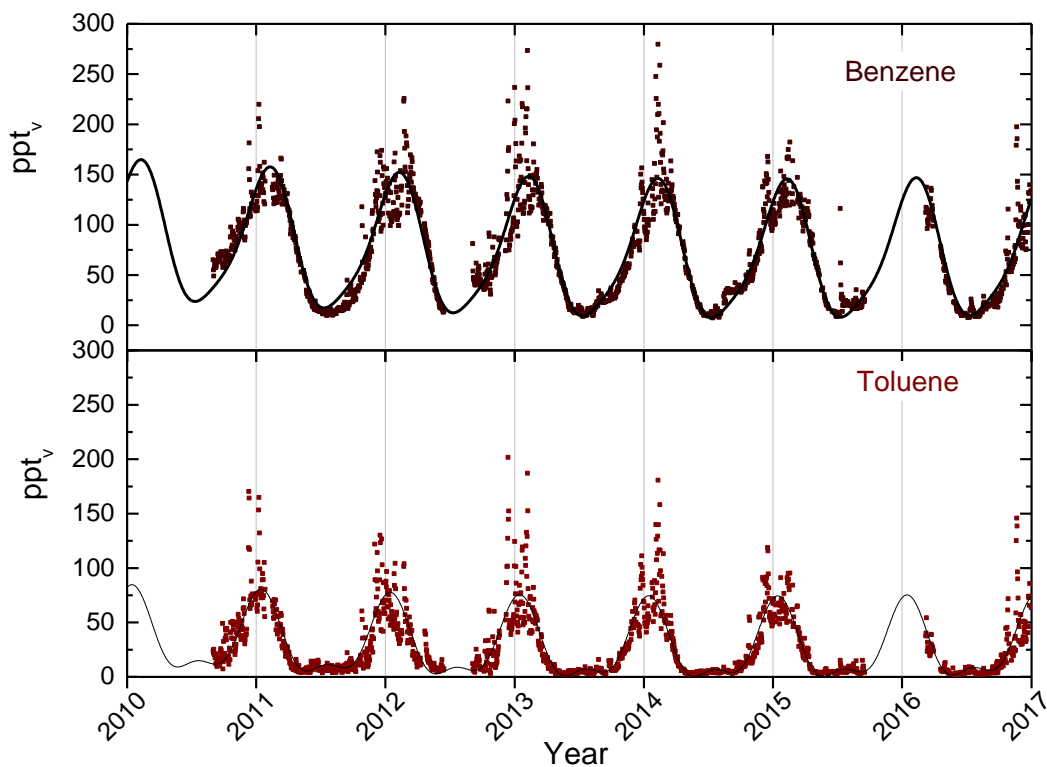


Figure 18: Observations of daily averaged mixing ratio of benzene (upper panel) and toluene (lower panel) for the period September 2010 - 2016 at the Zeppelin Observatory.

As can be seen from the Figure there is strong annual variations, mainly explained by the reactions induced by sunlight. For both component there seem to be a decreasing trend, but this is too early to conclude, due to the short time series available.

The annual means of benzene and toluene for the period 2010-2016 is presented in Figure 19. The period 2010 to 2016 was relatively stable for both components, with strong episodes during wintertime due to transport of urban polluted air from lower latitudes.

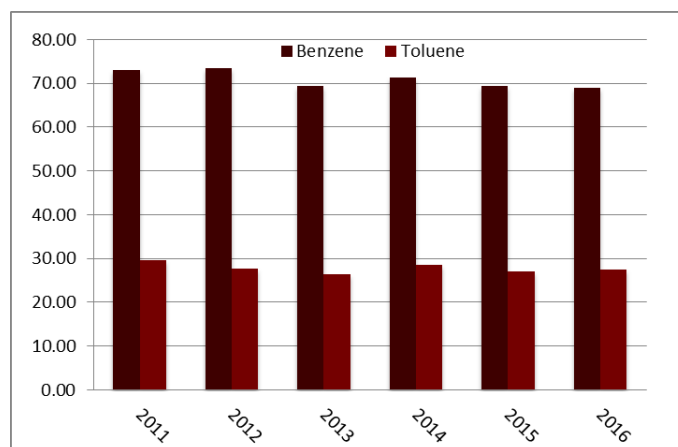


Figure 19: Development of the annual means of benzene (deep brown) and toluene (dark red) for the period September 2011 - 2016 at the Zeppelin Observatory. All concentrations are in ppt.

Key findings - VOCs: The hydrocarbon **ethane**, often co-emitted with fossil fuel methane, is increasing at Zeppelin, but **toluene** and **benzene**, show stable values since 2014. These are short lived indirect climate gases important for the levels of aerosols, ozone, CO and contribute to CO₂ and others, but with low direct greenhouse gas effects.

2.1.5 Carbon monoxide (CO)

Atmospheric carbon monoxide (CO) sources are the oxidation of various organic gases as VOCs emitted from fossil fuel, biomass burning, and also oxidation of methane is important. Additionally, emissions from plants, fires and ocean are important sources. CO is not considered as a direct greenhouse gas, mostly because it does not absorb terrestrial thermal IR energy strongly enough. However, CO is able to modulate the level of methane and production of tropospheric ozone, which are both very important greenhouse gas and hence CO is considered as a climate gas, although not a greenhouse gas. CO is closely linked to the cycles of methane and ozone and, like methane; CO plays a key role in the control of the OH radical.

CO at Zeppelin is included in the current monitoring programme and the observed CO mixing ratios for the period September 2001-2016 are shown in Figure 20.

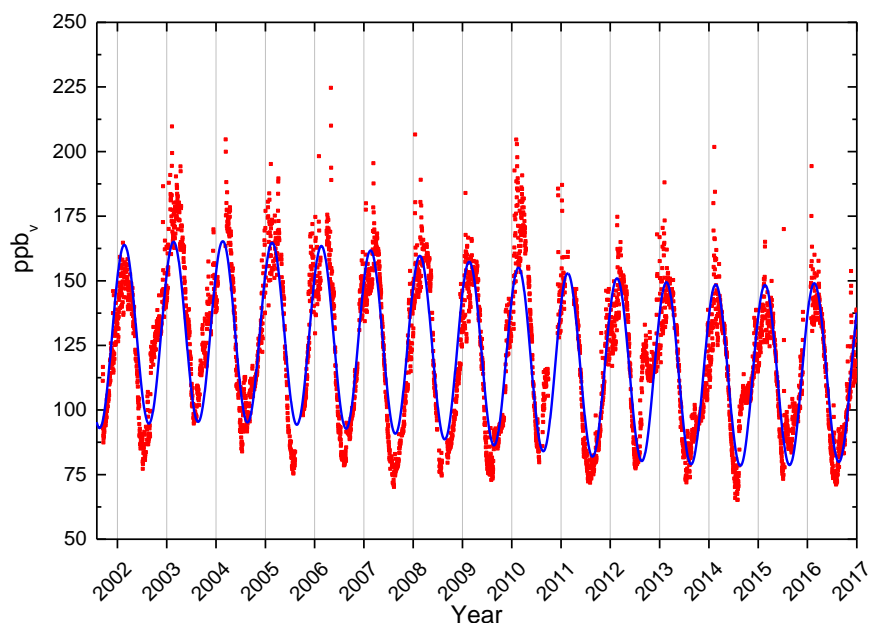


Figure 20: Observations of carbon monoxide (CO) from September 2001 to 2016 at the Zeppelin observatory. Red dots: daily averaged observed mixing ratios. The solid line is the empirical fitted background mixing ratio.

The concentrations of CO show characteristic seasonal variations with a clear annual cycle with a late winter (February/March) maximum and a late summer (August) minimum. This seasonal cycle is driven by variations in OH concentration as a sink, emission by industries and biomass burning, and transportation on a large scale. As seen from the Figure there are also peak values which are due to long-range transport of polluted air to Zeppelin and the Arctic. The highest mixing ratio of CO ever observed at Zeppelin; is 217.2 ppb on the 2nd of May 2006. The peak values are due to transport of polluted air from lower latitudes; urban pollution (e.g. combustion of fossil fuel) and in spring 2006 it was from agricultural fires in Eastern Europe. The maximum value in 2016 was on 1st of February; 194 ppb, and this was caused by transport of polluted air from North East Russia, the region with oil and gas installations and possible flaring emissions. We calculated a trend at Zeppelin of -1.3 ppb per year for the period 2001-2016.

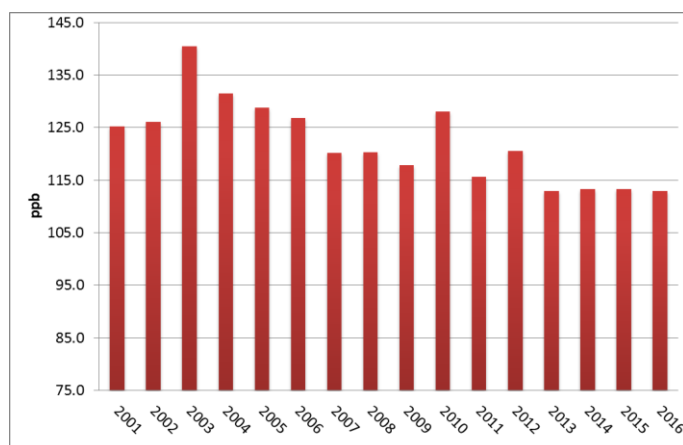


Figure 21: Development of the annual means of CO measured at the Zeppelin Observatory for the period 2001-2016. The concentrations are in ppb.

The development of the annual means for the period 2001-2016 are presented in Figure 21, clearly illustrating a maximum in the year of 2003. In general the CO concentrations measured at Zeppelin show a decrease during the period 2003 to 2009, and stable levels the last years with a small peak in 2010.

CO is an excellent tracer for transport of smoke from fires (biomass burning, agricultural- or forest fires). 2016 was not particularly influenced by this, it seems but 2015 was more a remarkably summer with respect to impact of fires at lower latitudes at the measurements at Zeppelin. The elevated concentrations back in July 2015 are related to long-range transport of smoke and ash from wildfires in Canada and Alaska. An analyse of the meteorological situation in the first two weeks of July 2015 shows a synoptically high pressure area over Greenland and Canada, with easterly wind direction from Canada towards the northwest, and air masses further arriving in the Arctic via the polar area. 7-days backwards trajectories from the FLEXTRA model, Figure 22, illustrates the synoptical situation on July 10th, 2015.

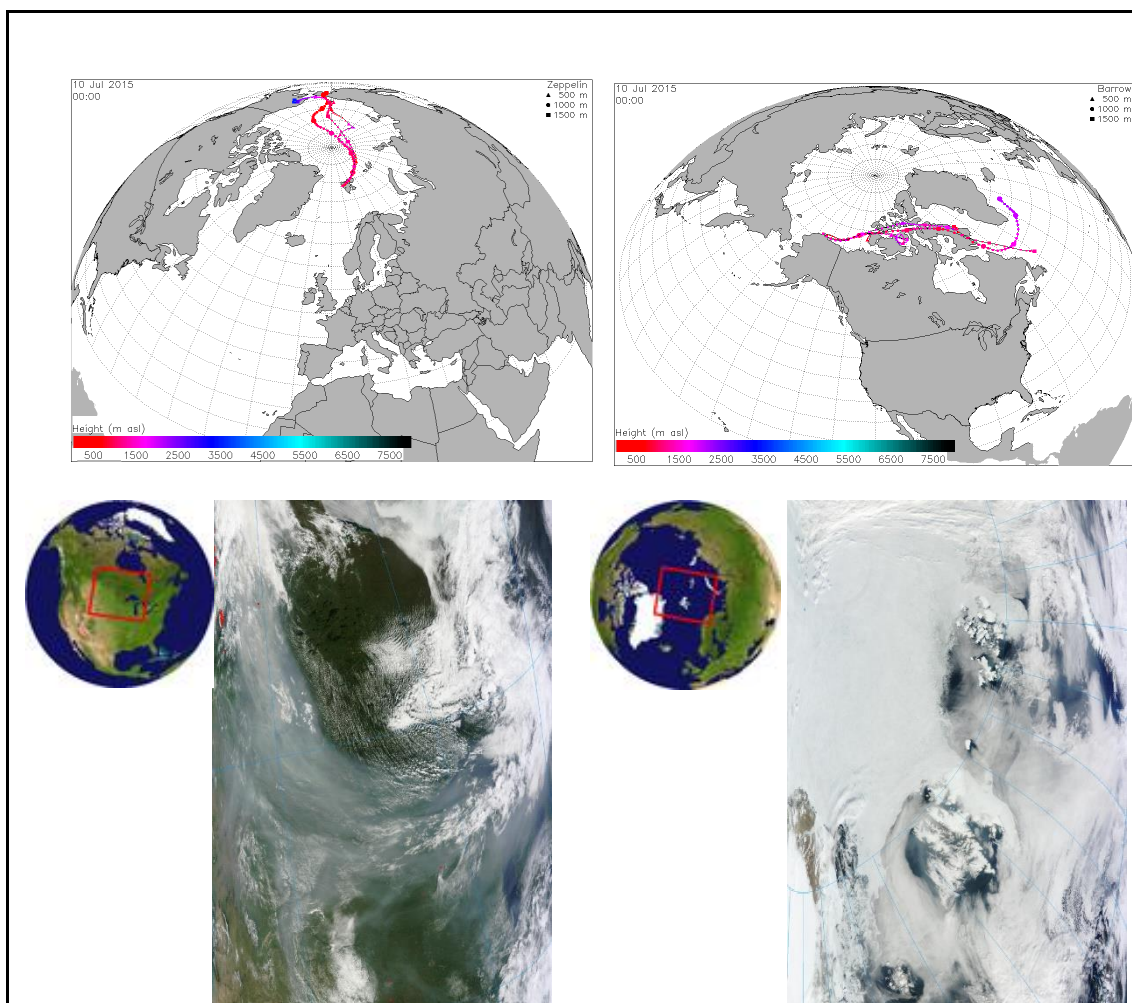


Figure 22: Upper panel: 7-days backwards trajectories from the FLEXTRA model and the synoptical situation on July 10th. Lower panel: the smoke as detected from the MODIS satellite instrument and spread out over North America on July 3rd 2015 (left) and visible above the Svalbard Islands on July 10th (right)

The increased CO concentrations arises as a result of air masses arriving at Zeppelin Observatory polluted with smoke and particles from more than 200 individual forest fires across British Columbia, Saskatchewan, and Alberta in July 2015, centred in the northwest of the continent. In western Canada, more than three times the area that's normally burned was affected. (<http://www.npr.org/2015/07/11/421995880/wildfires-in-canada-and-alaska-drive-thousands-from-homes>). High record temperatures in most of Alaska also underpinned the situation. The figure also shows the smoke as detected from the MODIS satellite instrument and spread out over North America on July 3rd 2015 (left) and visible above the Svalbard Islands on July 10th (right). The situation lasted until August 8, when the wind in the Arctic shifted to a more southerly direction again bringing air masses with CO concentrations close to the expected average for the season to Zeppelin.

2.1.6 Methyl Chloride at the Zeppelin Observatory

Methyl chloride (CH_3Cl) is the most abundant chlorine containing organic gas in the atmosphere, and it contributes approximately 16% to the total chlorine from the well-mixed gases in the troposphere (WMO, 2014b), and through this a strong contributor to ozone depletion. The main sources of methyl chloride are natural, and the dominating sources include ocean, biomass burning, fungi, wetlands, rice paddies, and tropical forests. Due to the dominating natural sources, this compound is not regulated through the Montreal or the Kyoto protocol. To reach the stratosphere, the lifetime in general needs to be in the order of 2-4 years, but this is also dependant on the source strength and the regional distribution of the gas. Methyl chloride has relatively high mixing ratio, and contributes to the stratospheric chlorine burden.

The result of the measurements of this gas for the period 2001-2016 is shown in Figure 23. The lifetime of methyl chloride is only one year, resulting in large seasonal fluctuations due to rapid changes in emission, as shown in Figure 23.

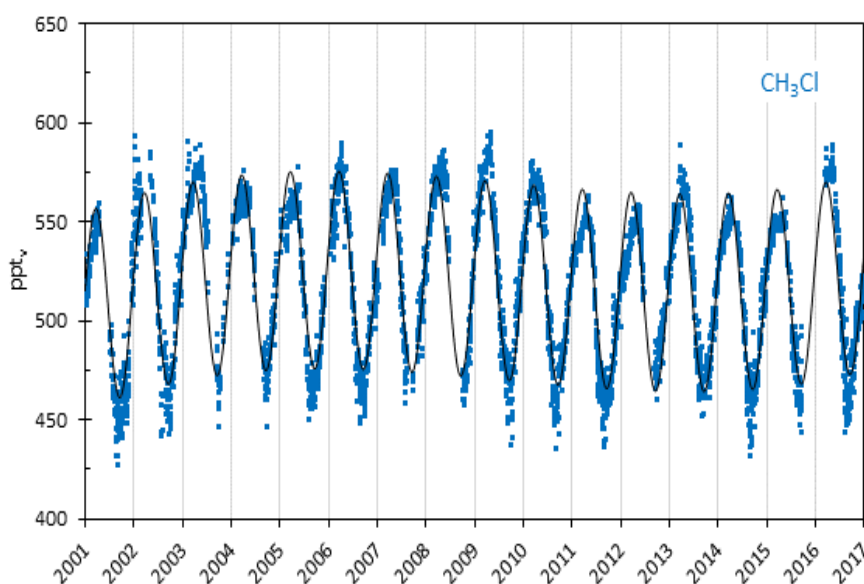


Figure 23: Observations of methyl chloride, CH_3Cl , for the period 2001-2016 at the Zeppelin Observatory. Blue dots: daily averaged concentrations from the observations, solid line: empirical fitted mixing ratios.

The annual means of methyl chloride for the period 2001-2016 are shown in Figure 24. Days with missing observations are filled with empirical fitted data. Only small changes have been observed since the measurements started in 2001. The trend for the period 2001-2016 is -0.16 ppt/yr (-0.5% for the entire period). From 2002 to 2009 the methyl chloride concentrations were relatively stable, but since 2009 there has been larger variability and a decreasing tendency. However, in 2016 the annual mean value was 10 ppt higher than previous year. The reason for this is not clear, and sources resulting in the rapid observational changes the last years need to be investigated. The black bar in Figure 24 shows that the global annual mean in 2016 (Hall et al., 2017) was 40 ppt (7%) higher than the annual mean value at the Zeppelin Observatory. This is likely explained by strong emission sources in the tropics, resulting in increased CH_3Cl mixing ratios towards lower latitudes (Umezawa et al., 2014).

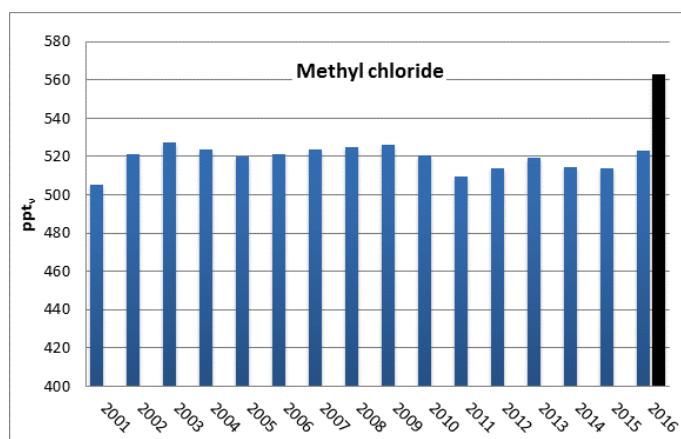


Figure 24: Development of methyl chloride annual means measured at the Zeppelin Observatory for the period 2001-2016. The global annual mean for 2016 (Hall et al., 2017) is included as a black bar. All units are in ppt.

Key findings - Methyl chloride: The atmospheric concentration of methyl chloride is relatively stable. The gas has a dominating natural origin and is not regulated through the Kyoto or Montreal protocol. The CH₃Cl concentration at Zeppelin has decreased by 0.5% since 2001, but in 2016 the annual mean value was 10 ppt higher than previous year.

2.1.7 Methyl bromide - CH₃Br at the Zeppelin Observatory

Methyl bromide (CH₃Br) is an important reservoir for atmospheric bromine reacting with ozone and reducing the ozone layer. CH₃Br has both natural and anthropogenic sources. The natural sources such as the ocean, plants, and soil, can also be a sink for this gas. The primary anthropogenic source of methyl bromide has been from its use as a fumigant, e.g. for pest control and pesticide in the control of weeds. Other anthropogenic sources of CH₃Br include the combustion of leaded gasoline, biomass burning, and emissions from certain crop species (e.g. canola, rice, mustard and cabbage). Even though methyl bromide is a natural substance, the additional contribution from anthropogenic sources contributes to the man-made depletion of the ozone layer. Total organic bromine from halons and methyl bromide peaked in the mid-1990s, but the tropospheric concentration has decreased by ~25% over the past 20 years. Also, the stratospheric abundance of bromide has started to decrease (WMO, 2014b).

The result of the daily averaged observations of methyl bromide for the period 2001-2016 is shown in Figure 25. Methyl bromide is a greenhouse gas which is twice as strong as CO₂ and has a lifetime of 0.8 years (Myhre et al, 2013b). The short lifetime explains the strong annual and seasonal variations of this compound.

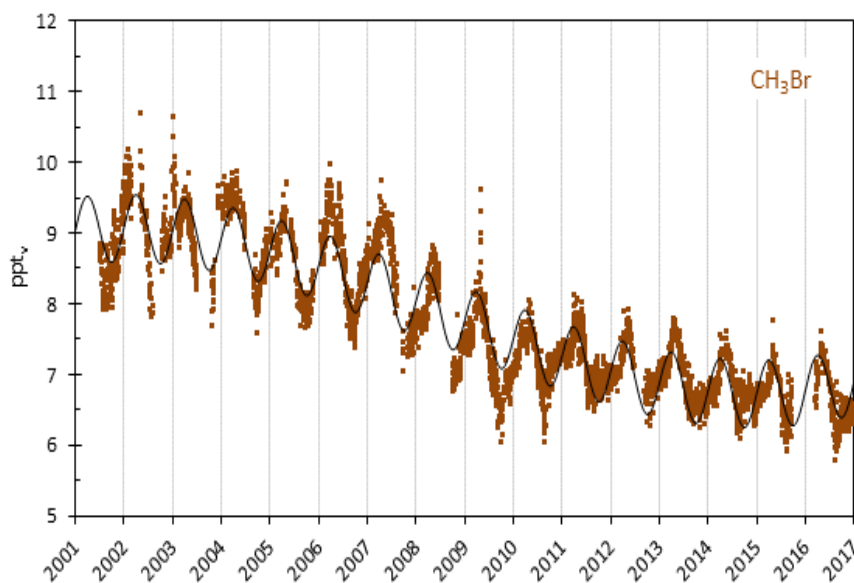


Figure 25: Observations of methyl bromide, CH_3Br , for the period 2001-2016 at the Zeppelin Observatory. Brown dots: daily averages mixing ratios from the observations, solid line empirical fitted mixing ratios.

The development of the annual means for the period 2001-2016 is presented in Figure 26. For this period there is a reduction in the mixing ratio of -0.19 ppt/yr. The overall observed change since 2001 is -2.2 ppt, i.e. -25% . Similar to CH_3Cl , the annual mean CH_3Br concentration in 2016 was higher than previous year (1% higher). CH_3Br shares many natural sources and sinks with CH_3Cl , which probably explains the high 2016 concentrations for both species. In general, the decline in methyl bromide is explained by considerable reduction in the emission; The uses of CH_3Br has decreased steadily as a result of the implementation of the Montreal Protocol, from over 50 000 tonnes/yr in the late 1990s to about 4 000 tonnes/yr in 2012 (WMO, 2014b).

The global mean mixing ratio published by BAMS in “State of the Climate” (Hall et al., 2017), presented by the black bar in Figure 26, was 6.9 ppt in 2016. This is close to the annual mean value observed at the Zeppelin observatory.

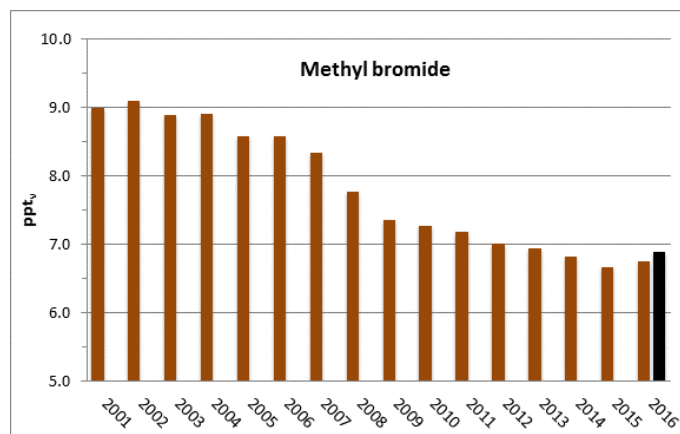


Figure 26: Development of the annual means of methyl bromide measured at the Zeppelin Observatory for the period 2001-2016. The global annual mean for 2016 (Hall et al. 2017) is included as a black bar.

Key findings - Methyl bromide: The atmospheric concentration of CH₃Br at Zeppelin has decreased by ~25% since the observations started in 2001. The decrease is a result of the implementation of the Montreal Protocol. However, CH₃Br has many natural sources with uncontrolled fluctuations from one year to another. Thus, in 2016 the annual mean CH₃Br concentration at Zeppelin was 1% higher than previous year.

2.2 Greenhouse gases with solely anthropogenic sources

All the gases presented in this chapter have solely anthropogenic sources. These man-made greenhouse gases include CFCs, HCFCs, HFCs, SF₆, NF₃, SO₂F₂ and halons, and most of these gases did not exist in the atmosphere before the 20th century. Although the gases have much lower concentration levels than most of the natural gases mentioned in the previous section, they are strong infrared absorbers, many of them with extremely long atmospheric lifetimes resulting in high global warming potentials (see Table 3). Together as a group, the gases contribute to around 12% to the overall global radiative forcing since 1750 (Myhre et al, 2013b). The annual mean concentrations for all years and all gases included in the monitoring program are given in Appendix I (Table A 1, page 112), whereas all trends, uncertainties and regression coefficients are found in Table A 2.

Some of these gases are ozone depleting, and consequently regulated through the Montreal protocol. Especially chlorine and bromine from CFCs, HCFCs and halons contribute to the depletion of the ozone layer, allowing increased UV radiation to reach the earth's surface, with potential impact not only on human health and the environment, but on agricultural crops as well. In 1987 the Montreal Protocol was signed in order to reduce the production and use of these ozone-depleting substances (ODSs) and the amount of ODSs in the troposphere reached a maximum around 1995. The amount of most ODSs in the troposphere is now declining slowly and the concentrations are expected to be back to pre-1980 levels around year 2050. In the stratosphere the peak ODS level was reached around year 2000. According to WMO (2014b) the amount of Equivalent Effective Stratospheric Chlorine (EESC) declined by about 10% in Polar region and 15% in Mid-latitude regions from 2000 to 2012.

There are two generations of substitutes for the CFCs. The first generation substitutes are included in the Montreal protocol as they also deplete the ozone layer. This comprises the components called HCFCs listed in Table 3. The second-generation substitutes, the HFCs, are included in the Kyoto protocol. In addition the agreement in Kigali in 2016, which is an extension of the Montreal Protocol, also aims to reduce the emission of HFCs. The general situation now is that the CFCs have started to decline, while their substitutes are increasing, and some of them are increasing rapidly.

2.2.1 Chlorofluorocarbons (CFCs) at Zeppelin Observatory

In total four chlorofluorocarbons (CFCs) are measured and analysed at the Zeppelin observatory: CFC-11, CFC-12, CFC-113, and CFC-115. These are the main ozone depleting gases. The anthropogenic emissions started around 1930s, and all these compounds were restricted in the first Montreal protocol from 1987. The main sources of these compounds were foam blowing, aerosol propellant, temperature control (refrigerators), solvent, and electronics industry. The highest production of the CFCs was around 1985 and maximum emissions were around 1987. The lifetimes of the compounds are long (see Table 3) and combined with strong infrared absorption properties the GWPs are high.

Figure 27 shows the daily averaged observed mixing ratios of the four CFCs. Before 2010/2011 the instrumentation for measurements of CFCs at Zeppelin was not in accordance with recommendations and criteria of AGAGE, and consequently there are relatively high uncertainties in the observations of these compounds, see also Appendix I. As a result, the trends are connected with relatively large uncertainties. From September 2010, new and improved instrumentation was installed at Zeppelin, providing more accurate observations of CFCs. The higher precisions are clearly visualised in Figure 27, but due to several severe instrumental problems in 2013/14 and 2015/16, there are some periods without CFC measurements⁹.

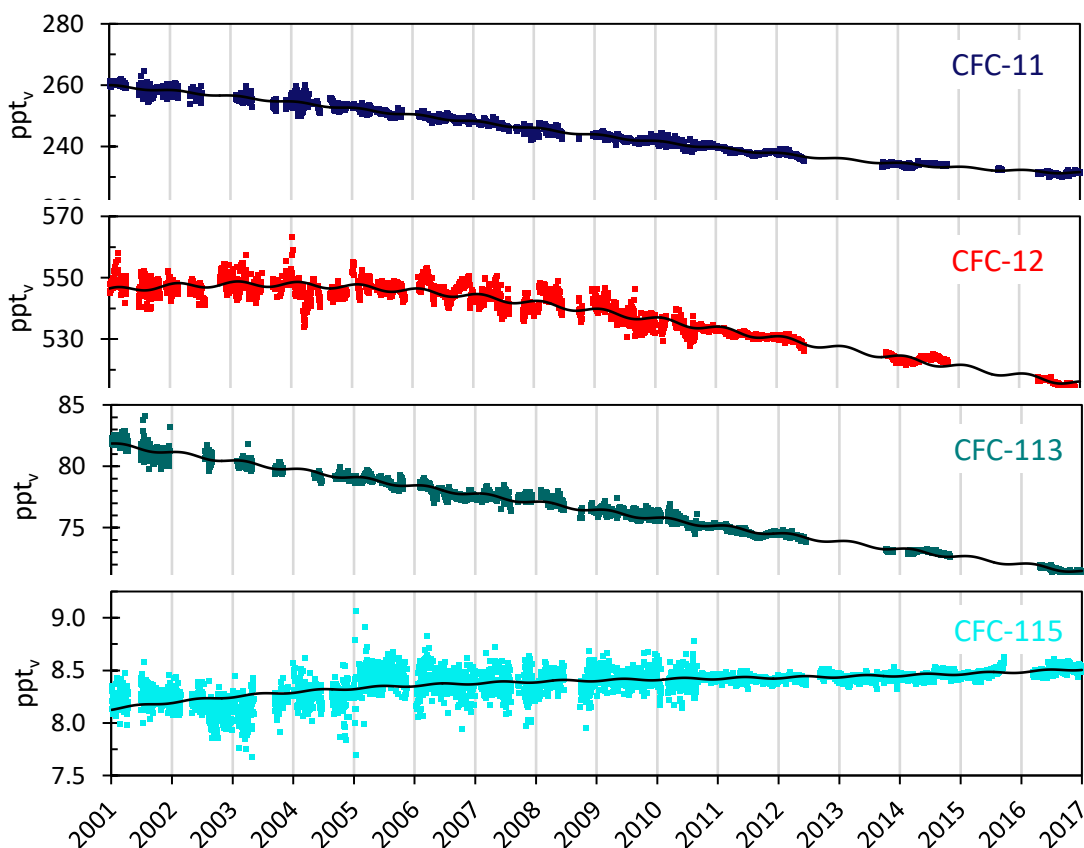


Figure 27: Daily averaged mixing ratios of the monitored CFCs at the Zeppelin observatory for the period 2001-2016: CFC-11 (dark blue), CFC-12 (red), CFC-113 (green) and CFC-115 (light blue). The solid lines are empirical fitted mixing ratios.

The trends per year for CFC-11, CFC-12 and CFC-113, given in Table 3, are all negative. The decreases are -1.9, -2.2, and -0.7 ppt/yr for CFC-11, CFC-12 and CFC-113, respectively. For the compound CFC-115 the trend is still slightly positive, +0.02 ppt/yr, and there has also been a small increase the last two years, after a stable period. It should be noted that the ambient concentration of CFC-115 is relatively low, and the trend of +0.02 ppt/yr is not dramatic. In total, the development of the CFC levels at the global background site Zeppelin is very promising and in accordance with the compliance of the Montreal protocol.

⁹ The current instrumentation is not in accordance with recommendations and criteria of AGAGE for measurements of the CFCs and there are larger uncertainties in the observations of this compound, see also Appendix I. This is also why these compounds are particularly sensitive to instrumental problems.

The 2001-2016 annual means for all the observed CFCs at Zeppelin are shown in Figure 28. Also, the global annual mean of 2016 as reported in “State of the Climate”, BAMS (Hall et al., 2017) are included as black bars for comparison. As can be seen, the observed concentrations at Zeppelin are close to the global mean for these compounds, as the lifetimes are long and there are hardly any present-day emissions.

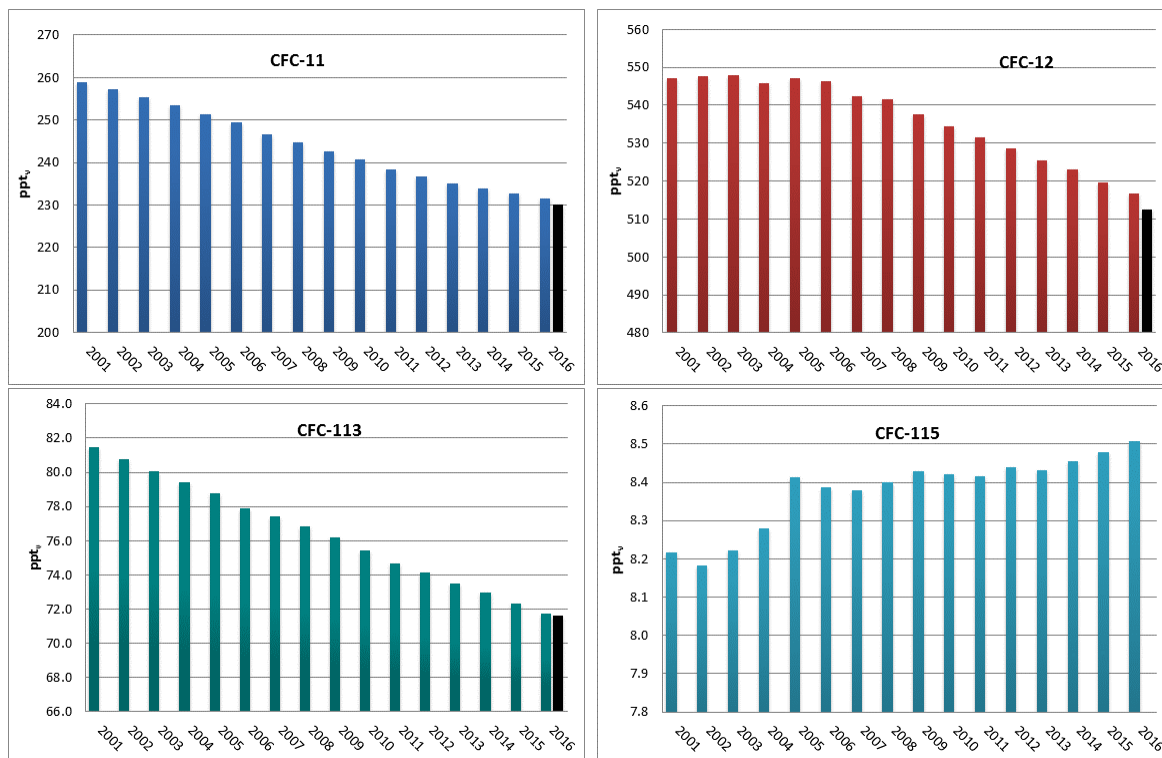


Figure 28: Development of CFC annual means at the Zeppelin Observatory for the period 2001-2016. Upper left panel: CFC-11, upper right panel: CFC-12, lower left panel: CFC-113, lower right panel: CFC-115. See Appendix I for data quality and uncertainty. The global annual means for 2016 (Hall et al., 2017) are included as black bars. All units are in ppt_v, when available.

According to WMO (2014b) the global mean mixing ratio of CFC-11 is decreasing with approximately 2.1 ppt/yr. This is in accordance with our results at Zeppelin. CFC-12 (the red diagram) has a very high GWP, 10 200, and it is also the most abundant CFC. This makes CFC-12 a very potent greenhouse gas. The global averaged atmospheric mixing ratio of CFC-12 decreased at a rate of 0.5%/yr over the period 2004-2008 (WMO, 2011). The same rate of decline was reported in WMO, 2014b. This fits well with our observations at Zeppelin. CFC-12 had a maximum around 2003-2005, but there has been a clear reduction over the last years: 30 ppt since 2005.

Key findings - CFCs: The development of the CFC levels at Zeppelin is very promising and in accordance with the compliance of the Montreal protocol. The concentrations of CFC-11, CFC-12 and CFC-113 are all declining. The mixing ratios of these gases are reduced with approx. 10.6%, 5.6% and 12.0% since 2001, respectively. However, CFC-115 was slightly higher in 2016 than in 2015, and the concentration has increase by 3.5% since 2001.

2.2.2 Hydrochlorofluorocarbons (HCFCs) at Zeppelin Observatory

Hydrochlorofluorocarbons, HCFCs, represent the first generation of replacement gases for CFCs. The lifetimes are rather long, see Table 3, but although not as stable and persistent in the atmosphere as CFCs, they can still end up in the stratosphere where they can destroy the ozone layer. Consequently, the gases are regulated through the Montreal protocol. The Norwegian monitoring programme includes three HCFC species: HCFC-22, HCFC-141b and HCFC-142b. These compounds are mainly used as refrigerants, foam blowing agents and solvents. The use of the gases is now frozen, but they are not completely phased out. All the gases have potentially a strong warming effect, depending on their concentrations and absorption properties, i.e. their GWPs (see Table 3). HCFC-142b has the highest GWP, with a warming potential 1980 times stronger than CO₂, per kg gas emitted.

The daily averaged observations of the three HCFCs are shown in Figure 29 for the period 2001-2016.

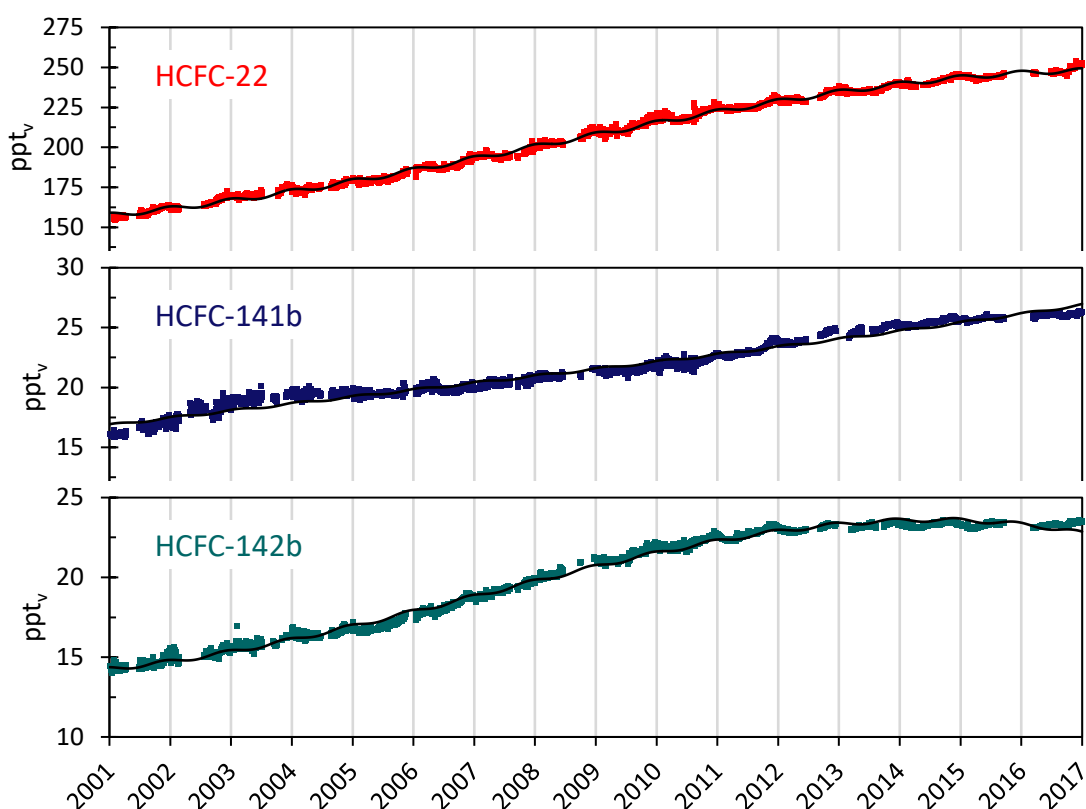


Figure 29: Daily averaged mixing ratios of the monitored HCFCs for the period 2001-2016 at the Zeppelin observatory: HCFC-22 (red), HCFC-141b (dark blue), and HCFC-142b (green). The solid lines are empirical fitted mixing ratios. All units are in ppt.

HCFC-22, HCFC-141b and HCFC-142b are all increasing over the period 2001-2016. HCFC-22 is the most abundant HCFC species and is increasing at a rate of 6.4 ppt/yr over the period 2001-2016. The concentration of the two other compounds, HCFC-141b and HCFC-142b, are a factor of ten lower than HCFC-22, and the increase in absolute annual means are also a factor of ten lower; HCFC-141b and HCFC-142b both increase by 0.6 ppt/yr over the period 2001-2016. However, the situation is very positive for HCFC-142b, which shows a slight decrease from 2015 to 2016. This is best illustrated in Figure 28, which shows the annual means for the full period. For all HCFCs there is a considerable increase from 2001 to 2010, but only HCFC-

142b has stabilized over the last years. With lifetimes in the order of 10-20 years, it is important to continue monitoring the development of the HCFCs for many years to come, as they have significant influence on the ozone layer and are also strong greenhouse gases. The global annual means in 2016 given in Hall et al. (2017) are included in Figure 28 as black bars. The observed concentrations at Zeppelin are 4-6% higher than the global means.

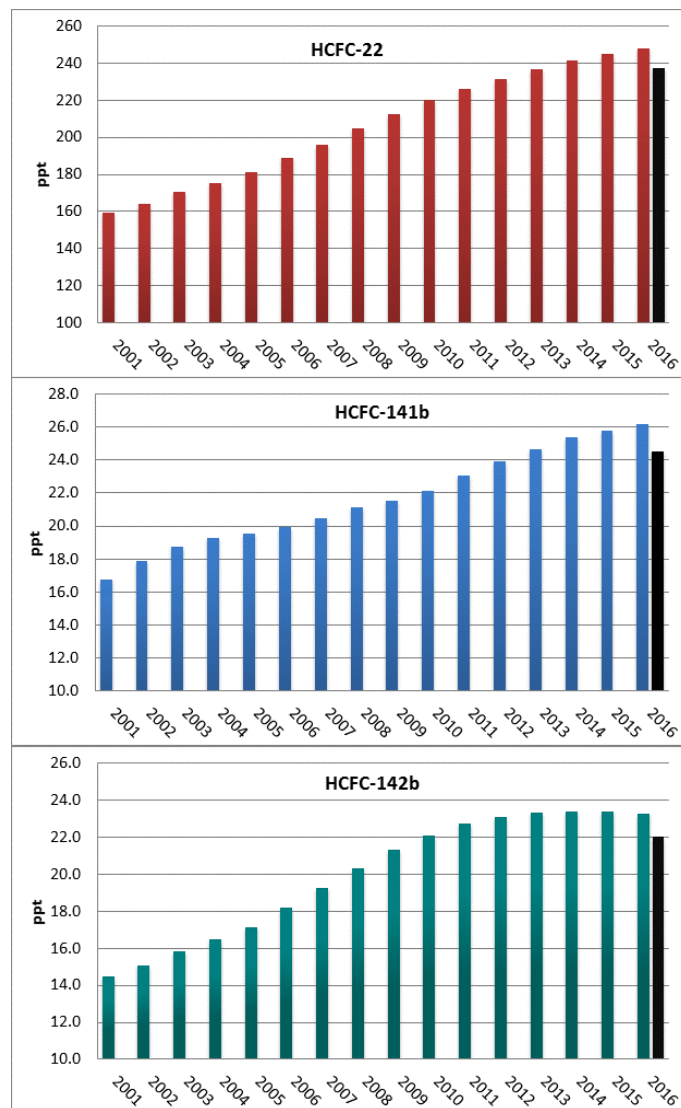


Figure 30: Development of the annual means of observed HCFCs at the Zeppelin Observatory for the period 2001-2016. HCFC-22 (red), HCFC-141b (blue), and HCFC-142b (green). The global annual means in 2016 as given in Hall et al. (2017) are included as black bars. All units are in ppt.

Key findings - HCFCs: The CFC substitutes HCFC-22, HCFC-141b and HCFC-142b have increased significantly since the measurements started at Zeppelin in 2001. HCFC-22 has a growth rate of 6.4 ppt/yr, whereas HCFC-141b has an average growth rate of 0.6 ppt/yr. For the 2001-2016 period HCFC-22, HCFC-141b and HCFC-142b increased by 56%, 56% and 61%, respectively. HCFC-22 and HCFC-141b are still increasing, but the situation is more positive for HCFC-142b, which has stabilized the last years.

2.2.3 Hydrofluorocarbons (HFCs) at Zeppelin Observatory

The substances called HFCs are the so-called second generation replacements of CFCs, which means that they are considered as better alternatives to the CFCs with respect to the ozone layer than HCFCs, as they do not contain chlorine or bromine. However, many of these compounds are strong greenhouse gases. 1 kg of HFC-23 is as much as 12 400 times more powerful greenhouse gas than CO₂ (see Table 3). The phase-down of HFCs under the Montreal Protocol has been under negotiation since 2009 and the successful agreement in Kigali, October 2016, represented an important progress (see also section 1.2). Presently, the contribution to global warming posed by HFCs are very limited. However, most of the compounds are increasing rapidly. The compounds are strong infrared absorbers with high GWP (see Table 3, page 25), hence it is crucial to reduce the future emission.

For the period 2001-2016 three compounds have been measured at the Zeppelin Observatory: HFC-125, HFC-134a, and HFC-152a. HFC-125 is mainly used as a refrigerant and fire suppression agent. HFC-134a is used as a temperature control for domestic refrigeration and automobile air conditioners, whereas HFC-152a is used as a refrigerant and propellant for aerosol sprays and in gas duster products. Since 1990, when HFC-134a was almost undetectable in the atmosphere, the concentration of this gas has risen massively, and HFC-134a is currently the HFC with highest atmospheric concentration.

In 2015 five new HFCs were included in the Norwegian monitoring programme: HFC-23, HFC-365mfc, HFC-227ea, HFC-236fa, and HFC-245fa. In 2016 three additional HFCs have been introduced to the programme: HFC-32, HFC-143a, and HFC-4310mee. All these species have been measured at Zeppelin since 2010, but they have not been analysed or reported to an international data base until 2016. The development of HFC-23 should be followed with extra care, since this gas has a relatively high concentration and an extremely high GWP. HFC-23 is used in the semiconductor industry, but it is also a useful refrigerant and fire suppressant.

Generally, the new HFCs are used for refrigeration and air conditioning, foam blowing, and fire extinguishing. Both HFC-245fa and HFC-365mfc are substitutes for HCFC-141b in foam blowing applications. HFC-236fa is also a foaming agent, in addition to a fire suppression agent and a refrigerant. HFC-227ea is mainly used to suppress fire in data equipment and telecommunication facilities, and in protection of flammable liquids and gases. HFC-227ea is also used as an aerosol propellant in pharmaceutical dose inhalers for e.g. asthma medication.

The three new HFCs introduced to the monitoring programme this year, are mainly used for refrigeration (HFC-32 and HFC-143a). In addition, HFC-143a is applied as propellant in canned air products for cleaning electronic equipment. HFC-4310mee is mainly used as a cleaning solvent in the electronics industry.

The seasonal cycle in HFC mixing ratios are closely linked to the variation in the incoming solar radiation and thus the lifetimes. HFC-152a has the shortest lifetime (1.5 year), and as seen in Figure 31 HFC-152a has the most distinct seasonal cycle. The gas is mainly destroyed in the lowest part of the atmosphere by photolysis and reactions with OH.

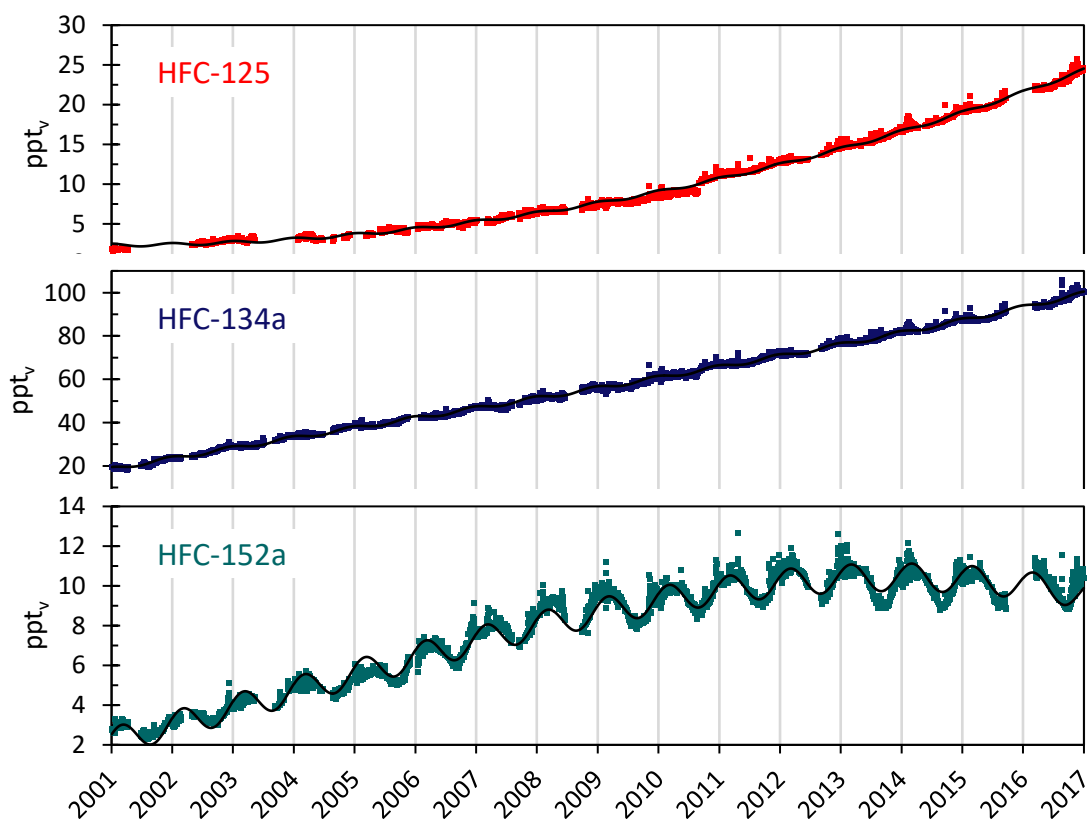


Figure 31: Daily averaged concentrations of the monitored HFCs for the period 2001-2016 at the Zeppelin observatory: HFC-125 (red), HFC-134a (dark blue), and HFC-152a (green). The solid lines are empirical fitted mixing ratios.

For the period 2001-2016 all HFCs shown in Figure 31 have increased significantly. HFC-134a has an increasing trend of 4.9 ppt/yr, which leaves this compound as the one with second highest change per year of the all the halocarbons measured at Zeppelin, next after HCFC-22. The mixing ratios of HFC-125, HFC-134a and HFC-152a have increased by as much as 935%, 362% and 269% since 2001, respectively. For HFC-125 we can even see an accelerating trend. HFC-152a, however, is the only HFC where the rapid increase has levelled off and thereafter started to decline, due to shorter life time and rapid response to emission changes. This is clearly illustrated in Figure 31 and Figure 33.

The eight new HFCs included in the programme in 2015 and 2016 are shown in Figure 32. The time series are too short for reliable trend calculations, but the concentrations of all the compounds have increased since 2010. The compounds have increased by 4-16%/yr, except from HFC-32 which has increased as much as 30%/yr.

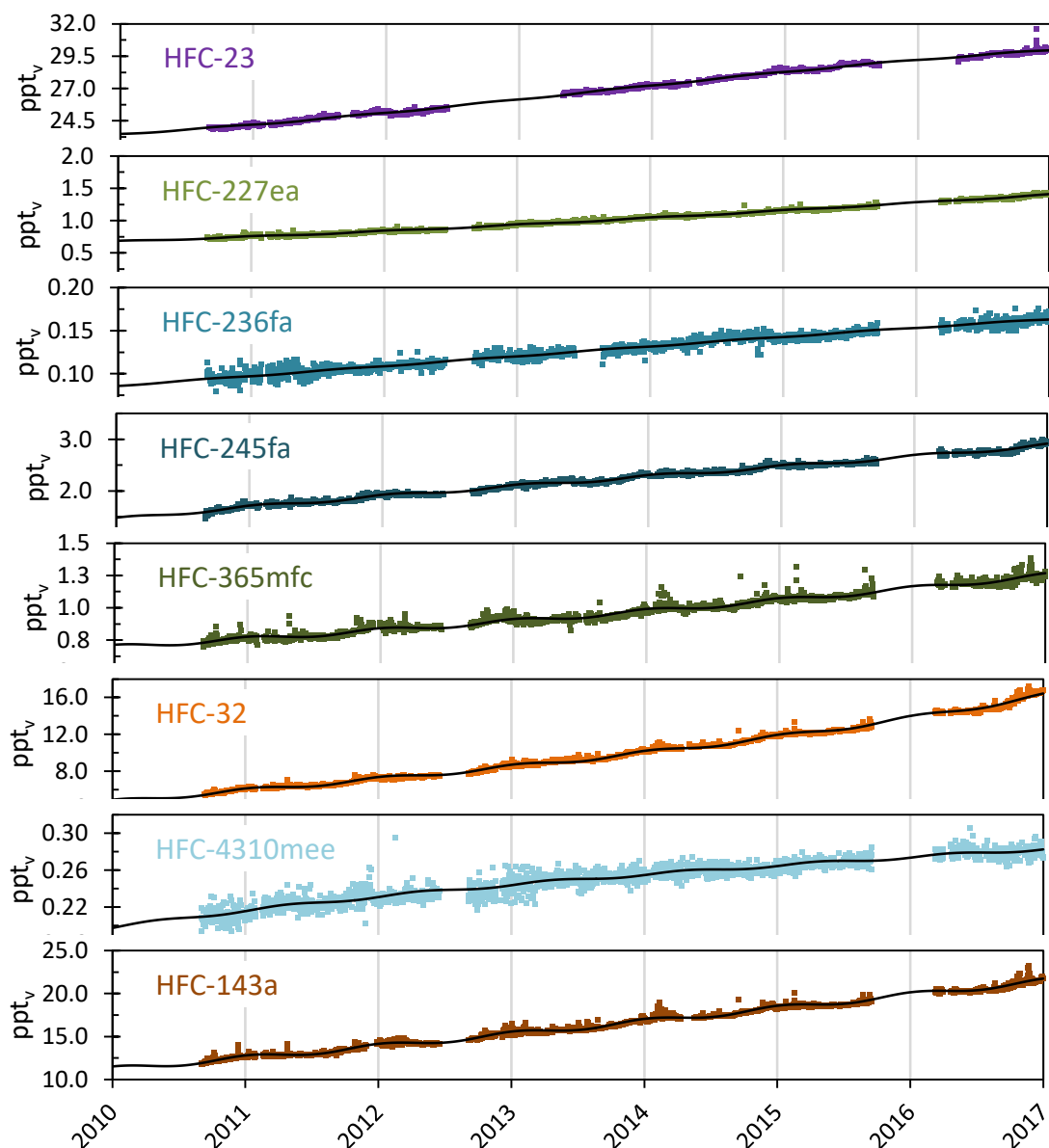


Figure 32: Daily averaged concentrations of monitored HFCs at the Zeppelin observatory for the period 2010-2016: HFC-23 (violet), HFC-227ea (light green), HFC-236fa (blue), HFC-245fa (dark blue), HFC-365mfc (dark green), HFC-32 (orange), HFC-4310mee (light blue), and HFC-143a (brown). The solid lines are empirical fitted mixing ratios.

The development of annual means of all reported HFCs are shown in Figure 33. The global annual means of 2016 as given in Hall et al. (2017) are included as black bars for comparison. As for HCFCs the concentrations at Zeppelin are slightly higher than the global means. Also, the increasing tendency for all HFCs is clear, even if the concentrations are still very low, particularly for the new HFC-365mfc, HFC-245fa, HFC-236fa, HFC-227ea, and HFC-4310mee, with 3 ppt as maximum for HFC-245fa.

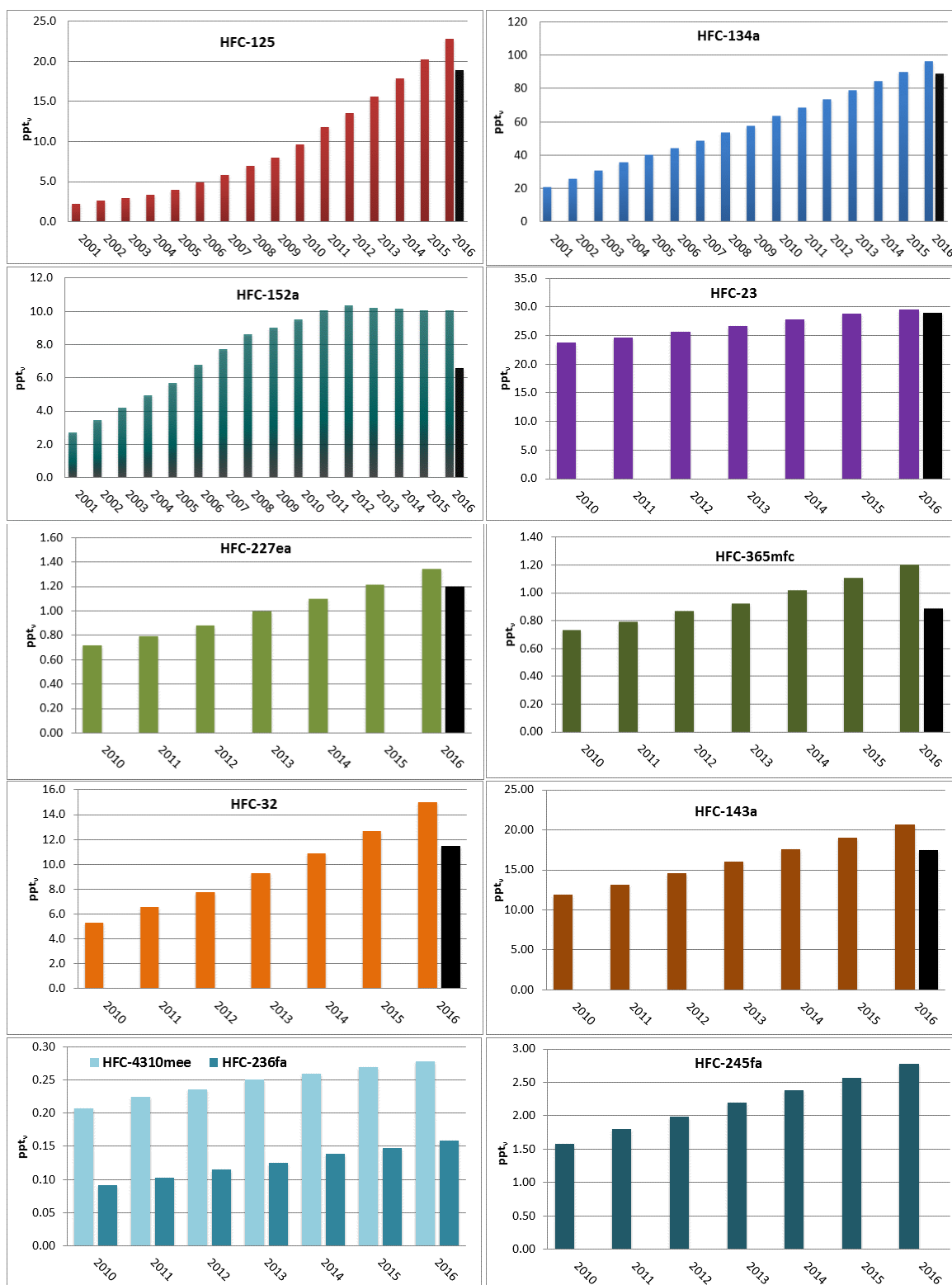


Figure 33: Development of the annual means of observed HFCs at the Zeppelin Observatory. For the period 2001-2016: HFC-125 (red), HFC-134a (blue), and HFC-152a (dark green). For the period 2010-2016: HFC-23 (violet), HFC-227ea (light green), HFC-365mfc (dark green), HFC-32 (orange), HFC-143 (brown), and light to dark blue: HFC-4310mee, HFC-236fa, and HFC-245fa. The global annual means in 2016 from Hall et al. (2017) are included as black bars, when available.

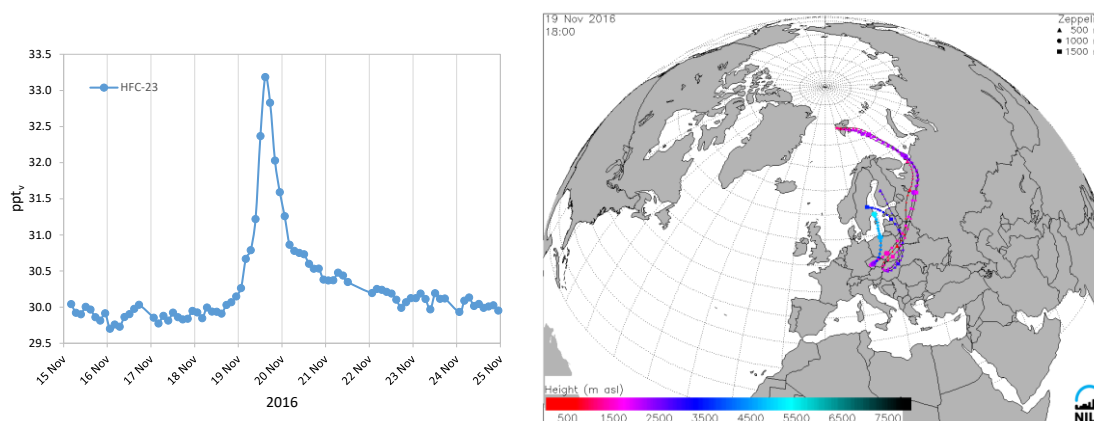


Figure 34: Left panel: HFC-23 observations at the Zeppelin observatory 15-25 November 2016, Right panel: 7-days backwards trajectories from the FLEXTRA model and the synoptical situation on November 19th

The atmospheric HFC concentrations increased gradually in 2016 and most days the daily average values were close to the empirical fitted trend lines. However, for some HFCs and HFC-23 in particular, there was an episode in November 2016 with enhanced concentrations at the Zeppelin Observatory. Figure 34 (left panel) shows HFC-23 observations 15.-25. November, measured every 3 hour. This Figure shows enhanced HFC-23 concentrations 19th and 20th November, with a maximum value of 33.2 ppt at 15:00 on November 19th. Figure 34 (right panel) shows 7-days backwards trajectories from the FLEXTRA model, illustrating the synoptical situation this day. According to the trajectory analysis the increased HFC-23 concentration arises from air masses arriving from Eastern Europe. HFC-23 is used in the semiconductor industry, as a refrigerant and fire suppressor. Important emission sources are most likely located in the abovementioned region. This resulted also in enhanced levels of many of the other gases, including the new compounds like NF_3 (see 2.2.6.1)

Key findings - HFCs: The hydrofluorocarbons (HFCs) have been introduced as replacements for the ozone depleting CFCs and HCFCs. They pose no harm to the ozone layer since they do not contain chlorine, but still they are strong greenhouse gases. The mixing ratios of HFC-125, HFC-134a, and HFC-152a have been measured at the Zeppelin observatory since 2001, and for the period 2001-2016 the concentrations have increased by 935%, 362% and 269%, respectively. Eight new HFCs were introduced to the monitoring programme in 2015 and 2016: HFC-23, HFC-365mfc, HFC-227ea, HFC-236fa, HFC-245fa, HFC-32, HFC-143a, and HFC-4310mee. The mixing ratios of these gases are analyzed back to 2010, showing an increase of 4-16%/yr for the period 2010-2016, except for HFC-32 which increased by as much as 30%/yr. HFC-152a is the only HFC which has levelled off and started to decline, - for all the other HFCs the steep growth rate continued in 2016. The contribution from the HFCs to the global warming is still relatively small, but given the rapid atmospheric increase it is crucial to follow the development of these gases. The phase-down of HFCs under the Montreal Protocol, agreed in Kigali in 2016, is important in curbing the growth in these gases

2.2.4 Halons measured at Zeppelin Observatory

Halons are greenhouse gases containing bromine, thus regulations of halons are also important to protect the ozone layer. Actually, bromine is even more effective in destroying ozone than chlorine. The halons are regulated through the Montreal protocol and the concentration of most substances are decreasing. The main source of halons were fire extinguishers.

Up to now two halons have been measured at the Zeppelin observatory: H-1301 and H-1211. In 2016 H-2402 was also included to the monitoring programme. H-2402 was used primarily in the former USSR and was the main halon fire suppressant in that region.

The ambient concentrations of the three halons are fairly low, all below 4 ppt. Figure 35 shows the daily average concentrations of the monitored halons at Zeppelin. The halon trend analyses, listed in Table 3 and visualized in Figure 35, show an increase for H-1301 during the period 2001-2016 and a relaxation for H-1211. The concentration of H-1211 is ~17% lower today than when the measurements started in 2001, whereas H-1301 has increased by ~14%. The new compound, H-2402, shows a relaxation of ~10% from 2010 to 2016. The development of the annual means for all three compounds are shown in Figure 36.

The annual means have not changed dramatically over the measured period, which is explained by low emissions and relatively long lifetimes (16 years for H-1211, 65 years for H-1301, and 20 years for H-2402). However, clear declines are evident for Halon-1211 and H-2402, which have the shortest lifetimes. According to the last Ozone Assessment report (WMO, 2014b) the total stratospheric bromine concentration decreased by $-0.6 \pm 0.1\%/yr$ between peak levels observed in 2000-2001 and 2012.

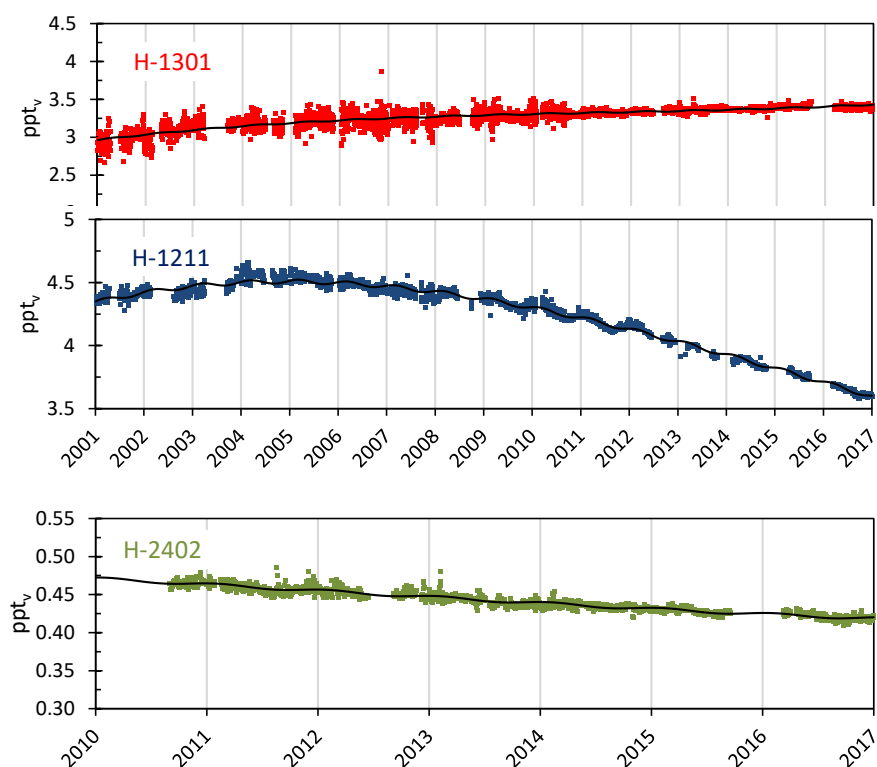


Figure 35: Daily averaged concentrations of the monitored halons at the Zeppelin Observatory. For the period 2001-2016: H-1301 (red) and H-1211 (blue). For the period 2010-2016: H-2402 (green). The solid lines are empirical fitted mixing ratios.

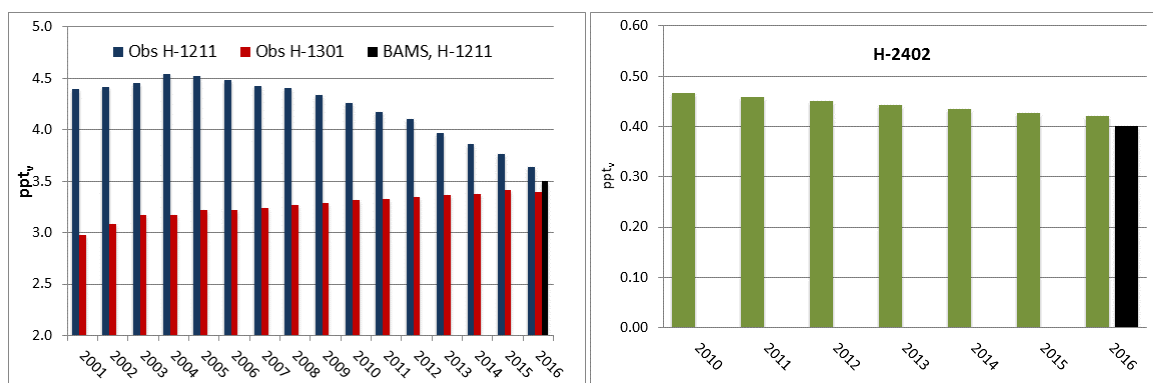


Figure 36: Development of the annual means of the observed halons at the Zeppelin Observatory. Red: H-1301, blue: H-1211, and green: H-2402. The global annual means in 2016 from Hall et al. (2017) are included as black bars. All units are in ppt, when available.

Key findings - Halons: Halons are bromine containing halocarbons that contribute both to the depletion of the ozone layer, and to global warming. Three halons are measured at Zeppelin: H-1211, H-1301, and H-2402. For H-1211 a maximum was observed in 2004, followed by a gradual decline. The concentration of H-1211 is ~17% lower today than when the measurements started in 2001. H-1301, however, has increased by ~14% during the same period, whereas H-2402 has decreased by ~10% from 2010 to 2016. According to the last Ozone Assessment (WMO, 2014b) the stratospheric bromine concentration has now started to decrease.

2.2.5 Other chlorinated hydrocarbons at Zeppelin Observatory

This section describes the following components measured at the Zeppelin Observatory: methyl chloroform (CH_3CCl_3), dichloromethane (CH_2Cl_2), chloroform (CHCl_3), trichloroethylene (TCE, CHClCCl_2), and perchloroethylene (PCE, CCl_2CCl_2). The daily average concentrations are shown in Figure 38. Additionally, a new compound was added in 2015; Carbon tetrachloride (CCl_4). The main sources of all these substances are solvents. Chloroform has also a natural sources, with offshore seawater as the largest single source.

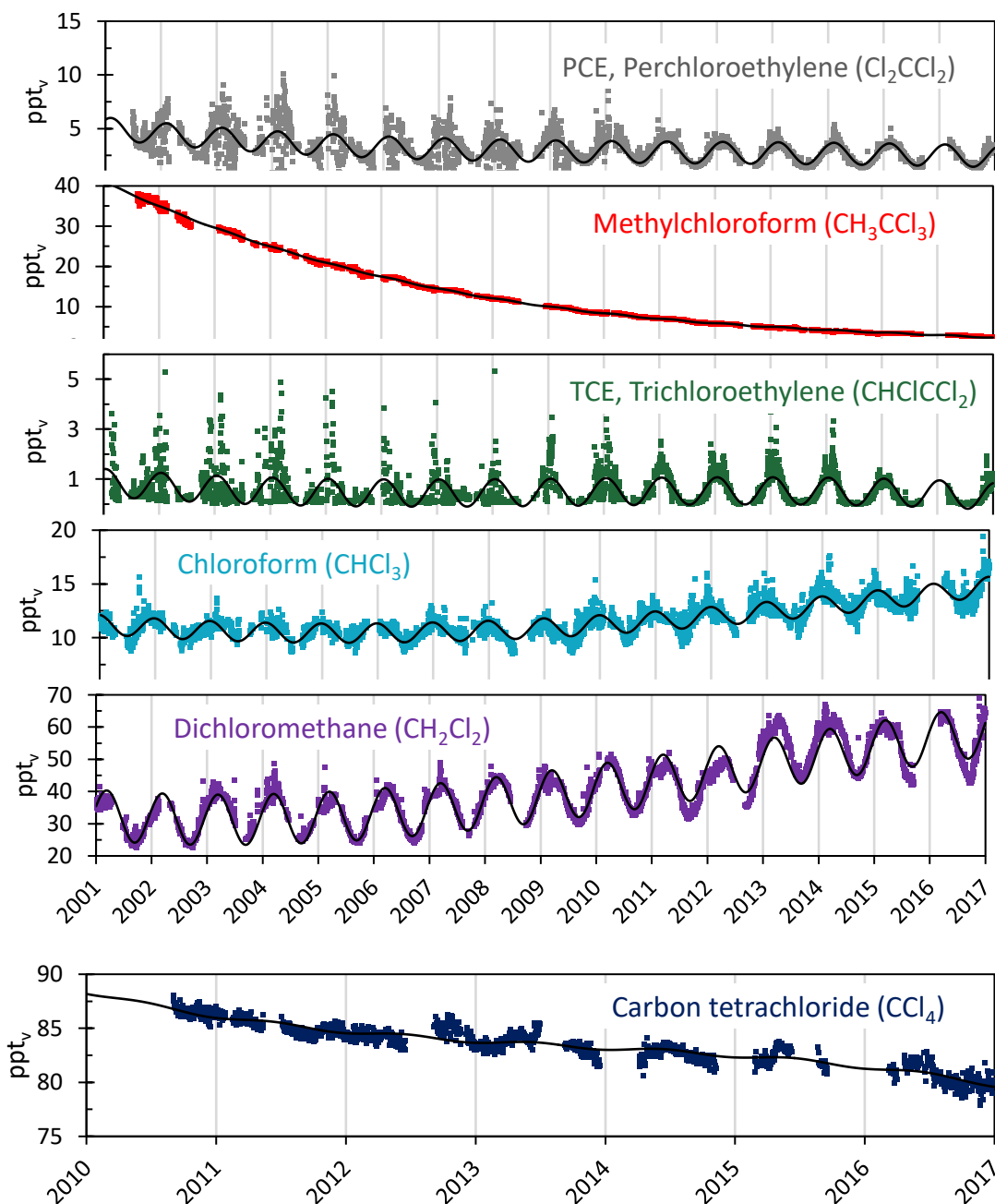


Figure 37: Daily averaged concentrations of chlorinated hydrocarbons at the Zeppelin observatory: For the period 2001-2016: perchloroethylene (grey), methylchloroform (red), trichloroethylene (green), chloroform (light blue), and dichloromethane (violet). For the period 2010-2016: carbon tetrachloride (dark blue). Solid lines are empirical fitted mixing ratios.

The global fraction of methyl chloroform (CH_3CCl_3), which is controlled under the Montreal Protocol, has been declining steadily since the peak values in the early 1990s. In 2012 the global mean mole fraction of 5.4 ppt was only 4% of its maximum value (WMO, 2011; 2014b). The measurements at Zeppelin show that the concentration has further decreased to 2.7 ppt in 2016, a reduction of 93% since the measurements started in 2001. Today methyl chloroform contributes negligible to the atmospheric chlorine burden.

It is worth noting the strong recent increase in dichloromethane (violet), and chloroform

(light blue) in Figure 37 and Figure 38. Dichloromethane has a lifetime of less than 6 months and responds rapidly to emissions changes, where about 90% has industrial origin. Its main applications are from paint strippers, degreasers and solvents; in foam production and blowing applications; and as an agricultural fumigant (WMO, 2011). The natural sources of dichloromethane, which account for ~10% of the total emission, is mainly from biomass burning and marine sources. At Zeppelin, the increase since 2001 is about 80%. The concentration is currently 56.6 ppt, a slight increase since 2015.

Chloroform (light blue) has a short lifetime of 1 year, thus the response to emission changes is also relatively rapid. The annual mean value of chloroform has increased with 28% since 2005 at Zeppelin, this is also observed at other sites (e.g. Mauna Loa at Hawaii and Barrow in Alaska). From known emissions of this compound this increase is not expected. The reason for this increase is not yet clear, and it might be explained by natural sources.

The atmospheric concentrations of trichloroethylene, TCE (green) and Perchloroethylene, PCE (grey) are low, and the annual variabilities are quite high, especially before 2011. This makes it difficult to draw conclusions about trends and development of these species. In 2016 the annual average concentrations of PCE and TCE were 2.54 ppt and 0.38 ppt, respectively.

The concentration of carbon tetrachloride (CCl_4) has been measured at Zeppelin since 2010. This compound was once a popular solvent in organic chemistry, but because of its adverse health effects it is rarely used today. Today CCl_4 is sometimes used as a solvent for infrared spectroscopy. For the period 2010-2016 the annual mean values have decreased by 1.3%/yr, i.e. from 87.2 ppt in 2010 to 80.7 ppt in 2016.

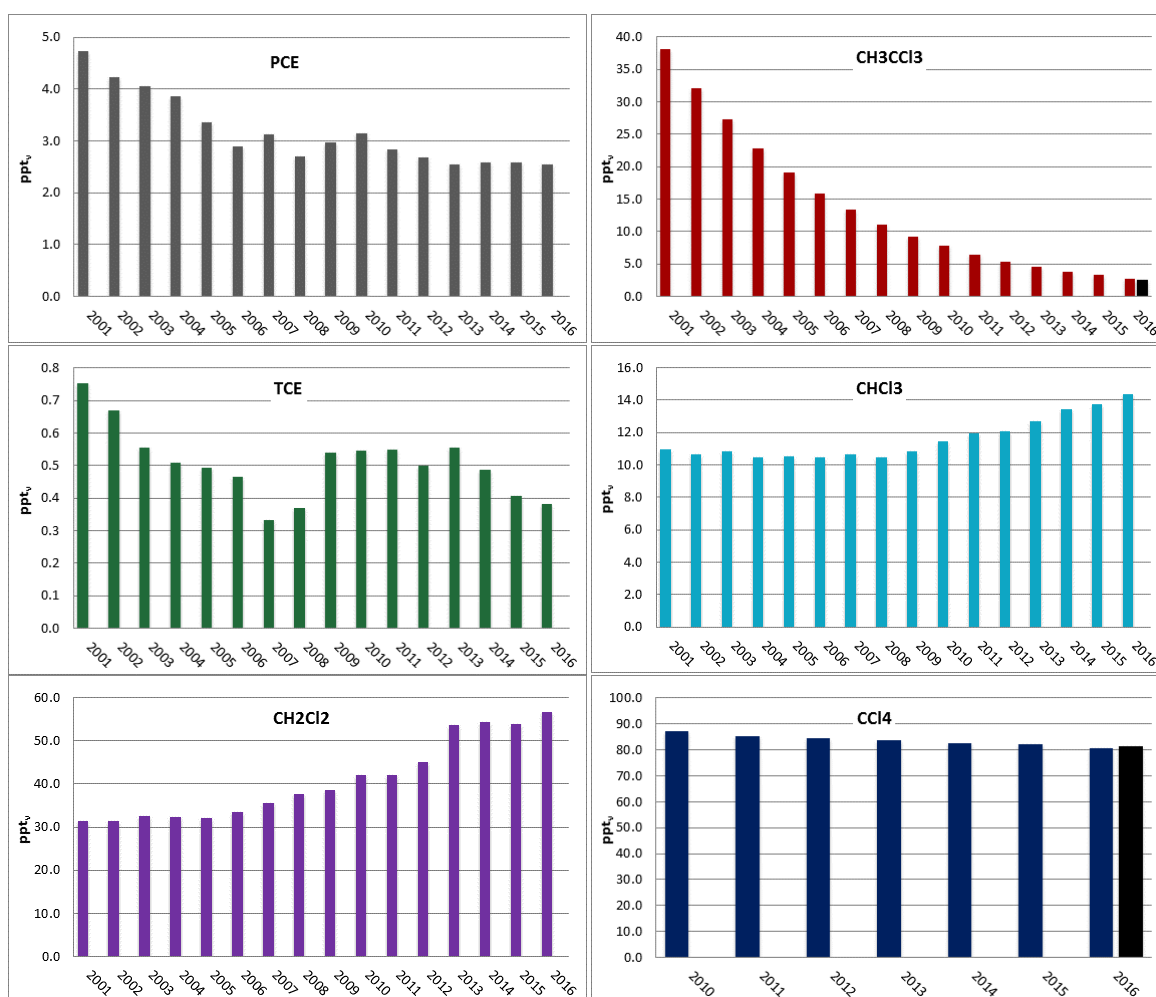


Figure 38: Annual means of the chlorinated hydrocarbons. Upper panel: perchloroethylene (grey) and trichloromethane (red). Mid panel: trichloroethylene (green) and chloroform (light blue). Lower panel: dichloromethane (violet) and carbon tetrachloride (dark blue). The global annual means for CH₃CCl₃ and CCl₄ in 2016 from Hall et al. (2017) are included as black bars. All units are in ppt, when available.

Key findings - Other Chlorinated greenhouse gases. In addition to Methyl chloride and Methyl bromide described in section 0 and 2.1.7, the following six chlorinated gases are measured at the Zeppelin Observatory: methyl chloroform (CH₃CCl₃), dichloromethane (CH₂Cl₂), chloroform (CHCl₃), trichloroethylene (TCE, CHClCCl₂), perchloroethylene (PCE, CCl₂CCl₂), and carbon tetrachloride (CCl₄). Two of these gases, **chloroform and dichloromethane, have increased by 31% and 80%, since 2001 respectively.** The other four compounds are decreasing. Methyl chloroform has decreased by 93% since 2001.

2.2.6 Perfluorinated compounds at Zeppelin Observatory

Perfluorinated compounds belong to a group of long-lived greenhouse gases, and their contribution to the Earth's radiative forcing has increased over the past several decades. The impact of these highly fluorinated compounds on climate change is a concern because of their exceptionally long atmospheric lifetimes, as well as their strong absorption in the infrared "window" region (Baasandorj et al., 2012).

Up to 2015, the Norwegian national monitoring programme only included measurements of one perfluorinated compound, SF₆. However, other perfluorinated compounds are also very powerful greenhouse gases with atmospheric lifetimes up to 50 000 years (See Table 3) and with increasing concentrations in the atmosphere. NILU has from 2010 extended the monitoring of perfluorinated compounds at Zeppelin as we have new and improved instrumentation. Several of these compounds, so-called perfluorocarbons (PFCs), were included in the current monitoring programme from 2015, with analysis back in time to September 2010. Two additional compounds have been included in the 2016 monitoring programme: Nitrogen trifluoride (NF₃) and Sulphuryl fluoride (SO₂F₂). For the latter compound data can be analysed back to 2010. The instrument at Zeppelin was re-build and optimized in 2015 and 2016, which made it possible to measure NF₃. Thus, NF₃ data are only available from 2016.

2.2.6.1 Sulphurhexafluoride (SF₆), Sulphuryl fluoride (SO₂F₂), Nitrogen trifluoride (NF₃)

Sulphurhexafluoride, SF₆ is an extremely strong greenhouse gas emitted to the atmosphere mainly from the production of magnesium and electronics industry. Measurements of this component has been a part of the programme since 2001. The atmospheric lifetime of this compound is 3 200 years, and the global warming potential is 23 500, which means that the emission of 1 kg of SF₆ has a warming potential which is 23 500 times stronger than 1 kg emitted CO₂ (Myhre et al, 2013b).

Sulphuryl fluoride (SO₂F₂) has a lifetime of 36 years and a GWP of 4 090. SO₂F₂ is normally used as a pesticide fumigant for dried fruits, nuts, and other agricultural commodities that must be kept pest-free during storage. It is one of the most common replacements for methyl bromide, an ozone-depleting substance whose use is being phased out.

Nitrogen trifluoride, NF₃, has a lifetime of 500 years and a GWP as high as 16 100, meaning that it also is an extremely strong greenhouse gas. NF₃ is used in the manufacturing of new generation solar panels, flat-screen televisions, touch-sensitive screens, and electronic processors. The use of NF₃ has widely increased in the past because of the rising demand in flat-screen televisions and microelectronics.

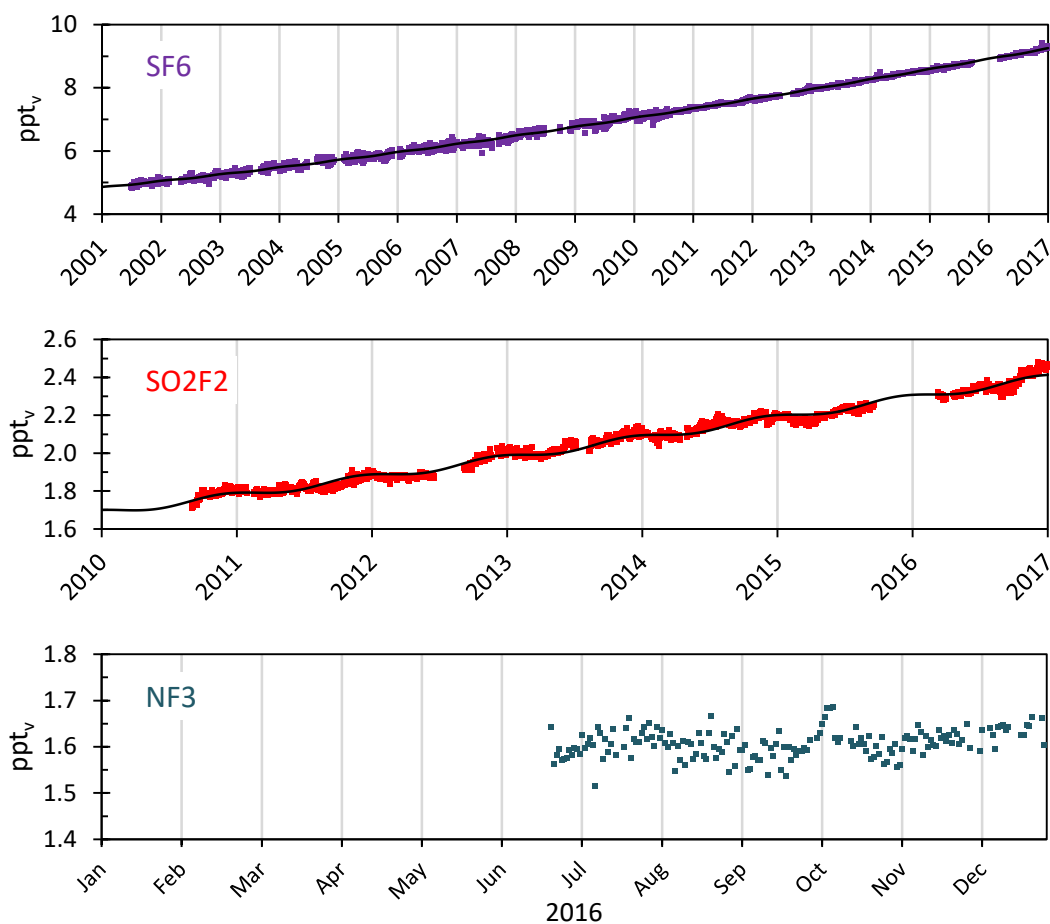


Figure 39: Daily averaged concentrations at the Zeppelin Observatory. Upper panel: SF_6 for the period 2001-2016. Middle panel: SO_2F_2 for the period 2010-2016. Lower panel: NF_3 from Jun-Dec 2016. Solid lines are statistical fitted mixing ratios.

The daily averaged concentrations of SF_6 , SO_2F_2 and NF_3 are presented in Figure 39. SF_6 is increasing with a rate of 0.28 ppt/yr and has increased as much as 83% since the start of our measurements in 2001. The instrumentation before 2010 was not optimal for measurements of SF_6 , thus there are higher uncertainties for this compound's mixing ratios than for most of the other compounds reported from 2001 to 2010 (see Appendix I).

The concentration of SO_2F_2 has also increased significantly the last years (see Figure 39). The increase for the period 2010-2016 is 0.6 ppt, which represents an increase of 35%. No trend is derived for NF_3 , as the measurements started in 2016. Daily average observations of NF_3 are visualized in Figure 39 (lower panel). The annual average NF_3 concentration in 2016 was 1.61 ppt.

Figure 40 shows annual average concentrations of SF_6 (left panel) and SO_2F_2 (right panel) measured at Zeppelin for the periods 2001-2016 and 2010-2016, respectively. The global annual means of SF_6 in 2016 (Hall et al., 2017) is included as a black bar for comparison. Again, the concentrations at Zeppelin are slightly higher than the global means.

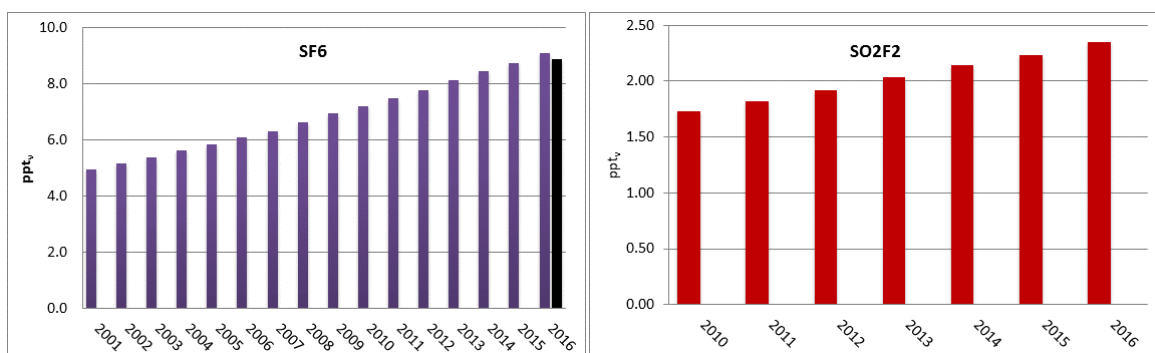


Figure 40: Annual means of SF₆ for the period 2001-2016 (left) and SO₂F₂ for the period 2010-2016(right) at the Zeppelin observatory. The global annual mean for SF₆ in 2016 (Hall et al., 2017) is included as a black bar.

2.2.6.2 Perfluorocarbons or PFC's: PFC-14, PFC-116, PFC-218, PFC-318

Perfluorocarbons or PFCs are compounds that contain only carbon and fluorine. Four of these compounds are currently measured and reported at Zeppelin: PFC-14, PFC-116, PFC-218, and PFC-318. Tetrafluoromethane (CF₄), PFC-14, is the most persistent PFC greenhouse gas with an atmospheric lifetime of 50 000 years and a greenhouse warming potential of 6 630. It is used as a low temperature refrigerant, in electronics microfabrication, and in neutron detectors. Another potent greenhouse gas is hexafluoroethane, PFC-116, which has an atmospheric lifetime of 10 000 years and a GWP of 11 100. The gas is used as an etchant in e.g. semiconductor manufacturing, and aluminium and the semiconductor manufacturing industries are the major emitters of PFC-116. Fraser et al (2013) showed that Hydro's aluminum plant in Australia release of PFC-14 was 10 times greater than PFC-116. Octafluoropropane, PFC-218, which has an atmospheric lifetime of 2 600 years and a GWP of 8 900, is also used in the electronics industry as a plasma etching material. In medicine, PFC-218 microbubbles reflect sound waves well and is used to improve the ultrasound signal backscatter. Octafluorocyclobutane, PFC-318, with an atmospheric life time of 3 200 years and a GWP of 9 540, is the third most abundant PFC in the atmosphere (Oram et al, 2012). Although a number of potential sources of PFC-318 have been reported, including the electronics and semi-conductor industries, there remains a large discrepancy in the atmospheric budget.

The daily averaged concentrations of the PFCs measured at Zeppelin are shown in Figure 41. For the period 2010-2016 PFC-116, PFC-218 and PFC-318 increased by 2.1%/yr, 2.6%/yr and 4.3%/yr, respectively. For PFC-14 no data exist until October 2014, but the measurements in 2015 and 2016 reveal that the concentration of PFC-14 increased by 1.0% from 2015 to 2016.

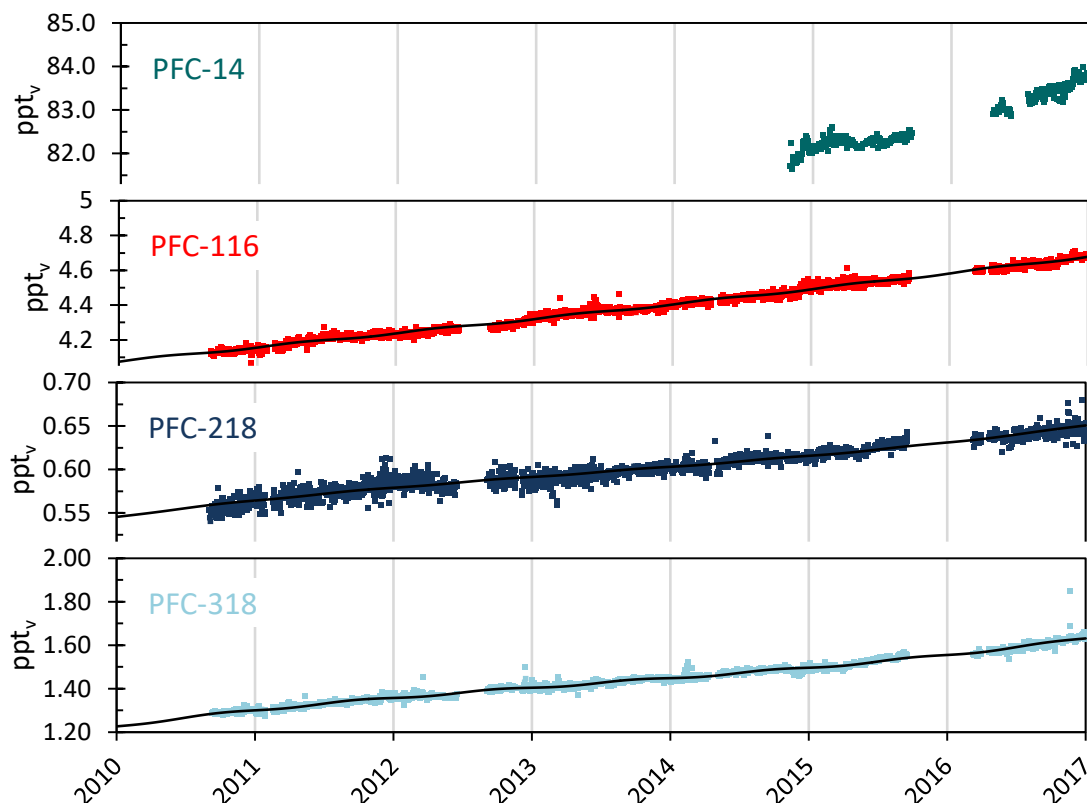


Figure 41: Daily averaged concentrations of perfluorocarbons at the Zeppelin observatory for the period 2010-2016: PFC-14 (green), PFC-116 (red), PFC-218 (dark blue), and PFC-316 (light blue). PFC-14 is only ranging back to autumn 2014. The solid lines are statistical fitted mixing ratios.

The development of the annual means of the PFCs are shown in Figure 42. For PFC-116 the global annual mean in 2016 (Hall et al., 2017) is shown as a black bar for comparison. The concentrations of most PFCs are relatively low. However, PFC-14 is an exception. With an annual mean concentration of 83.2 ppt in 2016, a lifetime of 50 000 years and GWP of 6 630, this is an important greenhouse gas that should be followed carefully.

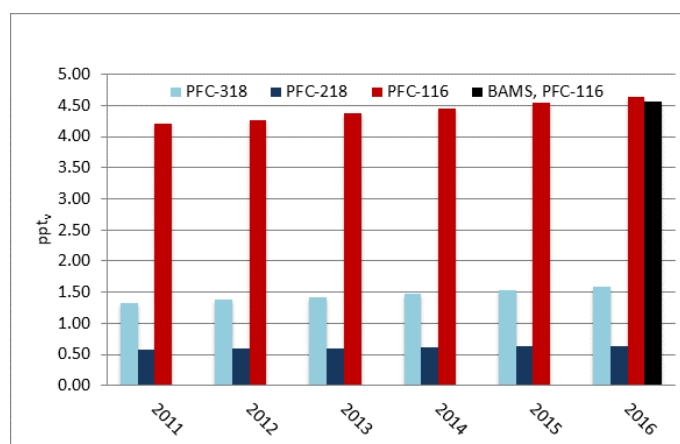


Figure 42: Annual mean concentrations of perfluorocarbons for the period 2010-2016 at the Zeppelin observatory: PFC-116 (red), PFC-218 (dark blue), and PFC-318 (light blue). The global annual mean for PFC-116 in 2016 (Hall et al., 2017) is included as a black bar.

Key findings - Perfluorinated compounds. This group of compounds include SF₆, SO₂F₂, NF₃, PFC-14, PFC-116, PFC-218, and PFC-318. Generally, these compounds are extremely potent greenhouse gases, but their concentrations are still low. An exception is PFC-14, which had a mixing ratio of 83.2 ppt in 2016, an increase of 0.9 ppt since 2015. SF₆ should also be followed closely, as this compound has an atmospheric life time of 3 200 years and an extremely high GWP of 23 500. This compound has increased by 83% since 2001.

2.3 Summary of measurements of climate gases

Increasing concentrations of greenhouse gases in Earth's atmosphere represent a long-term commitment by society to living in a changing climate and, ultimately, a warmer world (IPCC, 2013). The Norwegian greenhouse gas monitoring programme is set up to meet national and international needs for greenhouse gas measurement data, both for the scientific community, national environmental authorities and global policy making. The program includes measurements and trend calculations of 46 climate gases. The key findings from the monitoring program shows that concentration in the atmosphere of the main greenhouse gases with high anthropogenic emissions has been increasing over the period of investigation, since 2001, except for CFCs and a few halogenated gases. These gases have strong ozone depleting effect and are regulated through the successful Montreal protocol. The positive effect of this regulation on the recovery of the ozone layer is well documented. It is also a benefit for the climate.

More specific the programme shows for the main greenhouse gases CO₂, CH₄, and N₂O:

- **CO₂** concentrations have increased all years subsequently, in accordance with accumulation of gas in the atmosphere and the global development and increase in anthropogenic emissions. The new record levels in 2016 are 404.3 ppm at Zeppelin and 409.8 ppm at Birkenes. The increase from 2015 to 2016 is 3.1 ppm and 4.7 ppm, respectively, compared to global mean which was 3.3 ppm increase.
- **CH₄**: In 2016 the mixing ratios of methane increased to a new record level both at Zeppelin, Birkenes and globally. At Zeppelin the annual mean value reached 1932 ppb with an increase of as much as 12 ppb since 2015. The changes at Zeppelin the last 10 years are large compared to the evolution of the methane levels in the period 1998-2005, when the change was close to zero both at Zeppelin and globally, after a strong increase during the mid 20th Century.
- **N₂O**: The global mean level of N₂O has increased from around 270 ppb prior to industrialization and up to an average global mean of 328.9 ppb in 2016. This is slightly lower than at Zeppelin, where the annual mean is 329.0 ppb. The difference is not significant, hence the global mean concentration and the concentration at Zeppelin is the same.

The man-made greenhouse gases CFCs, HCFCs, HFCs, SF₆, NF₃, SO₂F₂, and halons did hardly exist in the atmosphere before the 20th century. The gases have relatively low concentrations, but most of them have extremely long atmospheric lifetimes and high global warming potentials. In total, the gases contribute to around 12% to the overall global radiative forcing. Some of these gases are ozone depleting, especially CFCs, HCFCs and halons, and consequently regulated through the Montreal protocol.

- The development of the **CFC** levels at Zeppelin is very promising and in accordance with the compliance of the Montreal protocol. The concentrations of CFC-11, CFC-12 and CFC-113 have declined significantly since the measurements started at Zeppelin in 2001. The positive effect of this regulation on the recovery of the ozone layer is well documented. It is also a benefit for the climate.
- The CFC substitutes **HCFC-22, HCFC-141b and HCFC-142b** have increased significantly the last decades. From 2001 to 2016 the concentrations of HCFC-22, HCFC-141b and HCFC-142b increased by 56%, 56% and 61%, respectively. The HCFC-22 and HCFC-141b concentrations are still increasing.
- The hydrofluorocarbons (**HFCs**) are newer replacements for CFCs and HCFCs. They are not ozone depleting, but instead they are strong greenhouse gases. Currently 11 HFCs are measured and reported at Zeppelin. All compounds have increased significantly since the measurements started, and the steep growth rate continued in 2016, except for HFC-152a. HFC-32 has the strongest increase with a trend of 30%/yr. The phase-down of HFCs under the Montreal Protocol, agreed in Kigali in 2016, is important for controlling future HFC emissions.
- **Halons** are bromine containing halocarbons and contribute both to the depletion of the ozone layer and to global warming. Three halons are measured at Zeppelin: H-1211, H-1301, and H-2402. H-1301 has increased by ~14% from 2001 to 2016, whereas H-1211 has declined by ~17% during the same period. There is also a decreasing trend for H-2402.
- Six **chlorinated gases** with solely anthropogenic origin are measured at the Zeppelin Observatory: methyl chloroform (CH₃CCl₃), dichloromethane (CH₂Cl₂), chloroform (CHCl₃), trichloroethylene (CHClCCl₂), perchloroethylene (CCl₂CCl₂), and carbon tetrachloride (CCl₄). Chloroform and dichloromethane have increased by 31% and 80% since 2001, respectively. The other four compounds are decreasing.
- The group of **fluorinated** compounds includes SF₆, SO₂F₂, NF₃, PFC-14, PFC-116, PFC-218, and PFC-318. Generally, these compounds are extremely potent greenhouse gases, but their concentrations are still low. An exception is PFC-14, which had a mixing ratio of 83.2 ppt in 2016, an increase of 0.9 ppt since 2015. SF₆ should also be followed closely, as this compound has an atmospheric lifetime of 3 200 years and an extremely high GWP of 23 500. This compound has increased by 83% since 2001.

Volatile Organic Compounds (VOCs) are a large group of carbon-based compounds that have a high vapor pressure and easily evaporate at room temperature. VOCs oxidation contributes to the production of tropospheric ozone and influences photochemical processing, both impacting climate and air quality. Their chemistry is essential for cleaning the atmosphere of a range of pollutants and greenhouse gases by initiating the oxidation of reduced compounds. In addition to volatile organic compounds (VOCs) carbon monoxide (CO) is measured at the Zeppelin observatory.

- **VOCs:** Six VOCs are measured at Zeppelin: ethane, propane, butane, pentane, benzene and toluene. Ethane, often co-emitted with fossil fuel methane, is increasing, whereas the concentrations of toluene and benzene have been stable since 2014.
- **CO:** In general the CO concentrations measured at Zeppelin show a decrease during the period 2003 to 2009, and stable levels the last years with a small peak in 2010. CO is an excellent tracer for transport of smoke from fires (biomass burning, agricultural- or forest fires). 2016 was not particularly influenced by such fire episodes.

3. Aerosols and climate

Atmospheric aerosol influences climate by scattering incoming solar radiation back into space, or absorb the radiation. This so called direct aerosol climate forcing results mostly in cooling, but can be moderated if the aerosol itself absorbs solar radiation, e.g. if it consists partly of light absorbing carbon or light absorbing minerals. In this case, the aerosol warms the surrounding atmosphere. Atmospheric aerosol influences climate as outlined in section 1.4. Atmospheric aerosol particles also affect the reflectivity and lifetime of clouds, which is termed the indirect aerosol climate effect. The effect can be cooling as well as warming for climate, but in most cases, the cloud reflectivity and lifetime are increased, leading again to a cooling effect (see Figure 3). Figure 43 gives an overview of the main natural and anthropogenic sources of atmospheric aerosols, also described in detail the annual report of Aas et al. 2017 on long range transport of air pollution.

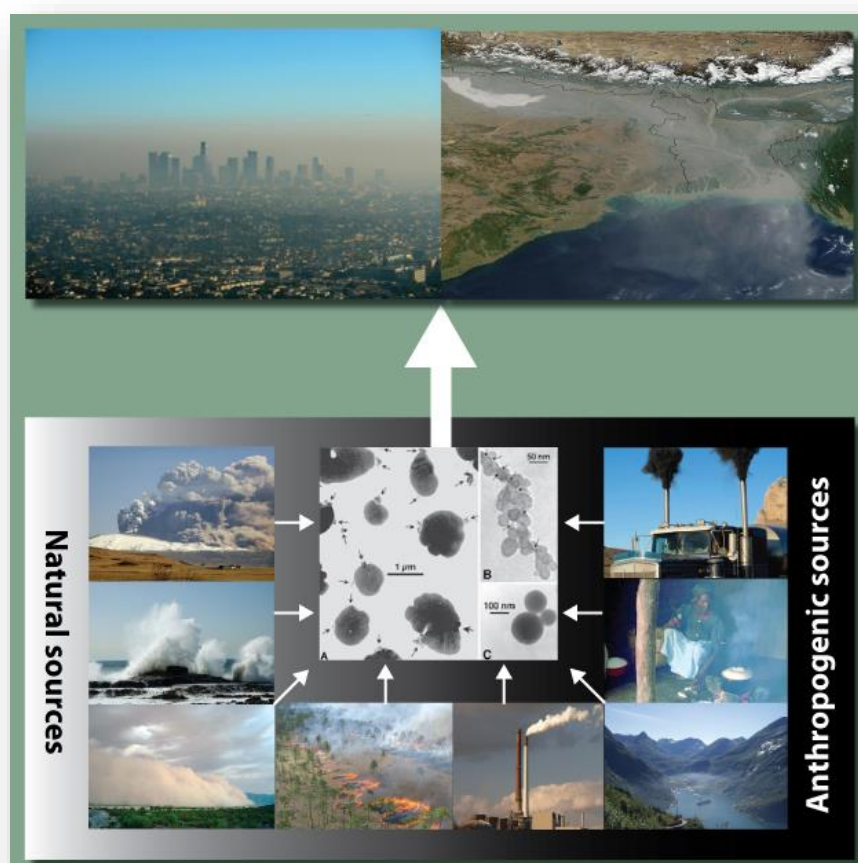


Figure 43: Illustration of the main natural and anthropogenic sources of atmospheric aerosols taken from Myhre et al (2013b). Top: local and large scale air pollution. Sources include (bottom, counter clockwise) volcanic eruptions (producing volcanic ash and sulphate), sea spray (sea salt and sulphate aerosols), desert storms (mineral dust), savannah biomass burning (BC and OC), coal power plants (fossil fuel BC and OC, sulphate, nitrate), ships (BC, OC, sulphates, nitrate), cooking* (domestic BC and OC), road transport (sulphate, BC, VOCs yielding OC). Additionally, Biogenic VOC to SOA and primary biological (e.g. pollen) from vegetation is crucial. Center: Electron microscope images of (A) sulphates, (B) soot, (C) fly ash, a product of coal combustion (Posfai et al., 1999).

Uncertainties in assessing aerosol climate forcing hamper the attribution of changes in the climate system. IPCC AR5 (IPCC, 2013) has high confidence in stating that total atmospheric aerosol negative radiative forcing in the past, has offset a significant fraction of greenhouse gas radiative warming, although the magnitude is connected with uncertainty. Due to the decline of aerosol concentrations as reported in Tørseth et al (2012), Collaud Coen et al., (2013), and Asmi et al., (2013), and summarized in Hartmann et al. 2013) the total anthropogenic radiative forcing (from both greenhouse gases and aerosols) will be even larger in the future, due to less negative forcing from cooling aerosols (sulphates etc.)

This monitoring programme includes measurements of aerosol properties relevant for quantifying the direct and indirect aerosol climate effect from 3 observatories NILU operates 3 observatories measuring aerosol properties relevant for quantifying the direct and indirect aerosol climate effects: 1) Zeppelin Observatory (in collaboration with the Norwegian Polar Institute and Stockholm University); 2) Birkenes Atmospheric Observatory, Aust-Agder, Southern Norway; 3) Trollhaugen Atmospheric Observatory, Antarctica (observatory operated by NILU, main station operated by Norwegian Polar Institute). Recent developments at these stations include:

1. **Zeppelin Observatory:** Within the Swedish - Norwegian co-operation operating the atmospheric observatory on Zeppelin mountain, Stockholm University maintains a set of instruments measuring the fine-range ($D_p < 1 \mu\text{m}$) particle number size distribution, as well as the aerosol particle scattering and absorption coefficients. Through funding from the Norwegian Ministry of environment for improving the monitoring at the Zeppelin observatory, a number of additional measurements have been installed. I.e. NILU is now operating a latest generation aethalometer at Zeppelin since June 2015. The Magee AE33 instrument is a filter absorption photometer providing the spectral aerosol particle absorption coefficient at 7 wavelengths from the UV to the infra-red. The instrument is designed to be less prone to systematic uncertainties than the previous instrument generation, and complements existing observations of that type at Zeppelin. The new instrument is due to replace a previous generation instrument operated at Zeppelin by the Greek Demokritos Research Institute (Athens). Both instruments are operated in collaboration between Greece and Norway. Moreover, NILU installed a Mobility Particle Size Spectrometer (MPSS) at Zeppelin that now measures the fine-range particle number size distribution in near-real-time, with data publicly available in NILU's EBAS database within 1 hour of measurement. During autumn 2016, this MPSS was extended to also measure the particle size distribution of the fine-range non-volatile aerosol as a proxy of the absorbing aerosol fraction.
2. **Birkenes Observatory:** In 2015, operation of the extended aerosol instrument set at Birkenes complied with the quality standards of EMEP, WMO GAW and the European infrastructure ACTRIS. A further improvement of the Birkenes aerosol observation programme is scheduled for late 2017. The station will be equipped with a new generation filter absorption photometer measuring the particle absorption coefficient with an extended spectral range (from ultraviolet to infrared) as compared to before (from blue to red). The intention behind this upgrade is to better distinguish sources of absorbing aerosol between fossil and biomass combustion, which are supposed to have different spectral absorption signatures in the extended wavelength range.

3. **Trollhaugen Observatory:** Activities at Trollhaugen Troll Atmospheric Observatory continued to follow up on a 2014 publication (Fiebig et al., 2014). The article investigates the annual cycle of the baseline aerosol at Troll as observed in the particle number size distribution and aerosol scattering coefficient data collected at Troll. It is shown that the baseline aerosol annual cycles in both parameters correspond. A comparison with data collected at the Antarctic stations South pole and Dome C, yields that the baseline air annual cycle observed at Troll is common to the whole Central Antarctic plateau. Following the Troll baseline air masses backwards with the Lagrangian transport model FLEXPART, the article demonstrates that these air masses descend over Antarctica after being transported in the free troposphere and lower stratosphere from mid-latitudes (there uplifted in fronts) or from the inter tropical convergence zone (uplifted by convection). The article shows further that the aerosol particles contained in Antarctic baseline air are formed in situ by photochemical oxidation of precursor substances. A project (AtmosCAire) following up on the discussed previous findings was applied for and approved by the Norwegian Antarctic Research Expeditions (NARE) programme. Among others, the project investigates the Antarctic background aerosol further by collecting an ultra-long exposure filter sample for chemical analysis despite the low concentrations, and use the cluster analysis method developed with Birkenes to identify the source regions and aerosol types found at Troll. This work is intended to further improve our knowledge about the aerosol and aerosol processes in pristine regions of the globe, which are often used as proxy for pre-industrial aerosol. Uncertainty about the climate effect of pre-industrial aerosol is still one of the main sources of uncertainty in climate predictions (Carslaw et al., 2013).

Table 4: Aerosol observations at Zeppelin, Birkenes and Troll Observatory following the ACTRIS recommendations. Parameters in green are funded by the Norwegian Environment Agency and included in this report.

	Zeppelin/Ny-Ålesund	Birkenes	Trollhaugen
Particle Number Size Distribution (fundamental to all aerosol processes)	fine mode ($0.01 \mu\text{m} < D_p < 0.8 \mu\text{m}$), NILU and in collaboration with Stockholm University	fine and coarse mode ($0.01 \mu\text{m} < D_p < 10 \mu\text{m}$)	fine mode ($0.03 \mu\text{m} < D_p < 0.8 \mu\text{m}$)
Aerosol Scattering Coefficient (addressing direct climate effect)	spectral at 450, 550, 700 nm, in collaboration with Stockholm University	spectral at 450, 550, 700 nm	spectral at 450, 550, 700 nm
Aerosol Absorption Coefficient (addressing direct climate effect)	single wavelength at 525 nm, (Stockholm University); single wavelength at 670 nm (Stockholm University); 7-wavelength (Demokritos Athens); 7-wavelength (NILU)	single wavelength (525 nm) and spectral at 3 wavelengths	single wavelength at 525 nm and spectral at 3 wavelengths.
Aerosol Optical Depth (addressing direct climate effect)	spectral at 368, 412, 500, 862 nm in collaboration with WORCC	spectral at 340, 380, 440, 500, 675, 870, 1020, 1640 nm, in collaboration with Univ. Valladolid	spectral at 368, 412, 500, 862 nm
Aerosol Chemical Composition (addressing direct + indirect climate effect)	inorganic ions (ion chromatography), heavy metals (inductively-coupled-plasma mass-spectrometry)	main components (daily resolution, offline filter-based, ion chromatography), heavy metals (inductively-coupled-plasma mass-spectrometry)	inorganic ions and POPs (ion chromatography), discontinued from 2011 due to local contamination.
Aerosol Chemical Speciation (direct + indirect climate effect, source attribution, transport)	Particle main chemical species (hourly resolution, online mass spectrometry)	Particle main chemical species (hourly resolution, online mass spectrometry)	---
Particle Mass Concentration	---	PM _{2.5} , PM ₁₀	PM ₁₀
Cloud Condensation Nuclei (addressing indirect climate effect)	size integrated number concentration at variable supersaturation in collaboration with Korean Polar Research Institute	Size integrated number concentration at variable supersaturation	---

An overview of all aerosol parameters currently measured at the 3 observatories can be found in Table 4. Parameters included in this report, are written in green.

3.1 Observed optical properties of aerosols

Aerosol absorption and scattering is decisive for the cooling or warming effect of aerosol in climate. All types of aerosols are scattering solar radiation, but the higher fraction of aerosol absorption, the more warming are the aerosols. The absorption is depending on the composition; black carbon (e.g. soot) and minerals absorb radiation.

3.1.1 Optical aerosol properties measured at the Birkenes Observatory

The comprehensive set of instruments observing in situ optical aerosol properties at Birkenes, i.e. those describing the direct effect of aerosol on climate, has now been in operation since 2010. The parameters covered include the scattering coefficient σ_{sp} and the absorption coefficient σ_{ap} at various wavelengths. Figure 44 summarises the essence of these observations for the years 2010 - 2016 in time series of the observations themselves and relevant directly derived parameters. All properties are measured for particles with aerodynamic diameter $D_{p,aero} < 10 \mu\text{m}$ and at relative humidity below 40%, thus avoiding water uptake by particles. This protocol follows the recommendations provided by of the European research infrastructure ACTRIS, also harmonised with the recommendations of the WMO GAW aerosol network. This is crucial to have comparable data at Zeppelin, Trollhaugen and Birkenes, and with other site on European and global scale. For more details concerning measurement principles and quality assurance routines, please see to Appendix II.

Panel a) of Figure 44 displays the time series of the spectral scattering coefficient σ_{sp} at 450, 550, and 700 nm wavelength. Thin lines represent daily average values for the respective wavelength, whereas the heavy green line represents the running 8-week median for easier visibility of seasonal averages (green wavelength at 550 nm only for clarity). The σ_{sp} time series exhibits significant variability on the time scale of days, illustrating that particle load in an air mass varies significantly with air mass type and thus air mass origin, i.e. with the synoptic weather situation on a time scale of 1 - 3 days. When focussing on the graph of the running median, a slight seasonal variation can be detected, with values higher in summer than winter.

For optical aerosol properties, information is contained both in the absolute level and in the values at different wavelengths relative to each other. In order to make this spectral information accessible, the Ångström coefficient has been defined, that can be calculated for optical aerosol properties. Higher values of the Ångström coefficient correlate with higher concentration ratios of particles in the fine size range ($D_p < 1 \mu\text{m}$) as compared to the coarse size range ($D_p > 1 \mu\text{m}$). Moreover, the relative size of particles determining an optical aerosol property decreases with wavelength, i.e. smaller wavelengths “look at” smaller particles in relative terms, larger wavelengths “look at” larger particles. Already with these simple qualitative rules, many features exhibited by spectral aerosol optical property data in general and Ångström coefficient data in particular can be interpreted meaningfully.

Panel b) of Figure 44 shows the time series of the Ångström coefficient \hat{a}_{sp} , calculated from $\sigma_{sp}(\lambda)$, again as daily averages (thin line) and running 8-week median (heavy line). As with σ_{sp} , the strongest variability is associated to a time scale of 1-3 days, indicative of changes associated with air mass type, origin, and synoptic weather situation. Looking at the running median however, the seasonal cycle is more pronounced for \hat{a}_{sp} as for σ_{sp} , with \hat{a}_{sp} values around 1.1 in winter and 1.8 in summer. This indicates a stronger contribution of smaller particles, i.e. particles with D_p smaller than about 120 nm, to σ_{sp} in summer than in winter.

This is consistent with number concentrations of particles in this size range exhibiting a similar seasonal cycle, as will be discussed below. The time series of σ_{sp} and \hat{a}_{sp} don't show any trend, which is consistent with the findings for other European continental background stations at Jungfraujoch (Switzerland, mountain top), Hohenpeissenberg (Southern Germany, elevated boundary layer), and Pallas (Northern Finland, boreal background) (Collaud Coen et al., 2013). Also the range of σ_{sp} values encountered, 3 - 50 Mm^{-1} with an annual average of about 12.5 Mm^{-1} , is consistent with findings at comparable stations (Delene & Ogren, 2002).

The observations of the particle absorption coefficient σ_{ap} at Birkenes were upgraded in 2012. The new instrument uses the same physical principle, but measures σ_{ap} at 3 wavelengths (470, 522, 660 nm) with considerable less electronic noise and significantly better long-term stability. Panel c) of Figure 44 displays the σ_{ap} time series of the newer, 3-wavelength filter absorption photometer, Panel d) the data of the older, one wavelength instrument. For the older instrument, the wavelength has been recalculated to the same green wavelength as observed by the nephelometer (550 nm). Both panels use thin lines for daily averages, heavy lines for the running 8-week medians.

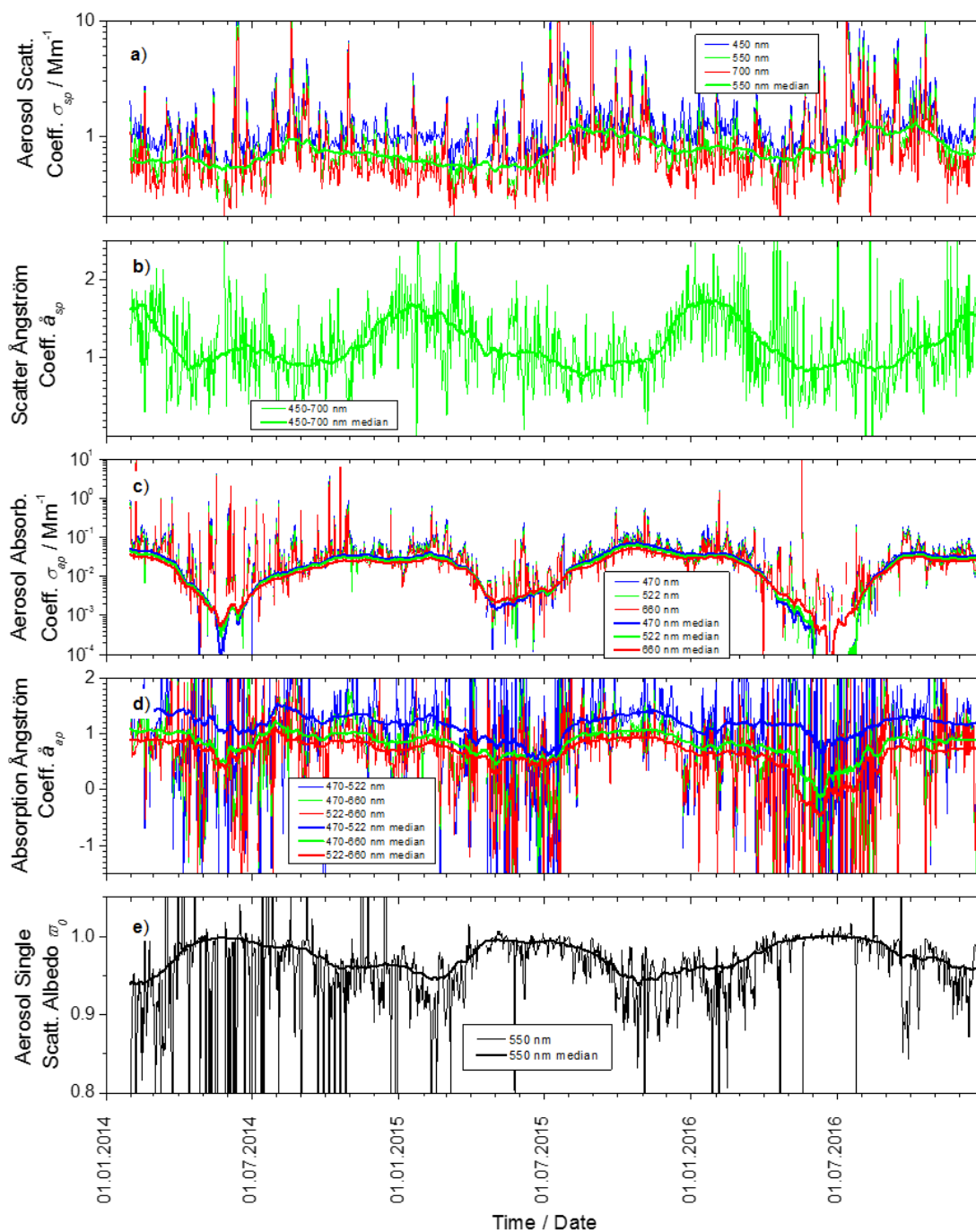


Figure 44: Time series of aerosol particle optical property daily means measured for 2010 - 2016 at Birkenes. Panel a) shows the aerosol scattering coefficient σ_{sp} at 450, 550, and 700 nm wavelength measured by integrating nephelometer. Panel c) the aerosol absorption coefficient σ_{ap} at 470, 522, and 660 nm wavelength measured by the newer filter absorption photometer, Panel d) the aerosol absorption coefficient σ_{ap} at 550 nm of the older filter absorption photometer, shifted from the instrument wavelength at 525 nm for consistent comparison assuming an absorption \AA ström coefficient of -1. Panels b) and e) show the derived properties scattering and absorption \AA ström coefficient \hat{a}_{sp} and \hat{a}_{ap} , respectively, while Panel f) depicts the single scattering albedo ω_0 . All plots also depict the running 8-week medians of the respective properties as heavy lines to visualize seasonal variations. To demonstrate consistency between old and new filter absorption photometer, respective comparison lines are displayed.

Panel d) also displays the σ_{ap} running median time series of the new filter absorption photometer (also recalculated to 550 nm wavelength) together with the data of the old instrument as an indicator for the goodness of overlap between the 2 instruments measuring the same property. Even though the older filter absorption photometer underwent quality assurance by off-site intercomparison within ACTRIS in 2013, a drift of the reading of the older compared to the newer instrument can be observed between 2013 - 2015. These stability issues of the old filter absorption photometer were discovered already during the 2013 intercomparison. Consequently, also the newer filter absorption photometer was subjected to an ACTRIS intercomparison in 2015. The intercomparison discovered no issues with the newer instrument and confirmed stability of calibration. As a result, the whole σ_{ap} time series obtained with the old filter absorption photometer has been corrected with the newer instrument as reference, yielding a consistent aerosol absorption time series for Birkenes for the years 2010 - 2016.

Apart from the variation with synoptic transport and air mass origin, σ_{ap} does not seem to exhibit significant seasonal variation. The values of σ_{ap} are in the range of 0.3 - 4 Mm^{-1} with annual means around 1 Mm^{-1} .

In order to cover the largest possible time period, panel f) of Figure 44 shows the time series of the aerosol particle single scattering albedo ω_0 based on the time series of the older filter absorption photometer (grey lines), again daily averages (thin line) and 8-week running median (heavy line), together with the respective time series of the new instrument (black lines). The single scattering albedo ω_0 quantifies the fraction of light scattered by the particles rather than absorbed. It thus quantifies how absorbing the average aerosol particle is, with ω_0 values decreasing with increasing absorption of the average particle. For a purely scattering aerosol, ω_0 is 1, and decreases with increasing fraction of light absorbing components in the aerosol particle phase. The most prominent feature in the ω_0 time series is the pronounced annual cycle, varying between 0.86 - 0.96, with lower ω_0 values and higher particle absorption in winter. The annual cycle in ω_0 has been discussed in previous reports of the Birkenes aerosol dataset, and has been connected to the combustion of biomass in wood stoves for domestic heating in the winter season.

Previous reports mentioned an increasing tendency in ω_0 (decreasing tendency in average particle absorption) until 2014 at Birkenes, with levelling out thereafter. A tendency towards less aerosol absorption has also been observed for stations in the continental U.S. and Alaska (Barrow), but only few stations in continental Europe (Hohenpeissenberg, Germany) (Collaud et al., 2013; Coen et al., 2013). After re-evaluating and drift correcting the Birkenes aerosol absorption coefficient time series following the ACTRIS inter-comparison in 2015, this tendency of increasing ω_0 cannot be confirmed. Both the time series and tabulated seasonal and annual averages of ω_0 (section 3.3) show rather stable values from year to year for corresponding seasons. This finding underlines the importance of careful quality management for long-term time series of climate relevant parameters. Even small trends of a few percent in these parameters usually have impact on climate, requiring a constant high accuracy in the measurement of the same order. Connection to frameworks like ACTRIS and GAW and associated traceability is key to achieving this accuracy.

Panels e) and of Figure 44 is based on data of the new filter absorption photometer, measuring σ_{ap} at 3 wavelengths, as opposed to 1 wavelength with the older instrument. Panel e) depicts the time series of the absorption Ångström coefficient \hat{a}_{ap} for all 3 wavelength pairs provided by the new instrument. For \hat{a}_{ap} , the information on relative particle size concerns

not the overall aerosol particle phase, but the fraction of absorbing particles. Thus, considering \hat{a}_{ap} data allows to investigate changes in source and transport of the absorbing particle fraction in the aerosol. When looking at the \hat{a}_{ap} data in panel e) of Figure 44, an annual cycle is apparent that is opposite of the annual cycles seen in scattering Ångström coefficient \hat{a}_{sp} and single scattering albedo ω_0 . Both \hat{a}_{sp} and ω_0 increase in summer as compared to winter, \hat{a}_{sp} because of a summer increase in small particles due to particle formation from biogenic precursors, ω_0 because of fewer combustion emissions in summer than in winter. For \hat{a}_{ap} , values increase in winter as compared to summer, indicating, in relative terms, higher abundance of smaller absorbing particles in winter than in summer. This observation is consistent with assuming emissions from domestic heating by wood stoves to contribute to the Birkenes winter aerosol, which is the explanation for the decreased winter values of ω_0 . The size of the absorbing aerosol particles increases with aerosol age. Consequently, a smaller size of the absorbing particles indicates a younger combustion aerosol and a closer combustion source, which is consistent with a scattered distribution of houses using wood stoves for heating, i.e. typical for Southern Norway. The previous instrument upgrade of aerosol absorption measurements in Birkenes has thus provided another indication for the contribution of wood stove emissions to the Birkenes winter aerosol. Further information can be expected from the additional upgrade extending the spectral range of particle absorption observations in November 2017.

Key findings aerosol optical properties Birkenes: The higher aerosol absorption, the more warming are the aerosols. The tendency from earlier years towards a decreasing trend in absorption of the average aerosol particle at Birkenes is not confirmed. Careful quality management revealed that this slight tendency observed in earlier years was due to calibration drift of the associated instrument. Aerosol absorption in 2016 was record low, consistent with record low EC as described in Aas et al. 2017. This is probably due to an unusually mild winter and spring. Trends in aerosol optical properties cannot be observed at Birkenes, which corresponds to findings at other European stations. The aerosol scattering show a stronger contribution of smaller particles in winter than in summer, and that there is no observed trend in the scattering properties. The reasons for these seasonal differences is that summer aerosols during summer are influence by biogenic emissions which tends to give larger particles compared to the dominant smaller combustion particles during winter

3.1.2 Optical aerosol properties measured the Zeppelin Observatory

The in situ optical properties of the particles at Zeppelin Observatory covered in this report are more limited as compared to Birkenes and Trollhaugen. NILU operates only a filter absorption photometer, an AE33 aethalometer, at Zeppelin measuring the absorption coefficient $\sigma_{ap}(\lambda)$ between 370-950 nm wavelength. A nephelometer providing the spectral scattering coefficient $\sigma_{sp}(\lambda)$ is also deployed at Zeppelin, but operated by Stockholm University, and data is therefore not available for this report. This excludes also calculation and discussion of the particle single scattering albedo.

Figure 45 summarises the first 1.5 years of spectral aerosol particle absorption coefficient $\sigma_{ap}(\lambda)$ data collected at Zeppelin Observatory since deployment of the aethalometer in June 2015. The top panel displays daily averaged $\sigma_{ap}(\lambda)$ data for all 7 wavelengths (thin lines), as well as running 8-week medians (bold lines), here only for 3 wavelengths to improve readability of the graph. The middle panel shows graphs of the absorption Ångström

coefficient \hat{a}_{ap} for 3 wavelength pairs representing short wave end, long wave end, and full range of the measured wavelength spectrum. The \hat{a}_{ap} data are plotted as 8-week median only since daily averages are too noisy due to the low particle load commonly observed at Zeppelin.

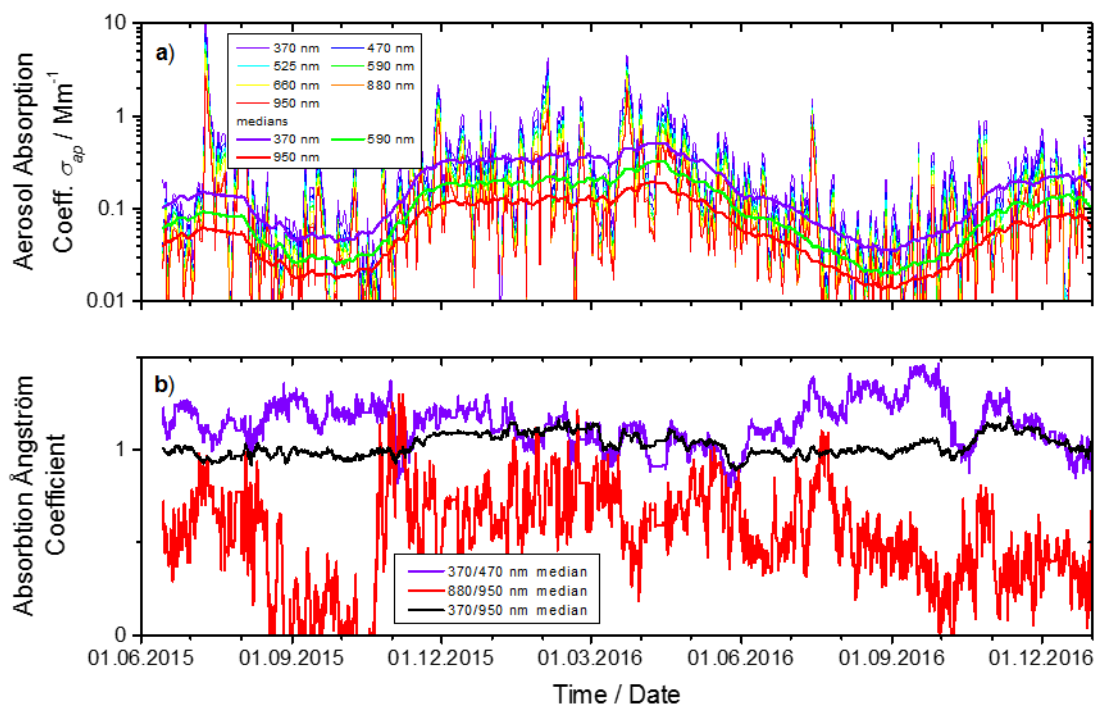


Figure 45: Time series graphs of the 1.5 years of data collected by the filter absorption photometer at Zeppelin Observatory since deployment in June 2015. Top: daily means of absorption coefficient at all 7 measured wavelengths (thin lines), and 8-week running medians for top, middle and bottom of observed spectral range (heavy lines). Bottom: 8-month running medians of absorption Ångström coefficient, top, bottom, and whole observed spectral range.

Even though the time series of the particle absorption data at Zeppelin spans only 1.5 years at this point, a few interesting features can be detected already now. The time series of σ_{ap} (top panel of Figure 45) exhibits the same annual cycle as described already in the data of the other aethalometer instrument at Zeppelin collected in earlier years (Eleftheriadis et al., 2009), with lower values in summer and higher ones in winter. These variations have been attributed to changes in combustion aerosol sources caused by emissions from domestic heating in the relevant source regions, e.g. Northern and Central Russia (Law & Stohl, 2007). This pattern is moderated by incidents of emissions from large forest fires reaching the Arctic, which can increase aerosol particle absorption in episodes also in summer (e.g. Stohl et al., 2007). Absolute values of σ_{ap} vary in the range of 0.02 - 2 Mm^{-1} at Arctic Zeppelin station, with median values roughly a factor of 5 lower than at boreal Birkenes, but a factor of 4 larger than at Antarctic Trollhaugen station.

Also interesting in the data provided by the new filter absorption photometer is the aerosol absorption Ångström coefficient \hat{a}_{ap} . The \hat{a}_{ap} values exhibit a distinct spectral dependence on wavelength, with \hat{a}_{ap} for shorter wavelengths at times being anti-correlated to \hat{a}_{ap} at larger wavelengths. An annual cycle of \hat{a}_{ap} seems possible at this point, but the time series is too short for any conclusions. An explanation of these phenomena needs to await further

measurements at Zeppelin. Also funded by the grant of the Norwegian Ministry of Climate and Environment, an instrument observing the size distribution of the non-volatile particle fraction as a proxy of the absorbing particle fraction will be installed at Zeppelin by NILU in autumn 2017.

Key findings aerosol optical properties Zeppelin: The aerosol absorption measurements at Zeppelin station are conducted in collaboration with the Greek Demokritos-Athens research institute, and continue a time series that has been in started 2001. The decreasing trend in aerosol absorption observed since 2001 by Eleftheriadis et al. (2009) fits with the corresponding trend observed at other surface in situ stations in the Arctic (Coen et al., 2013).

3.1.3 Optical aerosol properties measured at the Trollhaugen Observatory

This section covers the aerosol optical properties collected at the station after the relocation in January 2014 from the Troll main base to Trollhaugen located above and upwind of the previous location. At the location of the old station, up to 80% of the collected data were contaminated by diffuse (unavoidable) emissions from the main buildings, making the scientific value and interpretation of the data from the old location difficult.

At Trollhaugen station, the same comprehensive set of instruments for observing optical aerosol properties as used in Birkenes is deployed. These cover the spectral scattering coefficient $\sigma_{sp}(\lambda)$, the spectral absorption coefficient $\sigma_{ap}(\lambda)$, as well as the derived properties scattering and absorption Ångström coefficient \hat{a}_{sp} and \hat{a}_{ap} , parameterising the wavelength dependence of σ_{sp} and σ_{ap} , as well as the single scattering albedo ω_0 . Figure 46 summarises the corresponding data collected at Trollhaugen for the years 2014 - 2016.

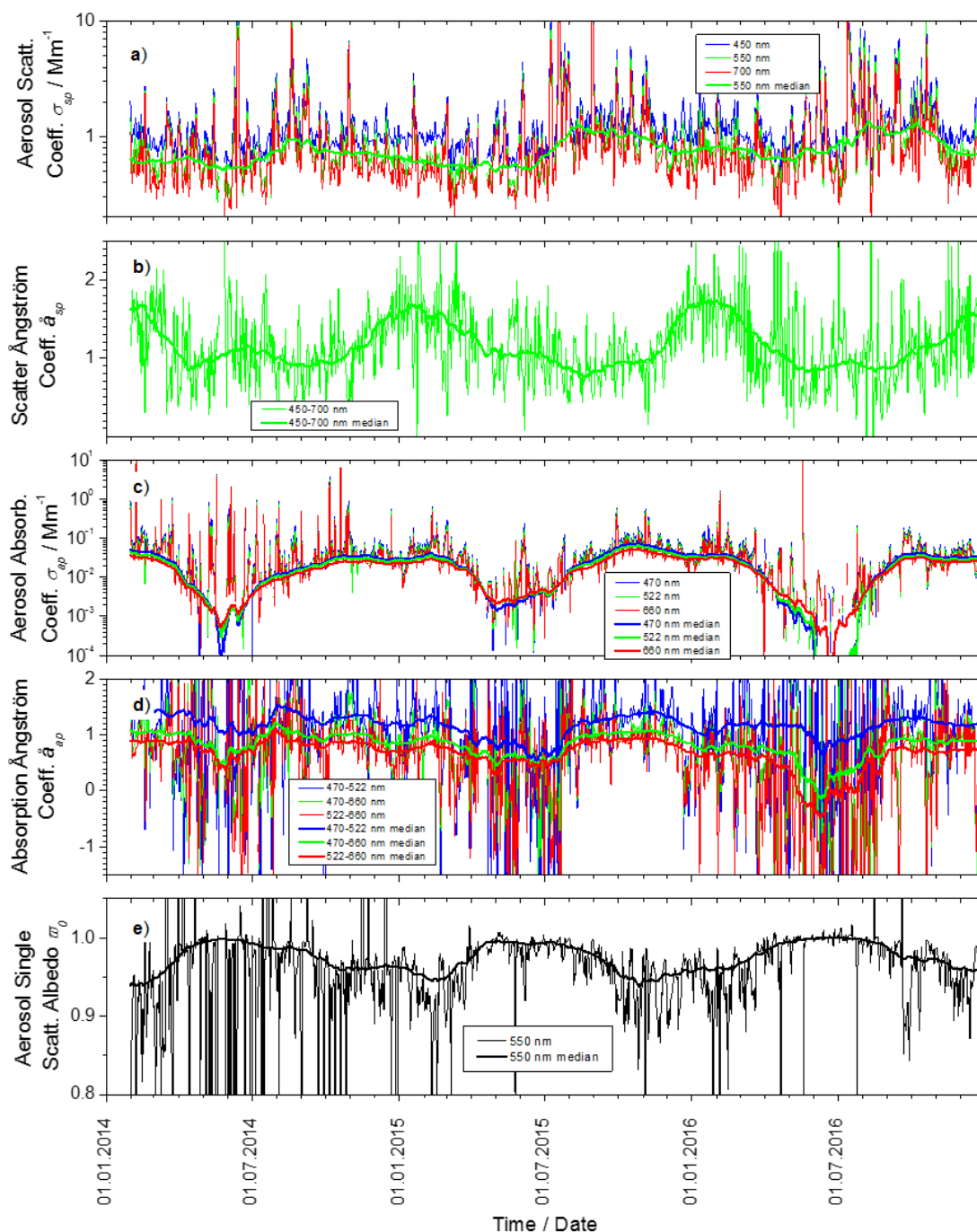


Figure 46: Time series of aerosol particle optical property daily means measured for 2014 - 2016 at Trollhaugen station. Panel a) shows the aerosol scattering coefficient σ_{sp} at 450, 550, and 700 nm wavelength measured by integrating nephelometer. Panel c) the aerosol absorption coefficient σ_{ap} at 470, 522, and 660 nm wavelength measured by filter absorption photometer. Panels b) and d) show the derived properties scattering and absorption Ångström coefficient \hat{a}_{sp} and \hat{a}_{ap} , respectively, while Panel e) depicts the single scattering albedo ω_0 . All plots also depict the running 8-week medians of the respective properties as heavy lines to visualize seasonal variations.

Starting with the time series of $\sigma_{sp}(\lambda)$ in panel a) of Figure 46, a slight annual cycle can be observed, with peaks throughout the year. The peaks are associated with intrusions of marine air during storm episodes, while the annual cycle is caused by an annual cycle of the particle number size distribution (PNSD) in Antarctic background air, with higher particle loads and larger particles in summer. The same annual cycle in the PNSD also explains the annual cycle

in the scattering Ångström coefficient \hat{a}_{sp} plotted in panel b). The scattering Ångström coefficient increases as the PNSD receives a relative peak at smaller particle sizes, which is the case in Antarctic background summer air.

An annual cycle can also be detected in the $\sigma_{ap}(\lambda)$ time series depicted in panel c) of Figure 46, even though the filter absorption photometer operates constantly around the detection limit. The minimum in the cycle occurs in Southern hemisphere winter when the Antarctic vortex decreases transport from lower latitudes through the lower and mid-troposphere. In the absorption Ångström coefficient \hat{a}_{ap} time series shown in panel d), the annual cycle is rather weakly pronounced, with the lowest values also occurring in winter.

The time series of the single scattering albedo ω_0 (panel e) of Figure 46) shows the highest values close to 1, i.e. almost no particle absorption at all, in Antarctic winter, coincident and consistent with the minimum in particle absorption. Lower ω_0 values, i.e. higher average particle absorption, occurs towards summer when the Antarctic continent is subject to stronger transport from mid-latitude sources through the lower part of the troposphere.

Optical aerosol properties are tightly connected to the physical aerosol properties, which is why they are ideally interpreted together in context. The annual cycle in the optical aerosol properties observed at Trollhaugen is caused by a corresponding annual cycle in the physical properties, which will be discussed in section 3.2.3.

Key findings aerosol optical properties Trollhaugen: The length of the time series of reliable data on optical aerosol properties at Trollhaugen is too short for drawing conclusions on trends. The annual cycle of the aerosol optical properties at Trollhaugen has been studied in detail, and is associated to a natural, hemispheric-scale atmospheric pattern. The same annual cycle with higher particle loads and larger particles in summer is observed also at other stations on the central Antarctic continent.

3.2 Measurements of aerosol number and size

3.2.1 Physical aerosol properties measured at the Birkenes Observatory

Figure 47 shows the time series of the particle number size distribution (PNSD) measured at Birkenes in 2016, separated into 4 different panels by season. In this plot type, the x-axis shows the time of the observation, whereas the y-axis holds the particle diameter D_p on a logarithmic scale. The logarithmic colour scale holds the particle concentration, normalised to the logarithmic size interval, $dN / d \log D_p$. The use of logarithmic axis is common when displaying PNSD information since both, particle diameter and particle concentration, tend to span several orders of magnitude while containing relevant information over the whole scale. In this report, the PNSD reported for Birkenes covers the whole size range between 0.01 - 10 μm by combining the information of 2 instruments, one each focussing on the fine ($D_p < 1 \mu\text{m}$) and coarse ($D_p > 1 \mu\text{m}$) size ranges, into a common PNSD product (see Appendix II for details). Existing, operating procedures and quality standards defined by the European research infrastructure ACTRIS have been used (Wiedensohler et al., 2012).

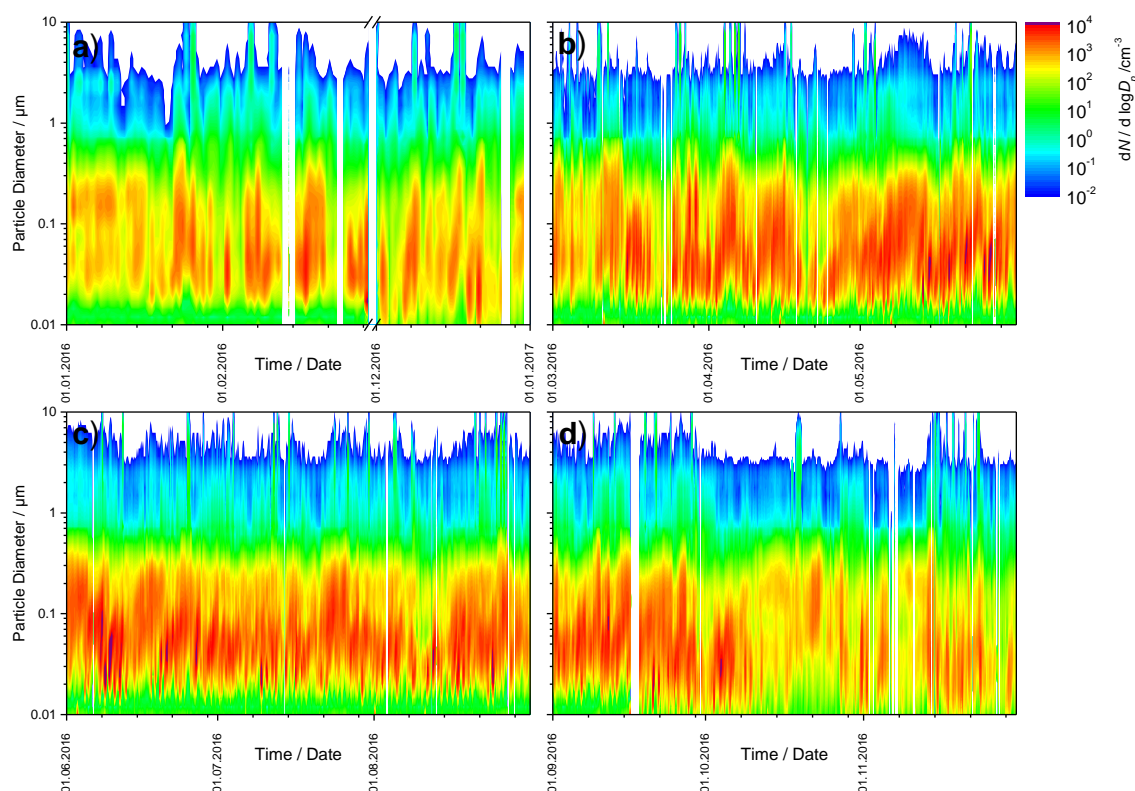


Figure 47: 2016 time series of particle number size distribution at Birkenes, panel a) winter, panel b) spring, panel c) summer, panel d) autumn.

There doesn't exist any unique connection between the PNSD and air mass type, but the PNSD still is normally fairly characteristic for the air mass, and can serve, together with the single scattering albedo ω_0 , and the scattering Ångström coefficient \hat{a}_{sp} , as valuable indication of air mass origin, which at Birkenes shifts with the synoptic weather situation. Consequently, the information content of a PNSD time series plot is too high to be discussed in detail in this overview-type annual report. The PNSD and ω_0 observations reconfirm findings from earlier years on the dominant air mass types at Birkenes, which consist of: 1) clean Arctic background aerosol; 2) Central and Eastern European aerosol; 3) biogenic aerosol, i.e.

vegetation emitted precursor gases condensing to the particle phase by photooxidation; 4) wood combustion aerosol from domestic heating.

Of particular interest in 2016 is an episode occurring around 22 October that year. Visible in panel d) of Figure 47, the episode is characterised by a PNSD dominated by a single accumulation mode peaking around 0.15-0.2 μm particle diameter, and almost absent ultrafine particles ($D_p < 0.1 \mu\text{m}$). The episode in the PNSD data coincides with a peak in particle absorption. Aerosols exhibiting such a PNSD have been subject to intense auto-processing, either by being closed off from surrounding air, and/or by maintaining high particle concentrations under transport. In coincidence with elevated particle absorption, such a PNSD is indicative of an aerosol originating from wildfires. In the present case, this notion could be confirmed by use of trajectory analysis and satellite fire products, which connects the Birkenes episode to wildfires in Eastern Ukraine.

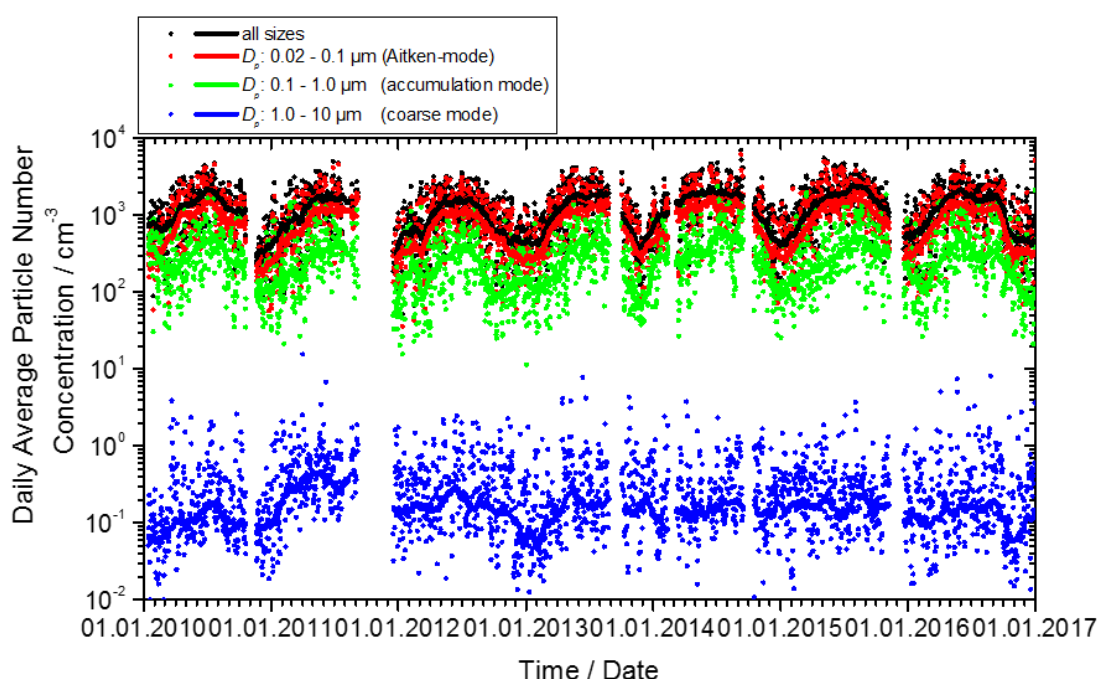


Figure 48: 2010-2016 time series of particle number concentration integrated over selected size ranges representing the different physical processes governing the atmospheric aerosol. The dotted graphs represent daily averages of the respective size range, the lines the 8-week running median.

In order to condense the information in the PNSD time series, Figure 48 shows the time series of selected PNSD integrals, i.e. the concentration of particles falling into selected size intervals. The size intervals are chosen to represent characteristic processes governing the atmospheric aerosol (see Appendix II for more details): 1) the Aitken-mode size range, 0.02 - 0.1 μm ; 2) the accumulation mode size range, 0.1 - 1 μm ; 3) the coarse mode size range, 1 - 10 μm . The time series in Figure 48 represent daily averages over these PNSD integrals for the whole period since the Birkenes station upgrade in 2010, as well as the corresponding running 8-week medians to highlight seasonal variations. The respective size range integral particle concentrations are denoted N_{ait} for the Aitken mode, N_{acc} for the accumulation mode, and N_{coa} for the coarse mode.

As to be expected, the particle concentration in the Birkenes aerosol in absolute terms is dominated by the Aitken mode particles, followed by the accumulation mode. Also the most prominent feature in Figure 48 is exhibited by the particle concentrations in these 2 modes, a clear annual cycle caused by the same underlying physical process. In summer, the vegetation emits gaseous aerosol precursors, which are photo-oxidised and condense onto Aitken-mode particles or form those directly. These particles coagulate, increasing the concentration of accumulation mode particles. These same processes increasing N_{ait} and N_{acc} in summer are also responsible for increasing the scattering Ångström coefficient \hat{a}_{sp} in summer. The processes controlling N_{coa} are decoupled from those controlling N_{ait} and N_{acc} . Coarse mode particles are formed from bulk material, their concentration is affected by wind speed (levitating dust, spores, pollen), snow cover, and rain (both inhibiting dust levitation).

Key findings aerosol physical properties Birkenes: Size segregated aerosol particle concentrations at Birkenes do not exhibit any obvious trend. This corresponds to findings obtained at other Nordic stations within ACTRIS and EMEP. The particle size distribution at Birkenes is governed by 5 major sources: 1) clean Arctic background aerosol; 2) Central and Eastern European aerosol; 3) Arctic haze; 4) fine fraction biogenic aerosol; 5) wood combustion aerosol from domestic heating. An episode observed in October 2016 can be traced to wildfires in Eastern Ukraine.

3.2.2 Physical aerosol properties measured in situ at the Zeppelin Observatory

An Differential Mobility Particle Sizer (DMPS) instrument, measuring particle size distribution, was installed in 2016 primarily to calibrate the ACSM instruments but included in continuous monitoring as an additional benefit. The same instrument type, operated in a different mode, is used to *measure* the particle number size distribution (PNSD) in the particle diameter range 0.01 μm - 0.8 μm at Birkenes and Trollhaugen stations. It was therefore decided to deploy the Zeppelin DMPS in the same way when not needed for calibrating the ACSM instrument.

As an additional feature, the Zeppelin DMPS will be upgraded in fall 2017 to also provide the PNSD of refractory (non-volatile) particles. The refractory particle fraction is often used as a proxy for the absorbing aerosol particle fraction, which will allow to study changes in particle absorption on a microphysical basis in the Arctic environment on a routine basis.

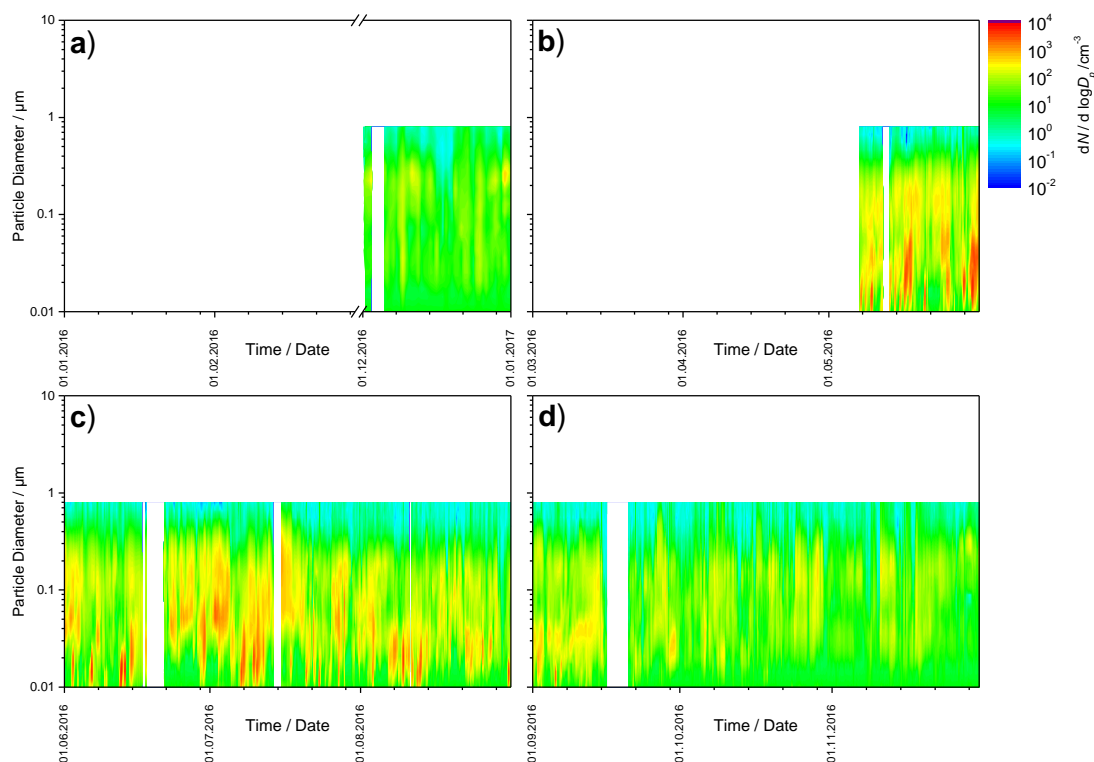


Figure 49: 2016 time series of particle number size distribution at Zeppelin, panel a) winter, panel b) spring, panel c) summer, panel d) autumn.

NILU's Zeppelin DMPS was deployed in June 2016, thus yielding half a year of data for the reporting year. At Zeppelin, the DMPS is not combined with an instrument covering the coarse particle size range larger 1 μm . This limits the available PNSD information the DMPS size range. Figure 49 presents the Zeppelin PNSD data available for this report for 2016 in the same way as for Birkenes and Trollhaugen, with one PNSD time series panel per season.

In contrast to mid-latitudes, air masses don't shift quite as rapidly at polar latitudes due to a smaller influence of frontal systems, making weather patterns more persistent at least in parts of the year. This allows to interpret the information on air mass types contained in PNSD data in more detail. Focussing in on Panel a) of Figure 49 displaying the PNSD data of December 2016, longer periods with a uni-modal size distribution are visible. This means the PNSD is dominated by a single mode, in this case the accumulation mode with a peak around 0.25 μm particle diameter. Such a PNSD is typical of early-phase Arctic haze (Heintzenberg, 1980), which is also detectable in late autumn (Panel d) of Figure 49). Arctic haze is formed by auto-processing of aerosol particles trapped under the winter Arctic vortex while the particle mass increases from industrial emissions under the vortex (e.g. Law & Stohl, 2007).

The late spring and summer PNSD at Zeppelin (Figure 49 panels c) and d) is somewhat more variable than in winter due to less stable atmospheric conditions. Particle formation events can be observed, with peak in the PNSD at particle diameters between 0.01 - 0.02 μm . These are triggered by photo-chemical production of chemical species that condense into the particle phase, and don't find enough existing particle surface to condense on, thus forming new particles. A more unusual event can be observed in the 2016 Zeppelin PNSD data around 15 July. The PNSD is dominated by a single mode peaking between 0.2 - 0.3 μm particle diameter. This indicated again strong auto-processing of the aerosol, which is unusual for Arctic summer. The peak in the PNSD coincides with a peak in particle absorption

(see section 3.1.2 to originate from Siberia, where wildfires were burning over huge areas in the warm 2016 summer.

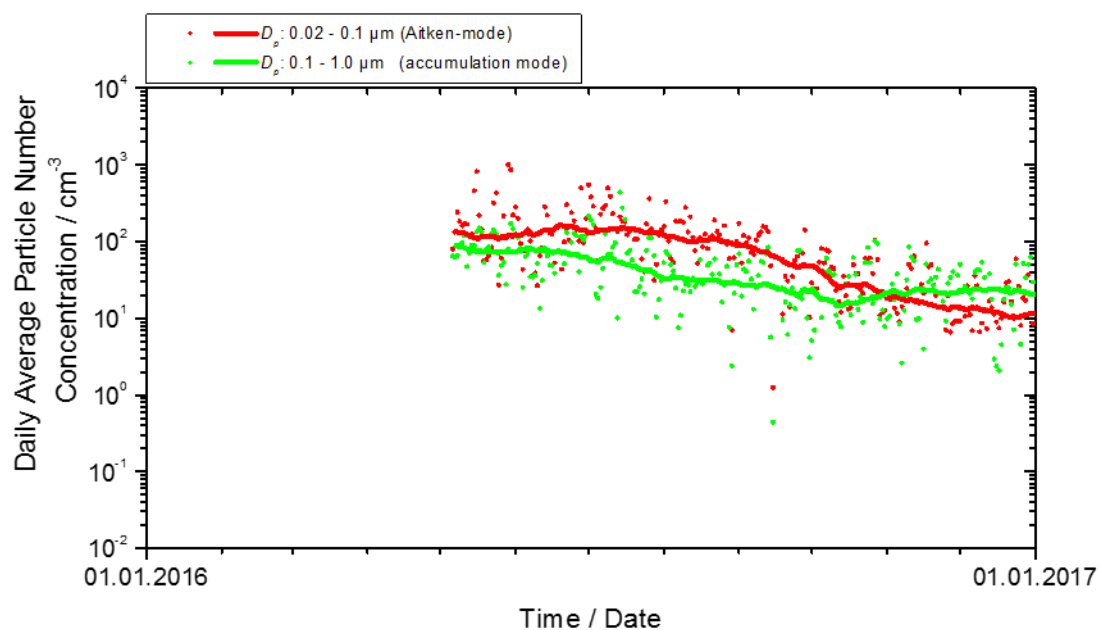


Figure 50: 2016 time series of particle number concentration integrated over selected size ranges representing the different physical processes governing the atmospheric aerosol. The dotted graphs represent daily averages of the respective size range, the lines the 8-week running median.

Figure 50 summarises the 2016 Zeppelin PNSD data by displaying time series of the PNSD size integrals for the Aitken mode N_{ait} ($0.02 \mu\text{m} < D_p < 0.1 \mu\text{m}$) and N_{acc} ($0.1 \mu\text{m} < D_p < 0.8 \mu\text{m}$). Apart from particle concentrations an order of magnitude lower than at boreal Birkenes, the most prominent and feature of the graph is the point in early November where the N_{acc} running median becomes consistently larger than N_{ait} running median. This behaviour is typical for auto-processed aerosols, and occurs normally only for shorter events. At Zeppelin, this point marks the onset of the Arctic haze period.

Key findings aerosol physical properties Zeppelin: Zeppelin particle size distribution data so far available for this report exhibit the well-known Arctic haze pattern. Trends in this pattern cannot be studied in this context due to too short the time series.

3.2.3 Physical aerosol properties measured in situ at the Trollhaugen Observatory

In contrast to mid-latitudes, polar latitudes exhibit more stable atmospheric conditions with less influence of frontal systems. This is especially true for the Antarctic continent due to colder inland temperatures and the absence of land masses in the mid- to high-latitude Southern hemisphere that could disturb the atmospheric air flow, as compared to the Northern hemisphere. This makes air masses well-defined in these regions, and their associated aerosol properties easier to interpret than under shifting Northern mid-latitude conditions.

This section only covers data collected at the station after the relocation in January 2014 from the Troll main base to Trollhaugen located above and upwind of the previous location. At the old station location, up to 80% of the collected data were locally contaminated by diffuse (unavoidable) emissions from the main station buildings, making a statistically meaningful interpretation of the data from the old location difficult.

The DMPS system measuring the PNSD at Trollhaugen station has been re-built on-site during the station maintenance visit of January / February 2016, causing a gap in the PNSD time series in January 2016. The system now conforms to the quality standards of the ACTRIS research infrastructure, and the observed size range has been extended from 0.03 - 0.8 μm to 0.01 - 0.8 μm , making it now suitable to study formation of new particles. As a consequence, absolute particle concentrations measured by the system before and after remodelling are not directly comparable. This disadvantage has been accepted in favour of a wider range of applications for the DMPS system.

Figure 51 plots the 2016 Trollhaugen PNSD data in the same way as for Birkenes. Due to the rather well-defined atmospheric conditions over the Antarctic continent, 2016 is rather representative also for previous years. Please observe that the times for the panels are the same as for the Northern hemisphere stations, but that seasons in the Southern hemisphere are shifted by 6 months.

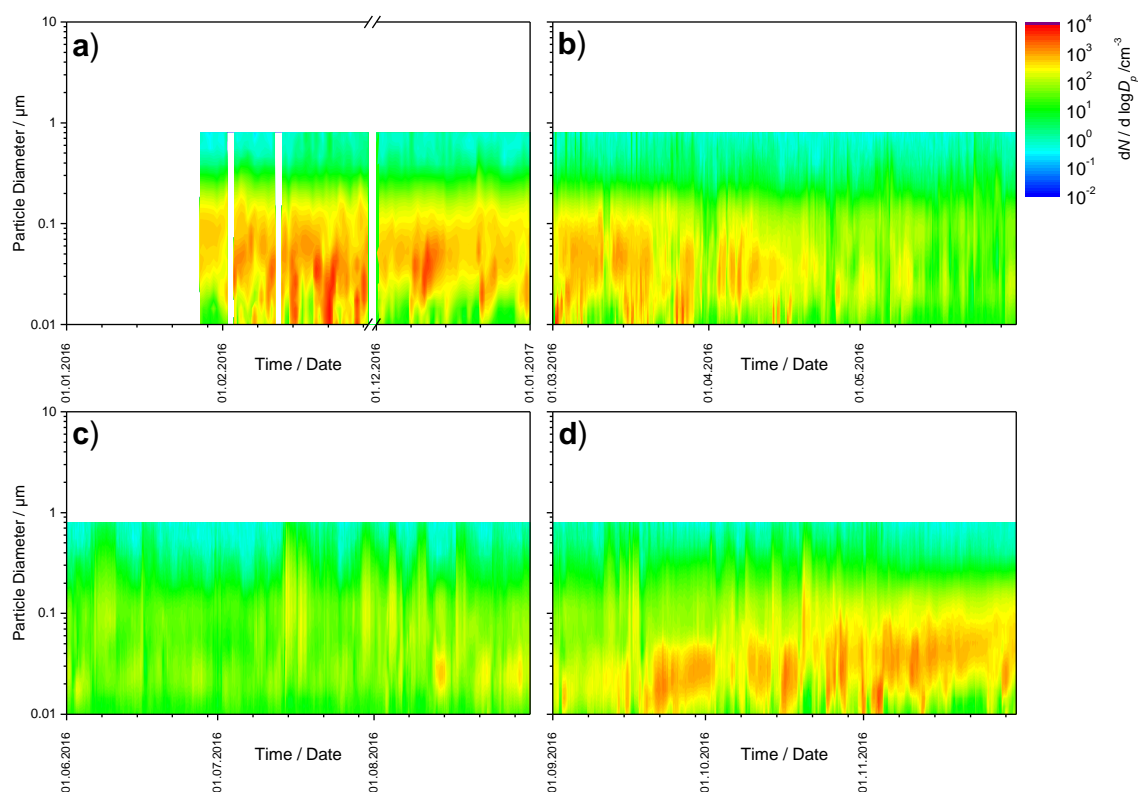


Figure 51: 2016 time series of particle number size distribution at Trollhaugen, panel a) summer, panel b) autumn, panel c) winter, panel d) spring.

Even though the Antarctic continent is among the most pristine regions on the globe, new particle formation events triggered by photo-chemical oxidation of precursor substances can be observed in Antarctic summer. Formation of new particles is not a function of available

condensable vapour alone, but also of the available particle surface. If the available particle surface becomes too small to accept the condensing vapour, new particles occur. This ratio doesn't depend on the absolute amount of aerosol particles. Thus, formation of new particles can occur anywhere on the globe.

A year-round feature observed at Trollhaugen are intrusions of marine air associated with marine storms. These have been observed even at South Pole, and are visible in the PNSD when the particle concentration at the upper end of the particle size range increases.

The probably most prominent feature in the Trollhaugen annual PNSD time series data is the annual cycle visible in the background aerosol. Particle concentrations are low in winter over the whole observed PNSD size range, and nucleation events lacking. In spring, particle concentrations in the diameter range 0.01 - 0.03 μm increase, and the central particle diameter of this peak increases throughout spring until reaching values around 0.09 μm in summer. Towards autumn and winter, the cycle reverses.

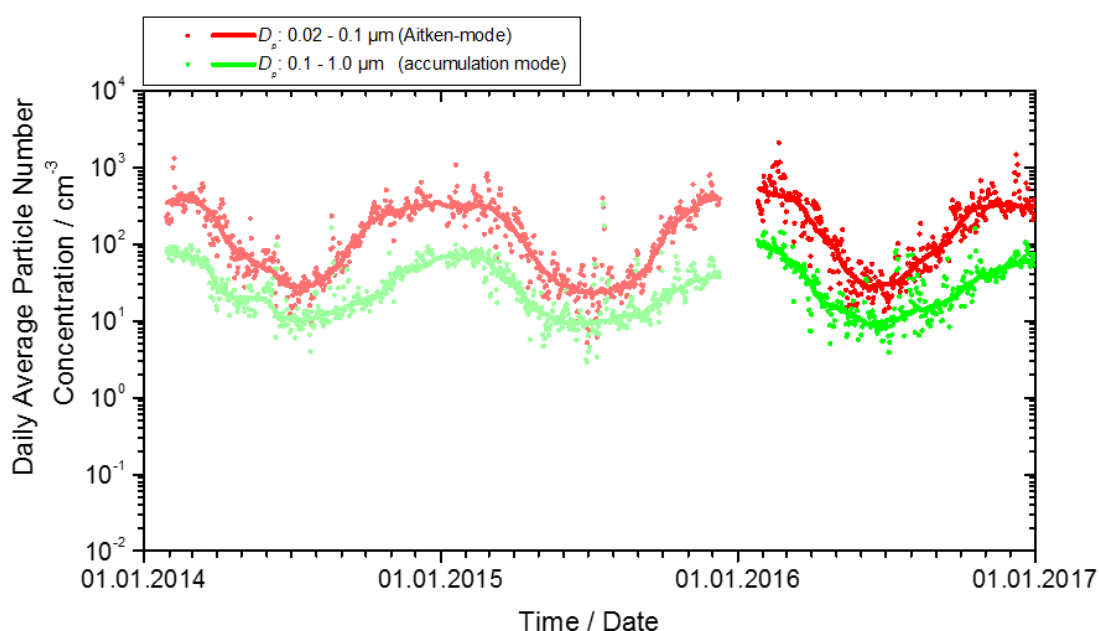


Figure 52: 2014-2016 time series of particle number concentration integrated over selected size ranges representing the different physical processes governing the atmospheric aerosol. The dotted graphs represent daily averages of the respective size range, the lines the 8-week running median. Data of the DMPS instrument prior to its upgrade are plotted in lighter colour as reminder that data before and after remodelling aren't directly comparable due to extension of the particle size range observed by the instrument.

This annual cycle in the Antarctic background PNSD is reflected by the PNSD size integrals for the Aitken mode N_{ait} ($0.02 \mu\text{m} < D_p < 0.1 \mu\text{m}$) and N_{acc} ($0.1 \mu\text{m} < D_p < 0.8 \mu\text{m}$) plotted in Figure 52, with higher particle concentrations in summer than in winter. A study based on data collected at Troll (Fiebig et al., 2014) connects the annual cycle to transport patterns seen by Antarctic background air. Antarctic background air descends over the central continent from the upper troposphere / lower stratosphere region, where it has been transported from mid-latitudes or even the tropics at the same altitude. At these lower latitudes, it had been uplifted by frontal conveyor belts (mid-latitudes) or tropical anvil clouds. The uplift process, associated with extensive wet removal of particles in the frontal or anvil cloud system, explains the cleanliness of the air.

Fiebig et al. (2014) raise the hypothesis that the annual cycle of the Antarctic background aerosol is caused by the annual variation of solar insolation seen by the air during this transport pattern. The hard UV radiation in the upper troposphere would oxidise water-insoluble vapours that survived wet removal during uplift of the air. The oxidation products would subsequently condense into the particle phase, causing the observed annual cycle in the Antarctic background PNSD. Studying this hypothesis further is subject of the currently ongoing AtmosCAir project funded by the Norwegian Antarctic Research Expedition (NARE) programme.

Key findings aerosol physical properties Trollhaugen: The length of the time series of reliable data on the aerosol particle number size distribution at Trollhaugen is **too short for drawing conclusions on trends**. The annual cycle of the PNSD at Trollhaugen has been studied in detail, and is associated to a natural, hemispheric-scale atmospheric pattern. Antarctic background air descends over the Central continent from the upper troposphere / lower stratosphere. At that altitude, it has been transported to the pole after being uplifted (and cleaned by wet removal) at mid- or tropical latitudes.

3.3 Summary of physical and optical aerosol properties

Aerosol absorption and scattering is decisive for the cooling or warming effect of aerosols in climate. All types of aerosols are scattering solar radiation, but the higher fraction of aerosol absorption, the more warming are the aerosols. The absorption is depending on the composition; black carbon (e.g. soot) and minerals absorb radiation. The size and number size distribution of the aerosols are also important for the scattering properties. In order to summarise the measurements of physical and optical aerosol properties observed at Birkenes, Trollhaugen, and Zeppelin stations, annual and seasonal means of the main parameters are collected in Table 5 for the physical parameters, and in Table 6 for the optical parameters.

Focussing first on the columns for Birkenes, Aitken-mode particle concentrations N_{ait} values for the summer show surprisingly little variation over the years. Relative to previous years, particle concentrations in 2016 are close to the multi-year average. Differences appear in comparison to the previous year. 2015 was unusual in the sense that the particle concentrations in Aitken and accumulation mode N_{ait} and N_{acc} were higher in winter, spring, and summer as compared to previous years. These deviations in 2015 as compared to 2016 were caused by the unusual meteorological conditions, with winter temperatures falling rarely below freezing, very early onset of spring, and high summer temperatures. These conditions caused stronger and prolonged biogenic emissions of aerosol precursor substances, leading to the observed higher particle concentrations on seasonal and annual average for Aitken and accumulation mode size range.

At Birkenes, N_{ait} values for winter are typically around 33% of their summer values due to lack of biogenic particle production from the gas-phase. They depend on emissions from domestic heating, with higher values for colder winters. With spring and autumn as transition periods between the winter and summer extreme values, the variability of N_{ait} in these seasons depends on the pace of transition between summer and winter. The same tendencies apply to the accumulation mode particle concentration N_{acc} .

Coarse mode particle concentrations at Birkenes have a tendency to be up to a factor of 2 smaller in winter than in summer due to less crustal particle production with a snow-covered ground. Particle concentrations at Birkenes don't exhibit any obvious trend over time.

Aitken and accumulation mode particle concentrations at Trollhaugen are an order of magnitude lower than at Birkenes, reflecting the pristine conditions in Antarctica. Their pronounced annual cycle and its cause has been discussed in section 3.2.3. Both concentrations show little variability over the years, reflecting the fact that atmospheric composition in Antarctica is still mostly governed by natural processes whose large scale pattern changes slowly.

The conclusion of no obvious trends applies also to the optical aerosol properties observed at Birkenes and Trollhaugen. At Birkenes, the annual and inter-annual variability is governed by the same processes mentioned when discussing the particle concentrations. More specifically, the aerosol is more absorbing in winter, and hence more warming, due to emissions from wood burning for domestic heating, which come on top of a baseline of absorbing aerosol emitted from traffic. This is reflected in higher particle absorption coefficient values in winter, and even more significantly in lower winter values of the single scattering albedo (lower meaning higher average particle absorption).

Table 5: 2010 - 2016 seasonal and annual means of integral particle concentrations in the ultrafine, fine and coarse particle size range for Birkenes, Trollhaugen, and Zeppelin stations, as far as available.

Year	Season	Birkenes				Trollhaugen ¹		Zeppelin	
		N _{ait} / cm ⁻³	N _{acc} / cm ⁻³	N _{coa} / cm ⁻³	N _{tot} / cm ⁻³	N _{ait} / cm ⁻³	² N _{acc} / cm ⁻³	N _{ait} / cm ⁻³	² N _{acc} / cm ⁻³
2009/10	Winter	440	384	0.087	824				
2010	Spring	1030	324	0.311	1354				
2010	Summer	1511	488	0.323	1999				
2010	Autumn	835	299	0.260	1135				
2010	Whole Year	973	362	0.256	1336				
2010/11	Winter	454	285	0.311	739				
2011	Spring	1127	369	0.639	1496				
2011	Summer	1391	438	0.572	1829				
2011	Autumn	1594	464	0.966	2059				
2011	Whole Year	1047	371	0.565	1418				
2011/12	Winter	424	213	0.305	637				
2012	Spring	1107	271	0.386	1378				
2012	Summer	1314	392	0.485	1706				
2012	Autumn	661	152	0.365	814				
2012	Whole Year	889	263	0.375	1152				
2012/13	Winter	383	183	0.183	566				
2013	Spring	1190	352	0.411	1543				
2013	Summer	1519	447	0.467	1967				
2013	Autumn	701	162	0.417	864				
2013	Whole Year	1020	304	0.391	1324				
2013/14	Winter	699	333	0.347	1033				
2014	Spring	1464	402	0.334	1866	183	32		
2014	Summer	1723	625	0.343	2349	43	19		
2014	Autumn	1122	446	0.385	1568	207	28		
2014	Whole Year	1279	456	0.338	1735	183	34		
2014/15	Winter	549	192	0.307	741	368	67		
2015	Spring	1425	332	0.348	1757	134	25		
2015	Summer	1979	559	0.395	2539	38	23		
2015	Autumn	1130	422	0.257	1553	221	28		
2015	Whole Year	1326	390	0.340	1717	171	32		
2015/16	Winter	542	233	0.297	776				
2016	Spring	1328	442	0.449	1770	170	26		
2016	Summer	1455	484	0.517	1940	47	18	156	64
2016	Autumn	895	290	0.312	1185	262	35	47	31
2016	Whole Year	1063	357	0.392	1421	231	37		

Cells shaded in grey mark values obtained with an older instrument version that can't be compared directly with later values.

¹Numbers given for the time when the respective season is present in the Northern hemisphere. Actual seasons in Southern hemisphere are shifted by 6 months.

²The accumulation mode integral particle concentration N_{acc} at Trollhaugen and Zeppelin extends only up to 0.8 µm particle diameter due to lack of an instrument covering larger particles. For Birkenes, N_{acc} includes particles up to 1 µm diameter

Table 6: 2010 - 2016 seasonal and annual means of optical aerosol properties scattering coefficient, absorption coefficient, and single scattering albedo for Birkenes, Trollhaugen, and Zeppelin stations, as far as available.

Year	Season	Birkenes			Trollhaugen ¹			Zeppelin		
		σ_{sp} (550 nm) / Mm ⁻¹	σ_{ap} (550 nm) / Mm ⁻¹	ω_0 (550 nm)	σ_{sp} (550 nm) / Mm ⁻¹	σ_{ap} (550 nm) / Mm ⁻¹	ω_0 (550 nm)	σ_{sp} (550 nm) / Mm ⁻¹	σ_{ap} (550 nm) / Mm ⁻¹	ω_0 (550 nm)
2009/10	Winter	16.82	3.09	0.88						
2010	Spring	12.33	0.78	0.93						
2010	Summer	11.30	0.70	0.94						
2010	Autumn	7.26	0.71	0.90						
2010	Whole Year	11.52	1.24	0.91						
2010/11	Winter	16.96	2.18	0.89						
2011	Spring	18.67	1.26	0.93						
2011	Summer	15.43	0.74	0.95						
2011	Autumn	29.74	2.87	0.92						
2011	Whole Year	20.26	1.69	0.93						
2011/12	Winter	11.29	1.00	0.91						
2012	Spring	15.10	0.86	0.93						
2012	Summer	12.62	0.67	0.95						
2012	Autumn	9.80	0.65	0.92						
2012	Whole Year	12.22	0.83	0.92						
2012/13	Winter	12.48	1.84	0.84						
2013	Spring	17.03	1.48	0.90						
2013	Summer	13.81	1.15	0.92						
2013	Autumn	8.89	1.25	0.85						
2013	Whole Year	13.73	1.40	0.88						
2013/14	Winter	22.89	2.64	0.87						
2014	Spring	12.95	2.09	0.87	0.74	-0.05	0.95			
2014	Summer	15.85	1.26	0.92	1.39	0.04	0.98			
2014	Autumn	18.76	3.41	0.82	1.02	0.15	0.93			
2014	Whole Year	16.99	2.30	0.87	1.01	0.09	0.95			
2014/15	Winter	13.98	1.30	0.89	0.74	0.04	0.94			
2015	Spring	12.72	1.48	0.89	0.65	0.02	0.97			
2015	Summer	12.45	1.46	0.90	2.44	0.02	0.98		0.30	
2015	Autumn	15.69	2.45	0.95	1.32	0.07	0.94		0.14	
2015	Whole Year	14.36	1.56	0.90	1.32	0.04	0.96			
2015/16	Winter	13.59	1.24	0.88	0.87	0.05	0.94		0.38	
2016	Spring	14.86	1.10	0.91	0.78	0.17	0.97		0.39	
2016	Summer	11.93	0.77	0.94	2.01	0.00	0.99		0.09	
2016	Autumn	11.47	1.46	0.85	1.54	0.04	0.95		0.12	
2016	Whole Year	12.26	1.12	0.89	1.31	0.06	0.97		0.24	

Values stated in cells shaded in grey are re-evaluated according to latest inter-comparisons within ACTRIS and therefore deviate from values given in earlier years.

¹Numbers given for the time when the respective season is present in the Northern hemisphere. Actual seasons in Southern hemisphere are shifted by 6 months.

3.4 Column optical aerosol properties measured by ground-based remote sensing

Ground-based remote sensing of the optical characteristics of aerosols in the atmospheric total column is conducted with multi-wavelength sun-photometers. A sun-photometer is oriented towards the sun to detect the solar radiation attenuated along the slant path from the top-of-atmosphere to the ground. The atmospheric aerosol load leads to a decrease in the solar radiation transmitted through the atmosphere. This decrease depends on the aerosol optical depth (AOD), which is given by the integral of the volume aerosol extinction coefficient along the vertical path of the atmosphere. The wavelength dependence of AOD, described by the Ångström exponent (\AA) is a qualitative indicator of the particle size and contains information about the aerosol type. The larger the Ångström exponent, the smaller the size of the particles measured.

Photos of instruments used for monitoring of spectral resolved AOD at Birkenes and Ny-Ålesund, their main characteristics are given in Appendix II, and detailed Tables with monthly data for all years are given in Appendix I.

3.4.1 Column optical aerosol properties measured by ground-based remote sensing at Birkenes Observatory

AOD measurements started at the Birkenes Observatory in spring 2009, utilizing an automatic sun and sky radiometer (CIMEL type CE-318, instrument #513). The retrieval method is that of the AERONET version 2 direct sun algorithm (for details: <http://aeronet.gsfc.nasa.gov>). Quality assured (Level 2) data are available for the eight years of operation, 2009 - 2016. The Cimel instrument was scheduled for calibration in spring 2016 at Valladolid (Spain), with the plan to restart measurements in July 2016 at the latest. Due to various circumstances, such as problems with Spanish customs and technical failure during the calibration, the instrument was not back in operation until end of October 2016. Shortly afterwards, further technical problems with both the instrument and the communication system at the observatory occurred and prohibited usable measurements until April 2017. As a consequence, only a very limited data set is available for 2016, mostly before 1 May. The few measurements from November 2016 lack a second calibration afterwards (which is planned for November 2017) and are only available as level 1.5 data.

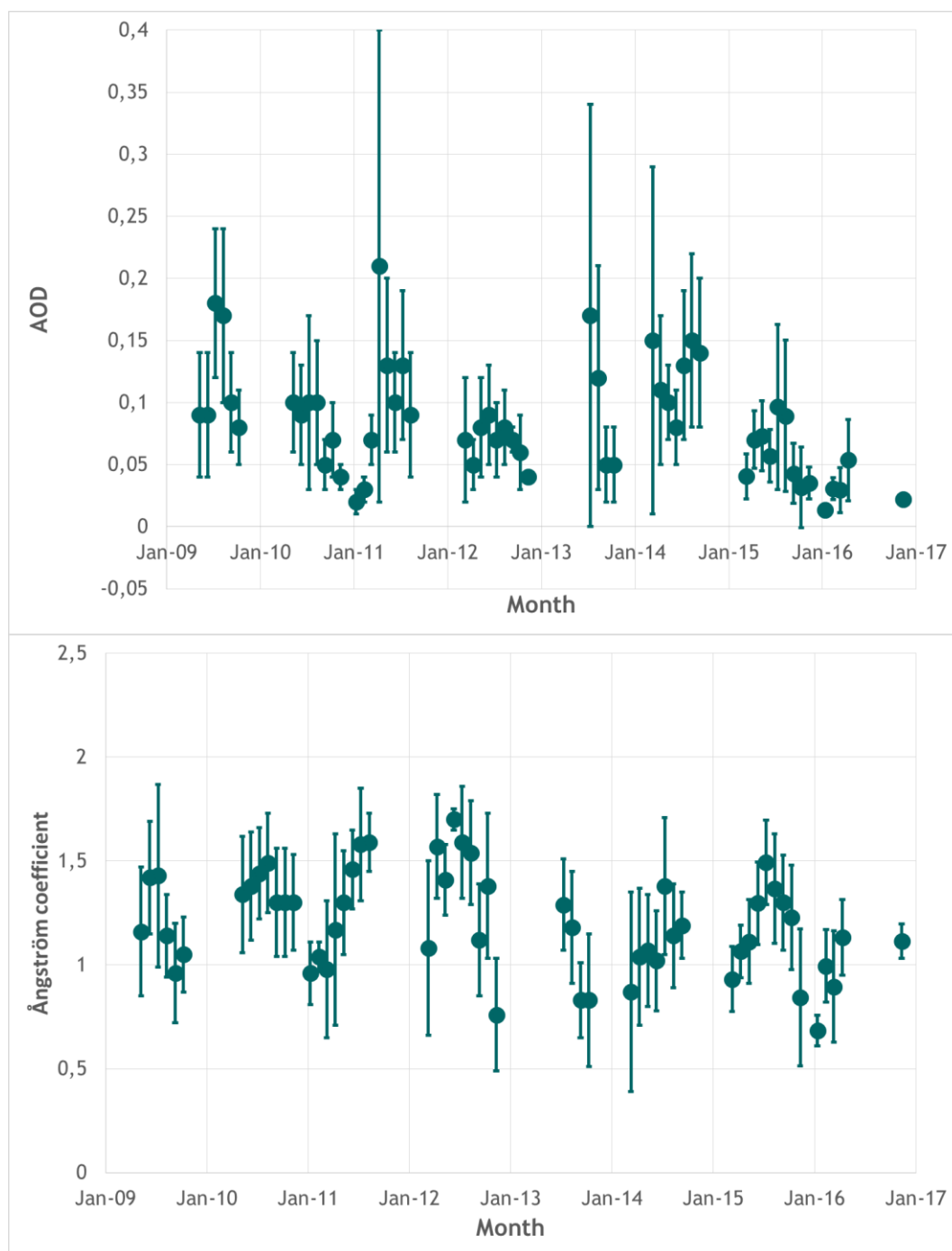


Figure 53: 2009 - 2016 time series of aerosol optical depth (AOD) at 500 nm wavelength in the atmospheric column above Birkenes (upper panel) and Ångström coefficient describing the AOD wavelength dependence (lower panel). Mean values and standard deviations are given.

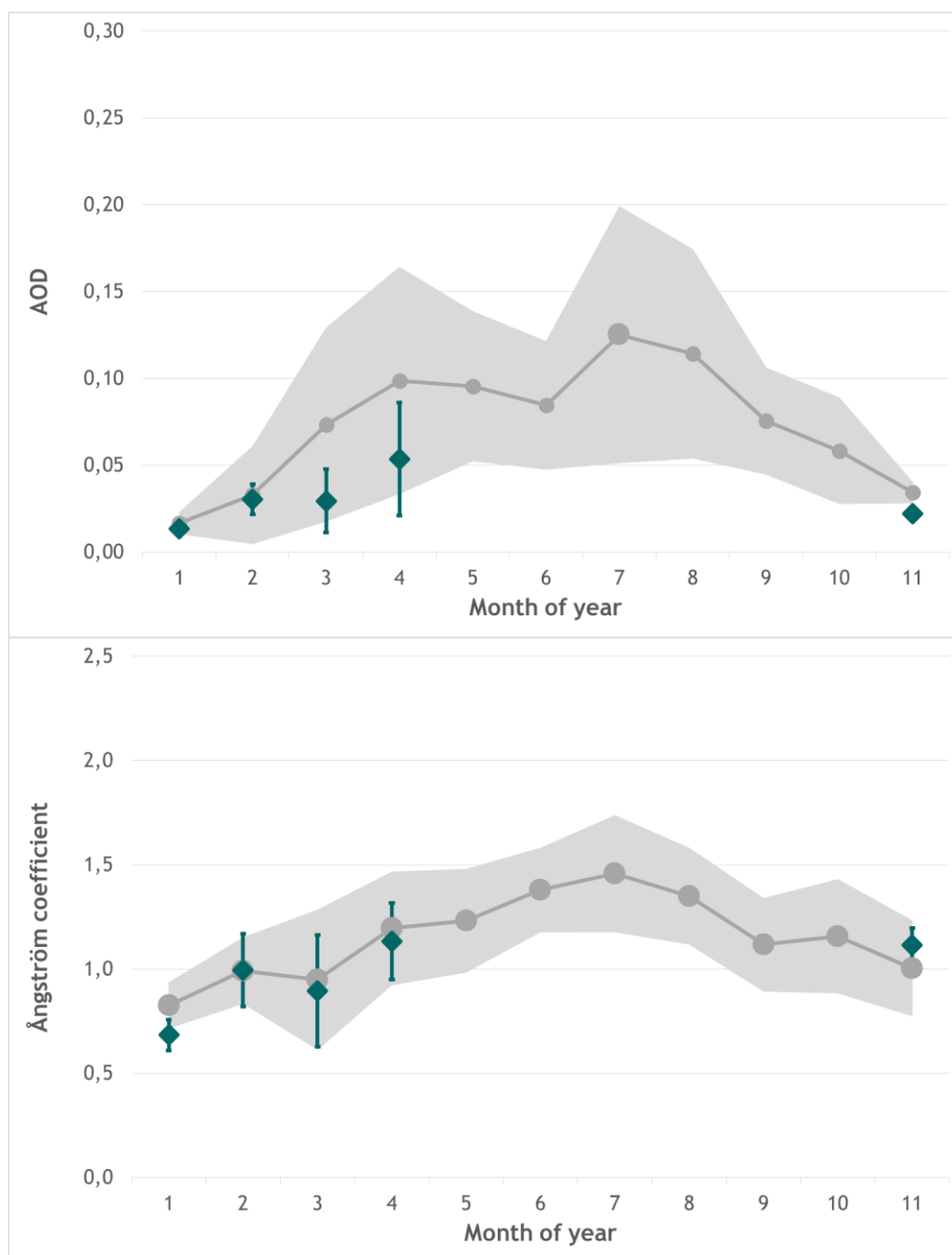


Figure 54: Monthly mean aerosol optical depth (AOD) at 500 nm wavelength in the atmospheric column above Birkenes (upper panel) and Ångström coefficient describing the AOD wavelength dependence (lower panel). Mean values and standard deviations are given. Values marked in grey are the mean and standard deviations for the time period 2009-2016.

The AOD and Ångström coefficient time series and seasonal variations are shown Figure 53 and Figure 54. The 2016 monthly mean and mean values for all years are shown in Table 7. Data for all years are given in Appendix I. There are no obvious trends visible in the eight years of observations. Missing data in the summer half-year were caused by a combination of various circumstances as described above. In general, AOD measured at Birkenes are relatively low, compared to central European observations. E.g., AERONET climatological values for Cabauw, the Netherlands, vary between 1.2 ± 0.06 in December and 3.1 ± 0.19 in April). In 2016, AOD values at Birkenes were very low, compared to previous years at this

station; none of the monthly mean AOT data were above average over the whole measurement series. The highest monthly average AOD of 0.05 was observed in April, but this is not significant as data from the summer months with generally higher AOT values are missing. There were no episodes with significantly higher AOT values during winter and spring.

Ångström exponent monthly means are close to the long-term means observed at Birkenes and also follow the seasonal variation of previous years, with monthly means close to 1.0 in the first months of the year and in November. All 2016 monthly means are within the standard deviations of all years at the station.

Table 7: Monthly mean values for 2016 and mean for the time period 2009-2016, plus standard deviations, for aerosol optical depth (AOD) and Ångström coefficient observed in Birkenes. In addition, the number of days with cloud free and quality assured observations are given.

Month/Year	Jan	Feb	Mar	Apr	May	Jun	Jul	Aug	Sep	Oct	Nov*
Aerosol optical depth (AOD)											
2016	0.01 ±0.00	0.03 ±0.01	0.03 ±0.02	0.05 ±0.03							0.02 ±0.00
Mean 09-16	0.02 0.01	0.03 ±0.01	0.07 ±0.05	0.10 ±0.07	0.10 ±0.04	0.08 ±0.04	0.13 ±0.07	0.11 ±0.06	0.08 ±0.03	0.06 ±0.03	0.03 ±0.01
Ångström coefficient (Å)											
2016	0.68 ±0.07	1.00 ±0.17	0.90 ± 0.27	1.13 ± 0.18							1.11 ±0.08
Mean 09-15	0.82 ±0.11	1.02 ±0.12	0.95 ±0.33	1.20 ±0.27	1.23 ±0.25	1.38 ±0.20	1.46 ±0.28	1.35 ±0.23	1.12 ±0.22	1.16 ±0.27	1.00 ±0.23
Number of days with cloud-free and quality assured observations (AERONET level 2)											
2016	2	11	12	9							2*
Total 09-16	9	13	61	63	93	114	127	107	68	52	13

*not yet approved as level-2 data

Key findings column-integrated optical aerosol properties Birkenes: There are **no trend in the eight years of AOD observations at Birkenes**. In 2016, AOD values at Birkenes were very low, compared to previous years at this station; none of the monthly mean AOT data were above average over the whole measurement series.

3.4.2 Column optical aerosol properties measured by ground-based remote sensing at Ny-Ålesund

In 2002, Physikalisch-Meteorologisches Observatorium Davos/*World Radiation Center* (PMOD/WRC) in collaboration with NILU, started AOD observations in Ny-Ålesund (at the Sverdrup station, 46 m a.s.l.) as part of the global AOD network on behalf of the WMO GAW program. A precision filter radiometer (PFR) measures the extinction in four narrow spectral bands at 368 nm, 415 nm, 500 nm and 862 nm. Data quality control includes instrumental control like detector temperature and solar pointing control as well as objective cloud screening. Ångström coefficients are derived for each set of measurements using all four PFR channels. Calibration is performed annually at PMOD/WRC. Quality assured data are available at the World Data Centre of Aerosols (WDCA), hosted at NILU (see <https://ebas.nilu.no>)

In Ny-Ålesund, the solar elevation is less than 5° before 4 March and after 10 October, limiting the period with suitable sun-photometer observations to the spring-summer-early autumn seasons (NILU contributes to a Lunar Arctic initiative to fill the gap in the wintertime AOD climatology by using Lunar photometer, see Appendix II). In 2016, sun-photometer observations started on 15 March and lasted until 12 September; reliable AOD values are available on 64 days. The AOD and Ångström coefficients time series of monthly means and standard deviation are shown in Figure 55, while the 2016 values on the background of the average data and their standard deviation from the whole 15-year period are shown in Figure 56. The 2016 monthly mean values and standard deviations for all years are given in Table 8. Data for all years are given in Appendix I.

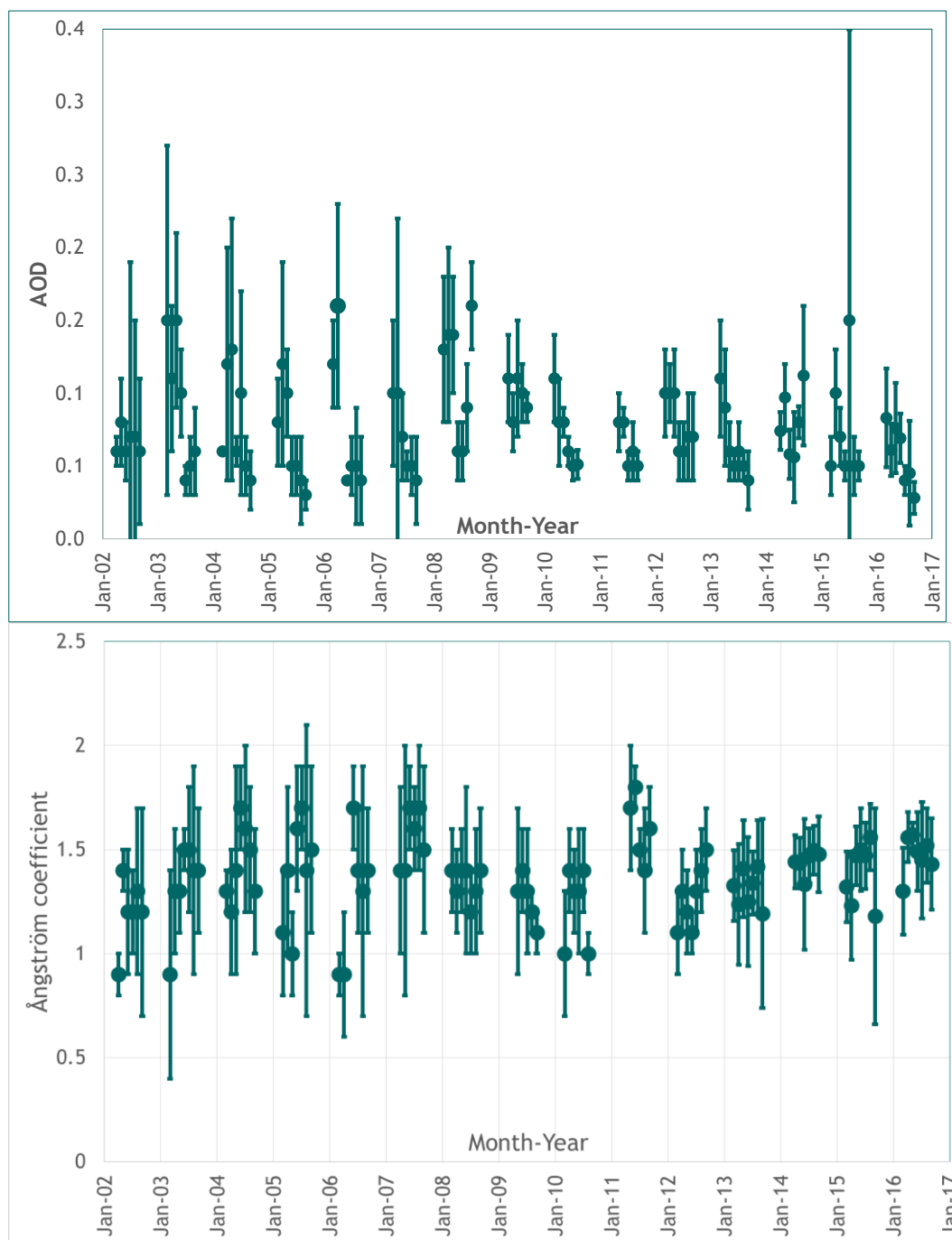


Figure 55: 2002 - 2016 time series of aerosol optical depth (AOD) at 500.5 nm wavelength in the atmospheric column above Ny-Ålesund (upper panel) and Ångström coefficient (lower panel). Monthly mean values and standard deviations are given.

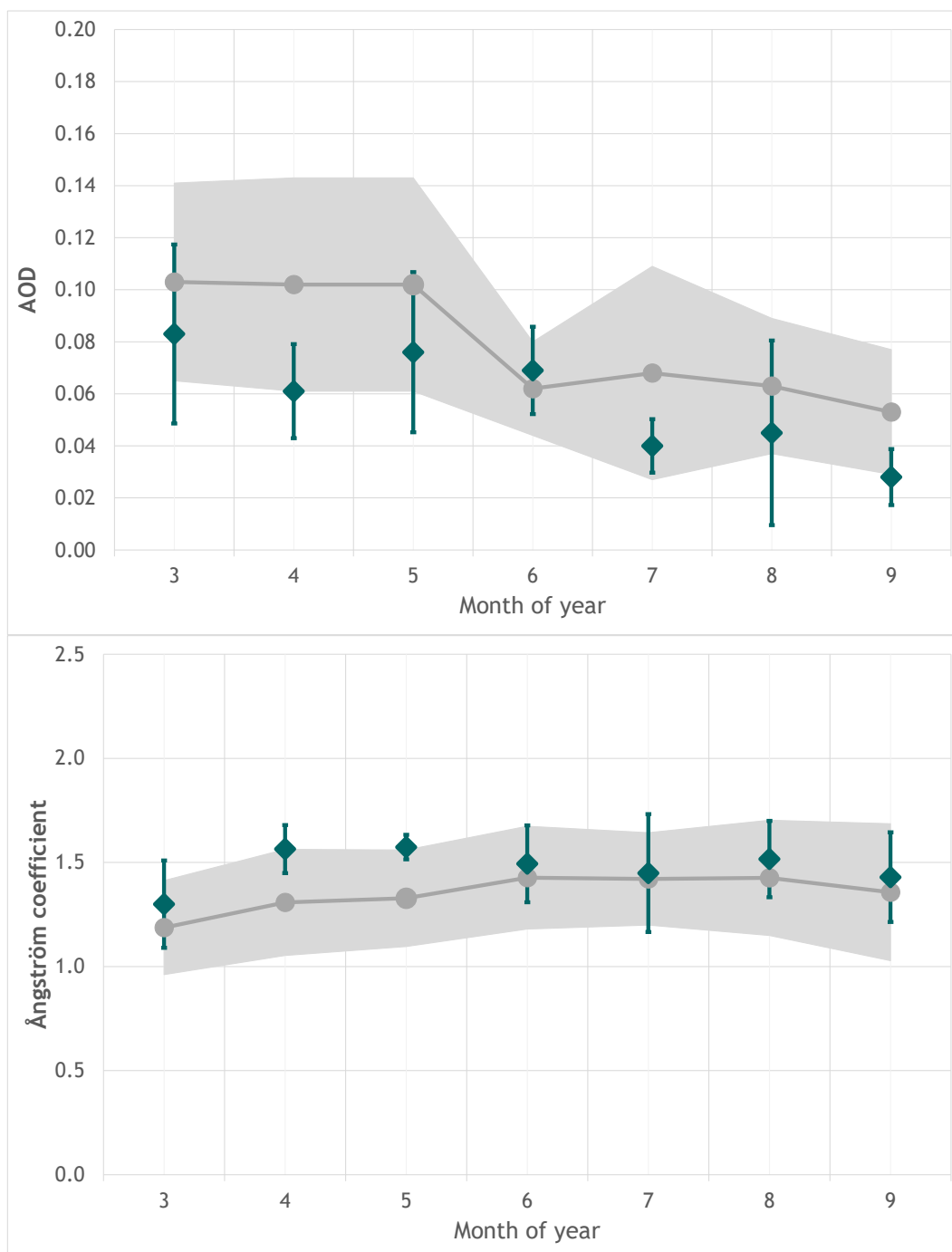


Figure 56: Seasonal variation of the aerosol optical depth (AOD) (upper panel) and Ångström coefficient (lower panel) observed in Ny-Ålesund. Values marked in grey are the mean and standard deviations for the time period 2009-2016; the 2016 monthly mean and standard deviations are shown in green.

In all months monthly mean AOD values were equal to or smaller than the long-term mean; in April the value was at the lower end of the standard deviation of all years. None of the daily average AOD values exceeded 0.2 and only 6 exceeded 0.1. Ångström coefficient monthly means relatively very stable throughout almost the whole measurement period close to a value of 1.5. Generally, in Ny-Ålesund seasonal variation of the Ångström coefficient is very weak, and the monthly mean Ångström coefficients in 2016 lie within the standard deviation range of the long-term monthly means, but in April and May at its upper end.

Table 8: Monthly mean values for 2016 and mean for the time period 2002-2016 for March to September, plus standard deviations, for aerosol optical depth (AOD) and Ångström coefficient observed in Ny-Ålesund. In addition, the number of days with cloud free and quality assured observations are given.

Month/Year	Mar	Apr	May	Jun	Jul	Aug	Sep
Aerosol optical depth (AOD)							
2016	0.08 ±0.03	0.06 ±0.02	0.08 ±0.03	0.07 ±0.02	0.04 ±0.01	0.05 ±0.04	0.03 ±0.01
Mean 2002-2016	0.10 ±0.04	0.10 ±0.04	0.10 ±0.04	0.06 ±0.02	0.07 ±0.04	0.06 ±0.03	0.05 ±0.02
Ångström coefficient (Å)							
2016	1.30 ±0.21	1.56 ±0.12	1.57 ±0.06	1.49 ±0.19	1.45 ±0.28	1.52 ±0.18	1.43 ±0.22
Mean 2002-2016	1.19 ±0.23	1.31 ±0.26	1.33 ±0.23	1.43 ±0.25	1.42 ±0.22	1.43 ±0.28	1.36 ±0.33
Number of days with cloud-free and quality assured observations							
2016	6	14	8	7	12	10	7
Total 2002- 2016	67	174	161	152	179	135	118

Key findings column-integrated optical aerosol properties Ny-Ålesund: In 2016, Ny-Ålesund monthly mean AOD values in all months were equal to or smaller than the long-term mean.

4. References

- Aas, W., Fiebig, M., Solberg, S., & Yttri, K. E. (2017) Monitoring of long-range transported air pollutants in Norway, annual Report 2016 (Miljødirektoratet rapport, M-780/2017) (NILU report, 18/2017). Kjeller: NILU.
- Asmi, A., Collaud Coen, M., Ogren, J. A., Andrews, E., Sheridan, P., Jefferson, A., Weingartner, E., Baltensperger, U., Bukowiecki, N., Lihavainen, H., Kivekäs, N., Asmi, E., Aalto, P. P., Kulmala, M., Wiedensohler, A., Birmili, W., Hamed, A., O'Dowd, C., G Jennings, S., Weller, R., Flentje, H., Fjaeraa, A. M., Fiebig, M., Myhre, C.E.L., Hallar, A. G., Swietlicki, E., Kristensson, A., Laj, P. (2013) Aerosol decadal trends - Part 2: In-situ aerosol particle number concentrations at GAW and ACTRIS stations. *Atmos. Chem. Phys.*, 13, 895-916. doi:10.5194/acp-13-895-2013.
- Baasandorj, M., Hall, B. D., Burkholder, J. B. (2012) Rate coefficients for the reaction of O(¹D) with the atmospherically long-lived greenhouse gases NF₃, SF₅CF₃, CHF₃, C₂F₆, C₄F₈, n-C₅F₁₂, and n-C₆F₁₄. *Atmos. Chem. Phys.*, 12, 11753-11764. doi:10.5194/acp-12-11753-2012.
- Coen, M.C., Andrews, E., Asmi, A., Baltensperger, U., Bukowiecki, N., Day, D., Fiebig, M., Fjaeraa, A. M., Flentje, H., Hyvärinen, A., Jefferson, A., Jennings, S. G., Kouvarakis, G., Lihavainen, H., Myhre, C.E.L., Malm, W. C., Mihapopoulos, N., Molenaar, J. V., O'Dowd, C., Ogren, J. A., Schichtel, B. A., Sheridan, P., Virkkula, A., Weingartner, E., Weller, R., Laj, P. (2013) Aerosol decadal trends - Part 1: In-situ optical measurements at GAW and IMPROVE stations. *Atmos. Chem. Phys.*, 13, 869-894. doi:10.5194/acp-13-869-2013.
- Coen, M.C., Weingartner, E., Apituley, A., Ceburnis, D., Fierz-Schmidhauser, R., Flentje, H., Henzing, J. S. (2010) Minimizing light absorption measurement artifacts of the Aethalometer: evaluation of five correction algorithms. *Atmos. Meas. Tech.*, 3, 457-474. doi: 10.5194/amt-3-457-2010.
- Dalsøren, S. B., Myhre, C.E.L., Myhre, G., Gomez-Pelaez, A. J., Søvde, O. A., Isaksen, I. S. A., Weiss, R. F., Harth, C. M. (2016) Atmospheric methane evolution the last 40 years. *Atmos. Chem. Phys.*, 16, 3099-3126. doi:10.5194/acp-16-3099-2016.
- Delene, D.J., Ogren, J.A. (2002) Variability of aerosol optical properties at four North American surface monitoring sites. *J. Atmos. Sci.*, 59, 1135-1150.
- Drinovec, L., G. Močnik, P. Zotter, A. S. H. Prévôt, C. Ruckstuhl, E. Coz, M. Rupakheti, J. Sciare, T. Müller, A. Wiedensohler, A. D. A. Hansen (2015) The "dual-spot" Aethalometer: an improved measurement of aerosol black carbon with real-time loading compensation. *Atmos. Meas. Tech.*, 8, 1965-1979. doi:10.5194/amt-8-1965-2015.
- Etioppe, G., Ciccioli, P. (2009) Earth's Degassing: A Missing Ethane and Propane Source. *Science* 323, 478. doi:10.1126/science.1165904.
- Etminan, M., G. Myhre, E. J. Highwood, and K. P. Shine (2016) Radiative forcing of carbon dioxide, methane, and nitrous oxide: A significant revision of the methane radiative forcing, *Geophys. Res. Lett.*, 43, 12,614-12,623, doi:10.1002/2016GL071930.
- Fiebig, M., D. Hirdman, C. R. Lunder, J. A. Ogren, S. Solberg, A. Stohl, R. L. Thompson (2014) Annual cycle of Antarctic baseline aerosol: controlled by photooxidation-limited aerosol formation. *Atmos. Chem. Phys.*, 14, 3083-3093. doi: 10.5194/acp-14-3083-2014

- Frasier, P., L. P. Steele, M. Cooksey (2013) PFC and Carbon Dioxide Emissions from an Australian Aluminium Smelter Using Time-Integrated Stack Sampling and GC-MS, GC-FID Analysis, *Light Metals 2013*, John Wiley & Sons, Inc., p.871 - 876.
- IPCC (2013) Summary for policymakers. In: *Climate Change 2013: The Physical Science Basis. Contribution of Working Group I to the Fifth Assessment Report of the Intergovernmental Panel on Climate Change*. Ed. by Stocker, T.F., Qin, D., Plattner, G.-K., Tignor, M., Allen, S.K., Boschung, J., Nauels, A., Xia, Y., Bex, V., Midgley, P.M. Cambridge, Cambridge University Press. pp. 3-29.
- Hall, B. D., S. A. Montzka, G. Dutton, J. Mühle, and J. W. Elkins (2017) Long-lived greenhouse gases [in "State of the Climate in 2016"]. *Bull. Amer. Meteor. Soc.*, 98 (8), S43-S46, doi:10.1175 /2017BAMSStateoftheClimate.1
- Hartmann, D.L., Klein Tank, A.M.G., Rusticucci, M., Alexander, L.V., Brönnimann, S., Charabi, Y., Dentener, F.J., Dlugokencky, E.J., Easterling, D.R., Kaplan, A., Soden, B.J., Thorne, P.W., Wild, M., Zhai, P.M. (2013) Observations: atmosphere and surface. In: *Climate Change 2013: The Physical Science Basis. Contribution of Working Group I to the Fifth Assessment Report of the Intergovernmental Panel on Climate Change*. Ed. by Stocker, T.F., Qin, D., Plattner, G.-K., Tignor, M., Allen, S.K., Boschung, J., Nauels, A., Xia, Y., Bex, V., Midgley, P.M. Cambridge, Cambridge University Press. pp. 159-254.
- Heintzenberg, J. (1980) Particle size distribution and optical properties of Arctic haze. *Tellus*, 32, 251-260. doi: 10.3402/tellusa.v32i3.10580
- Helmig D. et al. (2016) Reversal of global atmospheric ethane and propane trends largely due to US oil and natural gas production, *Nature Geosci.*, 9, 490-495. doi:10.1038/ngeo2721.
- Hewitt, C. Nicholas (ed.) (1999) *Reactive Hydrocarbons in the Atmosphere*. San Diego, CA, Academic Press. p. 313.
- Isaksen, I.S.A., Hov, Ø. (1987) Calculation of trends in the tropospheric concentration of O₃, OH, CO, CH₄ and NO_x. *Tellus*, 39B, 271-285.
- Mazzola, M., Vitale, V., Lupi, A., Wehrli, C., Kouremeti, N., Stone, R.S., Stebel, K. (2015) Moon-photometric aerosol optical depth measurements during polar night. Poster presented at the Lunar Photometry workshop, University of Valladolid, Spain, June 24 - 26, 2015.
- Myhre, C.E.L., Ferré, B., Platt, S.M., Silyakova, A., Hermansen, O., Allen, G., Pisso, I., Schmidbauer, N., Stohl, A., Pitt, J., Jansson, P., Greinert, J., Percival, C., Fjaeraa, A.M., O'Shea, S., Gallagher, M., Le Breton, M., Bower, K., Bauguitte, S., Dalsøren, S., Vadakkepuliambatta, S., Fisher, R., Nisbet, E., Lowry, D., Myhre, G., Pyle, J., Cain, M., Mienert, J. (2016) Large methane release from the Arctic seabed west of Svalbard, but small release to the atmosphere. *Geophys. Res. Lett.*, 43, 4624-4631. doi:10.1002/2016GL068999.
- Myhre, G., Myhre C. Lund, P. M. Forster, K. P. Shine, Halfway to doubling of CO₂ radiative forcing, *Nature Geoscience* 10, 710-711 (2017) doi:10.1038/ngeo3036
- Myhre, G., Myhre, C.E.Lund, Samset, B. H., Storelvmo, T. (2013a) Aerosols and their relation to global climate and climate sensitivity. *Nature Education Knowledge*, 4, 5,7. URL: <http://www.nature.com/scitable/knowledge/library/aerosols-and-their-relation-to-global-climate-102215345>

- Myhre, G., Shindell, D., Bréon, F.-M., Collins, W., Fuglestedt, J., Huang, J., Koch, D., Lamarque, J.-F., Lee, D., Mendoza, B., Nakajima, T., Robock, A., Stephens, G., Takemura, T., Zhang, H. (2013b) Anthropogenic and natural radiative forcing. In: *Climate Change 2013: The Physical Science Basis. Contribution of Working Group I to the Fifth Assessment Report of the Intergovernmental Panel on Climate Change*. Ed. by Stocker, T.F., Qin, D., Plattner, G.-K., Tignor, M., Allen, S.K., Boschung, J., Nauels, A., Xia, Y., Bex, V., Midgley, P.M. Cambridge, Cambridge University Press. pp. 659-740.
- Ng, N.L., Kroll, J.H., Chan, A.W.H., Chhabra, P.S., Flagan, R.C., Seinfeld, J.H. (2007) Secondary organic aerosol formation from m-xylene, toluene, and benzene. *Atmos. Chem. Physics*, 7, 3909-3922.
- Nicewonger, M.R., Verhulst, K.R., Aydin, M., Saltzman, E.S. (2016) Preindustrial atmospheric ethane levels inferred from polar ice cores: A constraint on the geologic sources of atmospheric ethane and methane. *Geophys. Res. Lett.*, 43, 214-221. doi:10.1002/2015GL066854.
- Oram, D. E., Mani, F. S., Laube, J. C., Newland, M. J., Reeves, C. E., Sturges, W. T., Penkett, S. A., Brenninkmeijer, C. A. M., Röckmann, T., and Fraser, P. J. (2012) Long-term tropospheric trend of octafluorocyclobutane (c-C₄F₈ or PFC-318), *Atmos. Chem. Phys.*, 12, 261-269. doi:10.5194/acp-12-261-2012.
- Prather, M., Ehhalt, D., Dentener, F., Derwent, R.G., Dlugokencky, E., Holland, E., Isaksen, I.S.A., Katima, J., Kirchhoff, V., Matson, P., Midgley, P.M., Wang, M. (2001) Atmospheric chemistry and greenhouse gases. In: *Climate Change 2001: The Scientific Basis, Contribution of Working Group I to the Third Assessment Report of the Intergovernmental Panel on Climate Change*. Ed. by: Houghton, J.T., Ding, Y., Griggs, D.J., Noguer, M., van der Linden, P.J., Dai, X., Maskell, K., Johnson, C.A. Cambridge, Cambridge University Press. pp. 239-287.
- Pisso, I., Myhre, C.E.L., Platt, S.M., Eckhardt, S., Hermansen, O., Schmidbauer, N., Mienert, J., Vadakkepuliambatta, S., Bauguitte, S., Pitt, J., Allen, G., Bower, K.N., O'Shea, S., Gallagher, M.W., Percival, C.J., Pyle, J., Cain, M., Stohl, A. (2016) Constraints on oceanic methane emissions west of Svalbard from atmospheric in situ measurements and Lagrangian transport modelling. *J. Geophys. Res.*, 121, 14188-14200. doi:10.1002/2016JD025590.
- Repo, M.E., Susiluoto, S., Lind, S.E., Jokinen, S., Elsakov, V., Biasi, C., Virtanen, T., Pertti, J., Martikainen, P.J. (2009) Large N₂O emissions from cryoturbated peat soil in tundra. *Nature Geosci.*, 2, 189-192.
- Simmonds, P.G., Manning, A.J., Cunnold, D.M., Fraser, P.J., McCulloch, A., O'Doherty, S., Krummel, P.B., Wang, R.H.J., Porter, L.W., Derwent, R.G., Grealley, B., Salameh, P., Miller, B.R., Prinn, R.G., Weiss, R.F. (2006) Observations of dichloromethane, trichloroethene and tetrachloroethene from the AGAGE stations at Cape Grim, Tasmania, and Mace Head, Ireland. *J. Geophys. Res.*, 111, D18304. doi:10.1029/2006JD007082.
- Svendby, T.M., Edvardsen, K., Hansen, G.H., Stebel, K., Dahlback, A. (2015) Monitoring of the atmospheric ozone layer and natural ultraviolet radiation. Annual report 2014. Kjeller, NILU (Miljødirektoratet rapport, M-366/2015) (NILU OR, 18/2015).
- Svendby, T.M., Hansen, G.H., Edvardsen, K., Stebel, K., Dahlback, A. (2016) Monitoring of the atmospheric ozone layer and natural ultraviolet radiation. Annual report 2015. Kjeller, NILU. (Miljødirektoratet rapport, M-561/2016) (NILU report, 12/2016).

- Stebel, K., Vik, A.F., Myhre, C.E.L., Fjæraa, A.M., Svendby, T., Schneider, P. (2013) Towards operational satellite based atmospheric monitoring in Norway SatMoNAir. Kjeller, NILU, (NILU OR, 46/2013).
- Toledano, C., Cachorro, V., Gausa, M., Stebel, K., Aaltonen, V., Berjón, A., Ortiz de Galisteo, J.P., de Frutos, A.M., Bennouna, Y., Blindheim, S, Myhre, C.E.L., Zibordi, G., Wehrli, C., Kratzer, S., Hakansson, B., Carlund, T., de Leeuw, G., Herber, A., Torres, B. (2012) Overview of sun photometer measurements of aerosol properties in Scandinavia and Svalbard. *Atmos. Environ.*, 52, 18-28. doi: 10.1016/j.atmosenv.2011.10.022.
- Tomasi, C., Kokhanovsky, A. A., Lupi, A., Ritter, C., Smirnov, A., O'Neill, N. T., Stone, R. S., Holben, B. N., Nyeki, S., Wehrli, C., Stohl, A., Mazzola, M., Lanconelli, C., Vitale, V., Stebel, K., Aaltonen, V., de Leeuw, G., Rodriguez, E., Herber, A. B., Radionov, V. F., Zielinski, T., Petelski, T., Sakerin, S. M., Kabanov, D. M., Xue, Y., Mei, L., Istomina, L., Wagener, R., McArthur, B., Sobolewski, P. S., Kivi, R., Courcoux, Y., Larouche, P., Broccardo, S., Piketh, S. J. (2015) Aerosol remote sensing in polar regions. *Earth Sci. Rev.*, 140, 108-157. doi:10.1016/j.earscirev.2014.11.001.
- Thompson, R.L., Sasakawa, M., Machida, T., Aalto, T., Worthy, D., Lavric, J. V., Myhre, C.E.L., Stohl, A. (2016) Methane fluxes in the high northern latitudes for 2005-2013 estimated using a Bayesian atmospheric inversion. *Atmos. Chem. Phys. Discuss.*, doi:10.5194/acp-2016-660, in review.
- Thompson, R.L., Dlugockenky, E., Chevallier, F., Ciais, P., Dutton, G., Elkins, J. W., Langenfelds, R. L., Prinn, R. G., Weiss, R. F., Tohjima, Y., Krummel, P. B., Fraser, P., Steele, L. P. (2013) Interannual variability in tropospheric nitrous oxide. *Geophys. Res. Lett.*, 40, 4426-4431. doi:10.1002/grl.50721.
- Tørseth, K., Aas, W., Breivik, K., Fjæraa, A. M., Fiebig, M., Hjellbrekke, A. G., Myhre, C.E.L., Solberg, S., Yttri, K. E. (2012) Introduction to the European Monitoring and Evaluation Programme (EMEP) and observed atmospheric composition change during 1972-2000. *Atmos. Chem. Phys.*, 12, 5447-5481. doi:10.5194/acp-12-5447-2012.
- Umezawa, T., A. K. Baker, D. Oram, C. Sauvage, D. O'Sullivan, A. Rauthe-Schöch, S. A. Montzka, A. Zahn, and C. A. M. Brenninkmeijer (2014), Methyl chloride in the upper troposphere observed by the CARIBIC passenger aircraft observatory: Large-scale distributions and Asian summer monsoon outflow, *J. Geophys. Res. Atmos.*, 119, 5542-5558, doi:10.1002/2013JD021396.
- Vik, A.F., Myhre, C.E.L., Stebel, K., Fjæraa, A.M., Svendby, T., Schyberg, H., Gauss, M., Tsyro, S., Schulz, M., Valdebenito, A., Kirkevåg, A., Seland, Ø., Griesfeller, J. (2011) Roadmap towards EarthCARE and Sentinel-5 precursor. A strategy preparing for operational application of planned European atmospheric chemistry and cloud/aerosol missions in Norway. Kjeller, NILU (NILU OR, 61/2011).
- Wiedensohler, A., Birmili, W., Nowak, A., Sonntag, A., Weinhold, K., Merkel, M., Wehner, B., Tuch, T., Pfeifer, S., Fiebig, M., Fjæraa, A.M., Asmi, E., Sellegri, K., Depuy, R., Venzac, H., Villani, P., Laj, P., Aalto, P., Ogren, J.A., Swietlicki, E., Williams, P., Roldin, P., Quincey, P., Hüglin, C., Fierz-Schmidhauser, R., Gysel, M., Weingartner, E., Riccobono, F., Santos, S., Grünig, C., Faloon, F., Beddows, D., Harrison, R., Monahan, C., Jennings, S.G., O'Dowd, C.D., Marinoni, A., Horn, H.-G., Keck, L., Jiang, J., Scheckman, J., McMurry, P.H., Deng, Z., Zhao, C.S., Moerman, M., Henzing, B., de Leeuw, G., Löschau, G., Bastian, S. (2012) Mobility particle size spectrometers: harmonization of technical standards and data structure to facilitate high quality long-term observations of

atmospheric particle number size distributions. *Atmos. Meas. Tech.*, 5, 657 - 685. doi:10.5194/amt-5-657-2012.

- WMO (2017) Greenhouse Gas Bulletin. The state of greenhouse gases in the atmosphere using global observations through 2016. Geneva, World Meteorological Organization (GHG Bulletin No. 13, 30 October 2017). URL: https://library.wmo.int/opac/doc_num.php?explnum_id=4022
- WMO (2016) Greenhouse Gas Bulletin. The state of greenhouse gases in the atmosphere using global observations through 2015. Geneva, World Meteorological Organization (GHG Bulletin No. 12, 24 October 2016). URL: http://library.wmo.int/pmb_ged/ghg-bulletin_12_en.pdf
- WMO (2015) Greenhouse Gas Bulletin. The state of greenhouse gases in the atmosphere using global observations through 2014. Geneva, World Meteorological Organization (GHG Bulletin No. 11, 9 November 2015). URL: http://library.wmo.int/pmb_ged/ghg-bulletin_11_en.pdf
- WMO (2014) Greenhouse Gas Bulletin. The state of greenhouse gases in the atmosphere using global observations through 2013. Geneva, World Meteorological Organization (GHG Bulletin No. 10, 9 September 2014). URL: http://library.wmo.int/opac/index.php?lvl=notice_display&id=16396#.VGHPz5-gQtK
- WMO (2014b) Scientific assessment of ozone depletion: 2014. Geneva, World Meteorological Organization (Global ozone research and monitoring project, Report No. 55). URL: <https://www.esrl.noaa.gov/csd/assessments/ozone/2014/chapters/2014OzoneAssessment.pdf>
- WMO (2013) Greenhouse Gas Bulletin. The state of greenhouse gases in the atmosphere using global observations through 2012. Geneva, World Meteorological Organization (GHG Bulletin No. 9, 6 November 2013). URL: http://www.wmo.int/pages/prog/arep/gaw/ghg/documents/GHG_Bulletin_No.9_en.pdf
- WMO (2012) Greenhouse Gas Bulletin. The state of greenhouse gases in the atmosphere using global observations through 2011. Geneva, World Meteorological Organization (GHG Bulletin No. 8, 19 November 2012). URL: http://www.wmo.int/pages/prog/arep/gaw/ghg/documents/GHG_Bulletin_No.8_en.pdf
- WMO (2011) Scientific assessment of ozone depletion: 2010. Geneva, World Meteorological Organization (Global ozone research and monitoring project, Report No. 52).
- Xiong, X., Barnet, C. D., Maddy, E., Sweeney, C., Liu, X., Zhou, L., Goldberg, M. (2008) Characterization and validation of methane products from the atmospheric infrared sounder AIRS. *J. Geophys. Res.*, 113, G00A01. doi:10.1029/2007JG000500.
- Xu, Y., Zaelke, D., Velders, G.J.M., Ramanathan, V. (2013) The role of HFCs in mitigating 21st century climate change. *Atmos. Chem. Phys.*, 13, 6083-6089. doi:10.5194/acp-13-6083-2013.

APPENDIX I: Data Tables

Table A 1: Annual mean concentration for all greenhouse gases included in the programme at Zeppelin and Birkenes. All concentrations are mixing ratios in ppt, except for methane and carbon monoxide (ppb) and carbon dioxide (ppm). The annual means are based on a combination of the measurements and the fitted background values; during periods with lacking observations, we have used the fitted background mixing ratios in the calculation of the annual mean. All underlying measurement data are open and accessible and can be downloaded directly from the database: <http://ebas.nilu.no/>

Component	2001	2002	2003	2004	2005	2006	2007	2008	2009	2010	2011	2012	2013	2014	2015	2016
Carbondioxide - Zeppelin											394.8	397.3	399.6	401.2	404.3	
Carbondioxide - Birkenes									393.2	394.0	396.7	397.8	400.7	402.8	405.2	409.9
Methane - Zeppelin	1842.9	1842.4	1855.4	1853.7	1852.8	1853.3	1863.6	1873.5	1888.2	1881.0	1879.6	1891.8	1897.9	1910.0	1920.3	1932.2
Methane - Birkenes									1887.6	1887.6	1896.2	1900.3	1902.4	1917.4	1926.2	1942.2
Carbon monoxide	124.6	126.0	140.3	131.2	128.3	126.5	120.1	119.8	117.7	127.3	115.2	120.5	113.0	113.4	113.6	113.0
Nitrous oxide											324.2	325.0	326.1	327.1	328.1	329.0
Chlorofluorocarbons																
CFC-11*	258.9	257.2	255.3	253.6	251.4	249.4	246.6	244.7	242.7	240.7	238.4	236.8	235.1	234.0	232.6	231.6
CFC-12*	547.1	547.5	547.8	545.8	547.0	546.3	542.4	541.5	537.6	534.4	531.5	528.6	525.5	523.0	519.5	516.6
CFC-113*	81.5	80.8	80.0	79.4	78.8	77.9	77.4	76.8	76.2	75.5	74.6	74.1	73.5	73.0	72.3	71.7
CFC-115*	8.22	8.18	8.22	8.28	8.41	8.39	8.38	8.40	8.43	8.42	8.42	8.44	8.43	8.45	8.48	8.51
Hydrochlorofluorocarbons																
HCFC-22	159.3	164.3	170.4	175.4	181.1	188.9	196.1	204.6	212.5	219.9	225.9	231.5	236.5	241.3	245.0	247.8
HCFC-141b	16.7	17.9	18.7	19.3	19.5	20.0	20.5	21.2	21.5	22.1	23.1	24.0	24.6	25.4	25.8	26.2
HCFC-142b*	14.5	15.1	15.8	16.5	17.2	18.2	19.3	20.3	21.3	22.1	22.7	23.1	23.3	23.4	23.4	23.3
Hydrofluorocarbons																
HFC-125	2.2	2.6	2.9	3.3	4.0	4.9	5.8	6.9	8.0	9.6	11.8	13.5	15.6	17.9	20.2	22.9
HFC-134a	20.9	26.0	30.8	35.6	40.0	44.2	48.7	53.5	57.8	63.5	68.5	73.5	78.9	84.4	90.0	96.5
HFC-152a	2.7	3.5	4.2	5.0	5.7	6.8	7.7	8.6	9.0	9.5	10.0	10.3	10.2	10.2	10.0	10.1

Component	2001	2002	2003	2004	2005	2006	2007	2008	2009	2010	2011	2012	2013	2014	2015	2016
HFC-23										23.8	24.7	25.6	26.7	27.8	28.8	29.6
HFC-365mfc										0.73	0.79	0.87	0.92	1.02	1.10	1.20
HFC-227ea										0.72	0.79	0.88	0.99	1.10	1.21	1.34
HFC-236fa										0.09	0.10	0.11	0.13	0.14	0.15	0.16
HFC-245fa										1.58	1.80	1.99	2.20	2.39	2.56	2.78
HFC-32										5.33	6.56	7.74	9.29	10.92	12.68	14.98
HFC-4310mee										0.21	0.23	0.24	0.25	0.26	0.27	0.28
HFC-143a										11.9	13.2	14.6	16.0	17.6	19.0	20.7
Perfluorinated compounds																
PFC-14															82.39	83.24
PFC-116										4.12	4.20	4.27	4.37	4.45	4.54	4.63
PFC-218										0.55	0.57	0.59	0.59	0.61	0.62	0.64
PFC-318										1.27	1.33	1.38	1.43	1.47	1.53	1.59
Sulphurhexafluoride*	4.95	5.14	5.37	5.61	5.82	6.09	6.31	6.64	6.93	7.19	7.49	7.78	8.11	8.43	8.74	9.08
Nitrogen trifluoride																1.61
Sulfuryl fluoride										1.73	1.82	1.92	2.04	2.14	2.23	2.35
Halons																
H-1211*	4.39	4.43	4.47	4.52	4.52	4.48	4.43	4.40	4.33	4.26	4.18	4.09	3.97	3.87	3.77	3.65
H-1301	2.98	3.07	3.14	3.17	3.22	3.23	3.24	3.28	3.29	3.32	3.32	3.35	3.36	3.38	3.40	3.40
H-2402										0.47	0.46	0.45	0.44	0.43	0.43	0.42
Other halocarbons																
Methylchloride	505.1	521.0	527.4	523.8	520.1	521.2	523.5	524.8	526.1	520.2	509.5	513.9	519.0	514.2	513.5	523.1
Methylbromide	9.00	9.11	8.90	8.90	8.58	8.59	8.34	7.77	7.36	7.28	7.19	7.02	6.94	6.83	6.68	6.76
Dichloromethane	31.43	31.44	32.54	32.36	32.00	33.42	35.51	37.63	38.55	42.03	42.06	45.13	53.69	54.33	54.00	56.57
Chloroform	10.98	10.66	10.82	10.46	10.51	10.48	10.67	10.45	10.85	11.45	11.96	12.10	12.70	13.45	13.72	14.35

Component	2001	2002	2003	2004	2005	2006	2007	2008	2009	2010	2011	2012	2013	2014	2015	2016
Carbon tetrachloride										87.21	85.26	84.37	83.50	82.70	82.03	80.68
Methylchloroform	38.11	32.05	27.25	22.83	19.12	15.93	13.31	11.05	9.23	7.76	6.49	5.40	4.52	3.79	3.25	2.73
Trichloroethylene	0.75	0.67	0.56	0.51	0.49	0.46	0.33	0.37	0.54	0.55	0.55	0.50	0.55	0.49	0.41	0.38
Perchloroethylene	4.72	4.23	4.06	3.86	3.36	2.90	3.12	2.71	2.97	3.14	2.83	2.69	2.55	2.58	2.58	2.54
Volatile Organic Compounds (VOC)																
Ethane										1431.2	1470.7	1587.1	1572.0	1652.6	1645.9	1581.7
Propane										504.2	529.2	562.7	578.2	569.0	541.1	562.8
Butane										169.9	187.3	198.7	204.5	193.3	178.8	163.3
Pentane										57.3	61.6	62.4	67.7	64.3	62.4	58.1
Benzene										88.2	73.0	73.7	69.3	71.3	69.5	69.0
Toluene										36.6	29.6	27.9	26.3	28.6	27.0	27.5

Table A 2: All calculated trends per year, error and regression coefficient for the fit. The trends are all in pptv per year, except for CH₄, N₂O, and CO which are in ppbv and CO₂ is in ppm. The negative trends are in blue, and the positive trends are shown in red. Generally the period is from 2001-2016 but for the compounds marked in green, the measurements started after September 2010. For these compounds, the trends are based on shorter time series, and more uncertain.

Component	Formula	Trend /yr	Error	R ²
Carbon dioxide - Zeppelin	CO ₂	2.46	0.052	0.831
Carbon dioxide - Birkenes		2.32	0.343	0.610
Methane - Zeppelin	CH ₄	5.63	0.047	0.838
Methane - Birkenes		7.56	0.200	0.502
Carbon monoxide	CO	-1.33	0.043	0.838
Nitrous oxide	N ₂ O	0.92	0.004	0.970
Chlorofluorocarbons				
CFC-11*	CCl ₃ F	-1.92	0.004	0.988
CFC-12*	CF ₂ Cl ₂	-2.21	0.011	0.936
CFC-113*	CF ₂ ClCFCl ₂	-0.65	0.001	0.987
CFC-115*	CF ₃ CF ₂ Cl	0.02	0.000	0.454
Hydrochlorofluorocarbons				
HCFC-22	CHClF ₂	6.36	0.005	0.997
HCFC-141b	C ₂ H ₃ FCl ₂	0.61	0.002	0.973
HCFC-142b*	CH ₃ CF ₂ Cl	0.61	0.002	0.973
Hydrofluorocarbons				
HFC-125	CHF ₂ CF ₃	1.36	0.001	0.997
HFC-134a	CH ₂ FCF ₃	4.93	0.003	0.999
HFC-152a	CH ₃ CHF ₂	0.53	0.001	0.976
HFC-23	CHF ₃	0.99	0.002	0.996
HFC-365mfc	CH ₃ CF ₂ CH ₂ CF ₃	0.08	0.000	0.969
HFC-227ea	CF ₃ CHFCF ₃	0.10	0.000	0.995
HFC-236fa	CF ₃ CH ₂ CF ₃	0.01	0.000	0.963
HFC-245fa	CHF ₂ CH ₂ CF ₃	0.20	0.000	0.993
HFC-32	CH ₂ F ₂	1.59	0.003	0.996
HFC-4310mee	C ₅ H ₂ F ₁₀	0.01	0.000	0.907
HFC-143a	CH ₃ CF ₃	1.47	0.004	0.992
Perfluorinated compounds				
PFC-14	CF ₄	-	-	-
PFC-116	C ₂ F ₆	0.09	0.000	0.989
PFC-218	C ₃ F ₈	0.01	0.000	0.932
PFC-318	c-C ₄ F ₈	0.05	0.000	0.985
Sulphurhexafluoride*	SF ₆	0.28	0.000	0.998
Nitrogen trifluoride	NF ₃	-	-	-
Sulphuryl fluoride	SO ₂ F ₂	0.10	0.000	0.987

Component	Formula	Trend /yr	Error	R ²
Halons				
H-1211*	CBrClF ₂	-0.05	0.000	0.99
H-1301	CBrF ₃	0.02	0.000	0.76
H-2402	CBrF ₂ CBrF ₂	-0.01	0.000	0.92
Halogenated compounds				
Methylchloride	CH ₃ Cl	-0.157	0.047	0.877
Methylbromide	CH ₃ Br	-0.186	0.001	0.881
Dichloromethane	CH ₂ Cl ₂	1.852	0.010	0.921
Chloroform	CHCl ₃	0.237	0.003	0.785
Carbon tetrachloride	CCl ₄	-0.992	0.011	0.881
Methylchloroform	CH ₃ CCl ₃	-2.192	0.001	0.999
Trichloroethylene	CHClCCl ₂	-0.012	0.002	0.377
Perchloroethylene	CCl ₂ CCl ₂	-0.128	0.004	0.456
Volatile Organic Compounds (VOC)				
Ethane	C ₂ H ₆	32.11	3.30	0.88
Propane	C ₃ H ₈	9.07	2.87	0.82
Butane	C ₄ H ₁₀	-0.98	1.36	0.75
Pentane	C ₅ H ₁₂	0.37	0.50	0.70
Benzene	C ₆ H ₆	-2.34	0.26	0.86
Toluene	C ₆ H ₅ CH ₃	-1.12	0.22	0.73

Table A 3: Monthly means and standard deviation of aerosol optical depth (AOD) at 500 nm at Ny-Ålesund.'

Month/Year	Mar	Apr	May	Jun	Jul	Aug	Sep
Aerosol optical depth (AOD)							
2002		0.06±0.01	0.08±0.03	0.06±0.02	0.07±0.12	0.07±0.08	0.06±0.05
2003	0.15±0.12	0.11±0.05	0.15±0.06	0.10±0.03	0.04±0.01	0.05±0.02	0.06±0.03
2004	0.06±0.00	0.12±0.08	0.13±0.09	0.06±0.01	0.10±0.07	0.05±0.02	0.04±0.02
2005	0.08±0.03	0.12±0.07	0.10±0.03	0.05±0.02	0.05±0.02	0.04±0.03	0.03±0.01
2006	0.12±0.03	0.16±0.07		0.04±0.00	0.05±0.02	0.05±0.04	0.04±0.03
2007		0.10±0.05	0.10±0.12	0.07±0.03	0.05±0.01	0.05±0.02	0.04±0.03
2008	0.13±0.05	0.14±0.06	0.14±0.04	0.06±0.02	0.06±0.02	0.09±0.03	0.16±0.03
2009			0.11±0.03	0.08±0.02	0.11±0.04	0.10±0.02	0.09±0.01
2010	0.11±0.03	0.08±0.03	0.08±0.01	0.06±0.01	0.05±0.01	0.05±0.01	
2011			0.08±0.02	0.08±0.01	0.05±0.01	0.06±0.02	0.05±0.01
2012	0.10±0.03	0.10±0.02	0.10±0.03	0.06±0.02	0.06±0.02	0.07±0.03	0.07±0.03
2013	0.11±0.04	0.09±0.04	0.06±0.02	0.05±0.01	0.06±0.02	0.05±0.01	0.04±0.02
2014		0.07±0.01	0.10±0.02	0.06±0.02	0.06±0.03	0.08±0.01	0.11±0.05
2015	0.05±0.02	0.10±0.03	0.07±0.02	0.05±0.01	0.15±0.20	0.05±0.02	0.05±0.01
2016	0.08±0.03	0.06±0.02	0.08±0.03	0.07±0.02	0.04±0.01	0.05±0.04	0.03±0.01
Mean (2002-2016)	0.10±0.04	0.10±0.04	0.10±0.04	0.06±0.02	0.07±0.04	0.06±0.03	0.05±0.02

Table A 4: Monthly means and standard deviation of the Ångström coefficient (\AA) at Ny-Ålesund. There are no observations of this parameter during the winter months due to polar night.

Month/Year	Mar	Apr	May	Jun	Jul	Aug	Sep
Ångström coefficient (\AA)							
2002		0.9±0.1	1.4±0.1	1.2±0.3	1.2±0.2	1.3±0.4	1.2±0.5
2003	0.9±0.5	1.3±0.3	1.3±0.2	1.5±0.1	1.5±0.3	1.4±0.5	1.4±0.3
2004	1.3±0.1	1.2±0.3	1.4±0.5	1.7±0.2	1.6±0.4	1.5±0.3	1.3±0.3
2005	1.1±0.3	1.4±0.4	1.0±0.2	1.6±0.3	1.7±0.2	1.4±0.7	1.5±0.4
2006	0.9±0.1	0.9±0.3		1.7±0.2	1.4±0.3	1.3±0.6	1.4±0.3
2007		1.4±0.4	1.4±0.6	1.7±0.2	1.6±0.2	1.7±0.3	1.5±0.4
2008	1.4±0.2	1.3±0.2	1.4±0.2	1.4±0.4	1.2±0.2	1.3±0.3	1.4±0.3
2009			1.3±0.4	1.4±0.2	1.3±0.3	1.2±0.1	1.1±0.1
2010	1.0±0.3	1.4±0.2	1.3±0.2	1.3±0.3	1.4±0.2	1.0±0.1	
2011			1.7±0.3	1.8±0.1	1.5±0.1	1.4 ±0.3	1.6±0.2
2012	1.1±0.2	1.3±0.2	1.2±0.2	1.1±0.1	1.3±0.2	1.4±0.2	1.5±0.2
2013	1.3±0.2	1.2±0.3	1.4±0.2	1.6±0.3	1.3±0.2	1.4±0.2	1.2±0.5
2014		1.4±0.1	1.4±0.1	1.3±0.3	1.5±0.1	1.5±0.1	1.5±0.2
2015	1.3±0.2	1.2±0.3	1.5±0.1	1.5±0.2	1.5±0.2	1.6±0.2	1.2±0.5
2016	1.3±0.2	1.6±0.1	1.6±0.1	1.5±0.2	1.4±0.3	1.5±0.2	1.4±0.2
Mean (2002 -2016)	1.2±0.2	1.3±0.3	1.3±0.2	1.4±0.2	1.4±0.2	1.4±0.3	1.4±0.3

Table A 5: Number of days with AOD observations at Ny-Ålesund made within the months.

Month/Year	Mar	Apr	May	Jun	Jul	Aug	Sep
Number of days with cloud-free and quality assured observations							
2002		4	15	11	6	9	14
2003	3	12	16	8	15	17	12
2004	2	8	13	9	5	12	12
2005	12	17	24	15	10		11
2006	6	12		5	12	4	13
2007		16	9	12	17	10	9
2008	15	12	14	20	16	13	2
2009			7	10	17	8	8
2010	7	18	7	10	12	3	1
2011			2	2	7	4	6
2012	6	18	12	15	16	11	4
2013	5	13	10	10	8	7	9
2014		13	9	9	9	14	4
2015	5	17	15	9	17	13	6
2016	6	14	8	7	12	10	7
Total (2002-2016)	67	174	161	152	179	135	118

Table A 6: Monthly means and standard deviation of aerosol optical depth (AOD) at 500 nm at Birkenes.

Month/Year	Jan	Feb	Mar	Apr	May	Jun	Jul	Aug	Sep	Oct	Nov
Aerosol optical depth (AOD)											
2009				0.29 ±0.00	0.09 ±0.05	0.09 ±0.05	0.18 ±0.06	0.17 ±0.07	0.10 ±0.04	0.08 ±0.03	
2010					0.10 ±0.04	0.09 ±0.04	0.10 ±0.07	0.10 ±0.05	0.05 ±0.02	0.07 ±0.03	0.04 ±0.01
2011	0.02 ±0.01	0.03 ±0.01	0.07 ±0.02	0.21 ±0.19	0.13 ±0.07	0.10 ±0.04	0.13 ±0.06	0.09 ±0.05			
2012			0.07 ±0.05	0.05 ±0.02	0.08 ±0.04	0.09 ±0.04	0.07 ±0.03	0.08 ±0.03	0.07 ±0.01	0.06 ±0.03	0.04 ±0.00
2013							0.17 ±0.17	0.12 ±0.09	0.05 ±0.03	0.05 ±0.03	
2014			0.15 ±0.14	0.11 ±0.06	0.10 ±0.03	0.08 ±0.03	0.13 ±0.06	0.15 ±0.07	0.14 ±0.06		
2015			0.04 ±0.02	0.07 ±0.02	0.07 ±0.03	0.06 ±0.02	0.10 ±0.07	0.09 ±0.06	0.04 ±0.02	0.03 ±0.03	0.04 ±0.01
2016	0.01 ±0.00	0.03 ±0.01	0.03 ±0.02	0.05 ±0.03							0.02 ±0.00*
Mean 09-15	0.02 0.01	0.03 ±0.01	0.07 ±0.05	0.10 ±0.07	0.10 ±0.04	0.08 ±0.04	0.13 ±0.07	0.11 ±0.06	0.08 ±0.03	0.06 ±0.03	0.03 ±0.01

* Level-1.5 data (no a-posteriori calibration)

Table A 7: Monthly means and standard deviation of the Ångström coefficient (Å) at Birkenes

Month/Year	Jan	Feb	Mar	Apr	May	Jun	Jul	Aug	Sep	Oct	Nov
Ångström coefficient (Å)											
2009				1.5 ±0.0	1.2 ±0.3	1.4 ±0.3	1.4 ±0.4	1.1 ±0.2	1.0 ±0.2	1.1 ±0.2	
2010					1.3 ±0.3	1.4 ±0.3	1.4 ±0.2	1.4 ±0.2	1.3 ±0.3	1.3 ±0.3	1.3 ±0.23
2011	1.0 ±0.2	1.0 ±0.1	1.0 ±0.3	1.2 ±0.5	1.3 ±0.3	1.5 ±0.3	1.6 ±0.3	1.6 ±0.1			
2012			1.1 ±0.4	1.6 ±0.3	1.4 ±0.4	1.7 ±0.1	1.6 ±0.3	1.5 ±0.3	1.1 ±0.3	1.4 ±0.4	0.8 ±0.3
2013							1.3 ±0.2	1.2 ±0.3	0.8 ±0.2	0.8 ±0.3	
2014			0.9 ±0.5	1.0 ±0.3	1.1 ±0.3	1.0 ±0.2	1.4 ±0.3	1.1 ±0.3	1.2 ±0.2		
2015			0.9 ±0.2	1.1 ±0.1	1.1 ±0.2	1.3 ±0.2	1.5 ±0.2	1.4 ±0.3	1.3 ±0.2	1.2 ±0.3	0.8 ±0.3
2016	0.7 ±0.1	1.0 ±0.2	0.9 ±0.3	1.1 ±0.2							1.1 ±0.1*
Mean 09-15	0.8 ±0.1	1.0 ±0.1	1.0 ±0.3	1.2 ±0.3	1.2 ±0.2	1.4 ±0.2	1.5 ±0.3	1.3 ±0.2	1.1 ±0.2	1.2 ±0.3	1.0 ±0.2

* Level-1.5 data (no a-posteriori calibration)

Table A 8: Number of days with AOD observations at Birkenes made within the months.

Month/Year	Jan	Feb	Mar	Apr	May	Jun	Jul	Aug	Sep	Oct	Nov
Number of days with cloud-free and quality assured observations (lev 2; lev 1.5 for 2013)											
2009				1	22	25	11	13	15	12	
2010					13	16	18	15	16	10	6
2011	7	2	20	23	18	20	15	13			
2012			11	12	10	7	16	18	9	12	2
2013							26	18	13	7	
2014			12	17	16	25	20	13	6		
2015			6	1	14	21	21	16	9	11	3
2016	2	11	12	9							2*
Total	9	13	61	63	93	114	127	107	68	52	13

* Level-1.5 data (no a-posteriori calibration)

APPENDIX II

Description of instruments and methodologies

ON THE , THE INSTRUMENTAL METHODS USED FOR THE MEASUREMENTS OF THE VARIOUS GREENHOUSE GASES AT BIRKENES AND ZEPPELIN OBSERVATORIES

In this section of the appendix, the instrumental methods used for the measurements of the various greenhouse gases are presented. Additionally we explain the theoretical methods used in calculation of the trends.

Details about greenhouse gas measurements and recent improvement and extensions

Table A 9: Instrumental details for greenhouse gas measurements at Zeppelin and Birkenes.

Component		Instrument and method	Time res.	Calibration procedures	Start - End	Comment
Methane (Birkenes)	CH ₄	Picarro CRDS G1301 CO ₂ /CH ₄ /H ₂ O	5 s	Working std. calibrated against GAW stds at EMPA	19. May 2009 ->	Data coverage in 2016: 98.1%
Methane (Zeppelin)	CH ₄	GC-FID/	1h	NOAA reference standards	Aug 2001- Apr 2012	
Methane (Zeppelin)	CH ₄	Picarro CRDS	5 sec	NOAA reference standards	20.Apr. 2012 ->	Data coverage 2016: 94%
Nitrous oxide (Zeppelin)	N ₂ O	GC-FID	30 min	Hourly, working std. calibrated vs. NOAA stds		Data coverage 2016 83%
Carbon monoxide (Zeppelin)	CO	GC-HgO/UV	20 min	Every 20 min, working std. calibrated vs. GAW std.	Sep. 2001 - 2012	
Carbon monoxide (Zeppelin)	CO	Picarro CRDS	5 sec	NOAA reference standards.	20.Apr 2012 ->	Data coverage 2016: 93%
Carbon dioxide (Zeppelin)	CO ₂	Picarro CRDS from 20.4.2012	1 h 5 sec	NOAA reference standards	1989 - 2012 20.Apr. 2012 ->	CO ₂ measurements in cooperation with ITM Stockholm University (SU). Data coverage 2016: 94%
Carbon dioxide (Birkenes)	CO ₂	Picarro CRDS G1301 CO ₂ /CH ₄ /H ₂ O	5 s	Working std. calibrated against GAW stds at EMPA	Measurements started 19 May 2009.	Data coverage in 2016: 98.1%
CFC-11 CFC-12 CFC-113 CFC-115 HFC-125 HFC-134a HFC-152a HFC-365mfc HCFC-22 HCFC-141b HCFC-142b H-1301 H-1211 H-2402	CFCl ₃ CF ₂ Cl ₂ CF ₂ ClCFCl ₂ CF ₃ CF ₂ Cl CHF ₂ CF ₃ CH ₂ FCF ₃ CH ₃ CHF ₂ CF ₃ CH ₂ CHF ₂ C H ₃ CHF ₂ Cl CH ₃ CFCl ₂ CH ₃ CF ₂ Cl CF ₃ Br CF ₂ ClBr	ADS-GCMS	4 h	Every 4 hours, working std. calibrated vs. AGAGE std.	4. Jan 2001- 2010	The measurements of the CFCs have higher uncertainty and are not within the required precision of AGAGE. See next section for details.

Table cont.:

Component		Instrument and method	Time res.	Calibration procedures	Comment
Methyl Chloride	CH ₃ Cl				
Methyl Bromide	CH ₃ Br				
Methylendichloride	CH ₂ Cl ₂				
Chloroform	CHCl ₃				
Methylchloroform	CH ₃ CCl ₃				
TriChloroethylene	CHClCCl ₂				
Perchloroethylene	CCl ₂ CCl ₂				
Sulphurhexafluoride	SF ₆				
Nitrogen trifluoride	NF ₃				
Tetrafluormethane	CF ₄				
PFC-116	C ₂ F ₆				
PFC-218	C ₃ F ₈				
PFC-318	c-C ₄ F ₈				
Sulphurhexafluoride	SF ₆				
Sulfuryl fluoride	SO ₂ F ₂				
HFC-23	CHF ₃				
HFC-32	CH ₂ F ₂				
HFC-125	CHF ₂ CF ₃				
HFC-134a	CH ₂ FCF ₃				
HFC-143a	CH ₃ CF ₃				
HFC-152a	CH ₃ CHF ₂				
HFC-227ea	CF ₃ CHFCF ₃				
HFC-236fa	CF ₃ CH ₂ CF ₃				
HFC-245fa	CF ₃ CH ₂ CHF ₂				
HFC-365mfc	CH ₃ CF ₂ CH ₂ CF ₃				
HFC-43-10mee	CF ₃ (CHF) ₂ CF ₂ CF ₃				
HCFC-22	CHClF ₂				
HCFC-141b	CH ₃ CCl ₂ F				
HCFC-142b	CH ₃ CClF ₂				
CFC-11	CCl ₃ F				
CFC-12	CCl ₂ F ₂				
CFC-113	CCl ₂ FCClF ₂				
CFC-115	CClF ₂ CF ₃				
H-1211	CBrClF ₂				
H-1301	CBrF ₃				
H-2402	C ₂ Br ₂ F ₄				
Methyl Chloride	CH ₃ Cl				
Methyl Bromide	CH ₃ Br				
Methylendichloride	CH ₂ Cl ₂				
Chloroform	CHCl ₃				
Methylchloroform	CH ₃ CCl ₃				
Dibromomethane	CH ₂ Br ₂				
TriChloroethylene	TCE				
Perchloroethylene	PCE				
Carbon tetrachloride	CCl ₄				
Ethane	C ₂ H ₆				
Propane	C ₃ H ₈				
Butane	C ₄ H ₁₀				
Pentane	C ₅ H ₁₂				
Benzene	C ₆ H ₆				
Toluene	C ₆ H ₅ CH ₃				
Ozone	O ₃		5 min		

DATA QUALITY AND UNCERTAINTIES

HALOCARBONS

In 2001 - 2010 measurements of a wide range of hydrochlorofluorocarbons, hydrofluorocarbons (HCFC-141b, HCFC-142b, HFC-134a etc.), methyl halides (CH₃Cl, CH₃Br, CH₃I) and the halons (e.g. H-1211, H-1301) were measured with good scientific quality by using ADS-GCMS. The system also measured other compounds like the chlorofluorocarbons, but the quality and the precision of these measurements was not at the same level. Table A 10 shows a list over those species measured with the ADS-GCMS at Zeppelin Observatory. The species that are in blue are of acceptable scientific quality and in accordance with recommendations and criteria of the AGAGE network for measurements of halogenated greenhouse gases in the atmosphere. Those listed in red have higher uncertainties and are not within the required precision of AGAGE. There are various reasons for this increased uncertainties; unsolved instrumental problems e.g. possible electron overload in detector (for the CFC's), influence from other species, detection limits (CH₃I, CHClCCl₂) and unsolved calibration problems (CHBr₃). Since 1. September 2010 the ADS-GCMS was replaced by a Medusa-GCMS system. The uncertainties improved for almost all species (Table A 11 for details), but there are periods where measurements of the CFC's were still not satisfactory. This is an unsolved problem within the AGAGE network.

Table A 10: ADS-GCMS measured species at Zeppelin from 4. January 2001 to 1. September 2010. Good scientific quality data in Blue; Data with reduced quality data in Red. The data are available through <http://ebas.nilu.no>. Please read and follow the stated data policy upon use.

Compound	Typical precision (%)	Compound	Typical precision (%)
SF ₆	1.5	H1301	1.5
HFC134a	0.4	H1211	0.4
HFC152a	0.6	CH ₃ Cl	0.6
HFC125	0.8	CH ₃ Br	0.8
HFC365mfc	1.7	CH ₃ I	5.1
HCFC22	0.2	CH ₂ Cl ₂	0.4
HCFC141b	0.5	CHCl ₃	0.3
HCFC142b	0.5	CHBr ₃	15
HCFC124	2.3	CCl ₄	0.5
CFC11	0.3	CH ₃ CCl ₃	0.6
CFC12	0.3	CHClCCl ₂	1.2
CFC113	0.2	CCl ₂ CCl ₂	0.7
CFC115	0.8		

Table below gives an overview over the species measured with the Medusa-GCMS systems at the AGAGE stations and the typical precision with the different instruments. The Medusa-GCMS instrument at the Zeppelin Observatory meet the same criteria as shown in the Table.

Table A 11: AGAGE measured species.

Compound	Typical precision (%)	Compound	Typical precision (%)
NF ₃	1		
CF ₄	0.15	H-1301	1.5
C ₂ F ₆	1	H-1211	0.5
C ₃ F ₈	3	H-2402	2
c-C ₄ F ₈	1.4	CH ₃ Cl	0.2
SF ₆	0.4	CH ₃ Br	0.6
SO ₂ F ₂	2	CH ₂ Cl ₂	0.5
HFC-23	0.7	CH ₂ Br ₂	1.5
HFC-32	3	CCl ₄	1
HFC-134a	0.5	CH ₃ CCl ₃	0.7
HFC-152a	1.4	CHClCCl ₂	2.5
HFC-125	0.7	CCl ₂ CCl ₂	0.5
HFC-143a	1.2	C ₂ H ₆	0.3
HFC-365mfc	5	C ₃ H ₈	0.3
HFC-43-10mee	3	C ₄ H ₁₀	0.6
HCFC-22	0.3	C ₆ H ₆	0.5
HCFC-141b	0.5	C ₇ H ₈	0.6
HCFC-142b	0.4		
CFC-11	0.15		
CFC-12	0.05		
CFC-113	0.2		
CFC-115	0.8		

METHANE

Methane is measured using a Picarro CRDS (Cavity Ring-Down Spectrometer) monitor which is calibrated against NOAA reference standards. The instrument participates in yearly INGOS cucumber ring tests. The continuous data are also compared to weekly flask samples sent to NOAA CMDL, Boulder Colorado. All data will be available for download from the EBAS database <http://ebas.nilu.no>.

The Picarro instrument had some problems with an internal laser that needed adjustments/fine tuning in January 2016, resulting in a period of reduced data coverage. After service from the instrument manufacturer, the instrument has performed well with full coverage for the rest of the year.

N₂O MEASUREMENTS

N₂O is measured using a gas chromatograph with an electron capture detector. Due to malfunctioning valves, data are missing from mid June to early August 2016. The instrument is old and worn and will be replaced by a new mid-IR Cavity Ring Down instrument in 2017. This new instrument will perform continuous measurements with improved precision.

CO₂ MEASUREMENTS

At the Zeppelin station carbon dioxide (CO₂) is monitored in cooperation with Stockholm University (Institute of Applied Environmental Research, ITM). NILU is running the Picarro Cavity Ring-Down Spectrometer used for continuous measurements, calibrated against SU-ITM's set of NOAA reference standards as a cooperation between the two institutes. The instrument participates in yearly INGOS cucumber ring tests. The continuous data are also compared to weekly flask samples sent to NOAA CMDL, Boulder Colorado. All data will be available for download from the EBAS database <http://ebas.nilu.no>.

IMPLEMENTATION OF MEASUREMENTS FROM BIRKENES AND ZEPPELIN INTO ICOS RESEARCH INFRASTRUCTURE -

Integrated Carbon Observation System (ICOS) is a European research infrastructure forming an observation system that will measure and assess atmospheric green CO₂, CH₄ and CO concentrations ensuring independent and reliable measurements. ICOS-Norway (<https://no.icos-cp.eu>) contributes to the network of atmospheric measurements with two observatories, Birkenes and Zeppelin.

ICOS has divided their sites into two levels, Class 1 and Class 2, dependent on their instrumental setup. At Class 1 sites a wider range of measurements of different species are required. Whilst, Class 2 is the low cost option where less parameters are mandatory.

Category	Gases, continuous	Gases, periodical	Meteorology, continuous	Eddy Fluxes
Class 1 Mandatory parameters	<ul style="list-style-type: none"> • CO₂, CH₄, CO : at each sampling height 	<ul style="list-style-type: none"> • CO₂, CH₄, N₂O, SF₆, CO, H₂,¹³C and ¹⁸O in CO₂: weekly sampled at highest sampling height† • ¹⁴C (radiocarbon integrated samples): at highest sampling height 	<ul style="list-style-type: none"> • Air temperature, relative humidity, wind direction, wind speed: at highest and lowest sampling height* • Atmospheric Pressure • Planetary Boundary Layer Height** † 	
Class 2 Mandatory parameters	<ul style="list-style-type: none"> • CO₂, CH₄ : at each sampling height 		<ul style="list-style-type: none"> • Air temperature, relative humidity, wind direction, wind speed: at highest and lowest sampling height* • Atmospheric Pressure 	
Recommended parameters***	<ul style="list-style-type: none"> • ²²²Rn, N₂O, O₂/N₂ ratio • CO for Class 2 stations 	<ul style="list-style-type: none"> • CH₄ stable isotopes, O₂/N₂ ratio for Class 1 stations: weekly sampled at highest sampling height 		<ul style="list-style-type: none"> • CO₂ : at one sampling height

* Atmospheric temperature and relative humidity recommended at all sampling heights

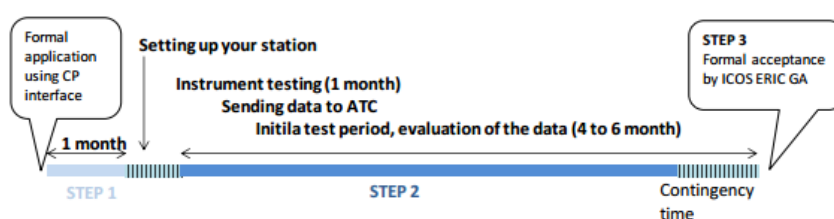
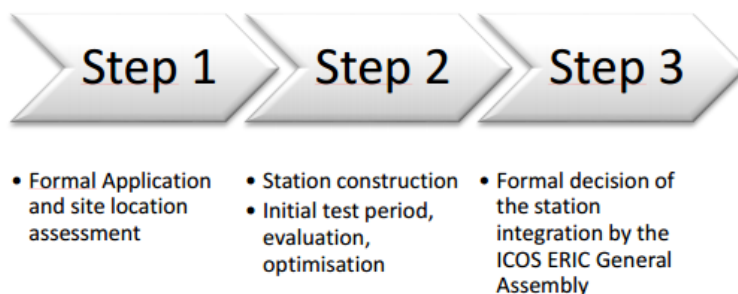
** Only required for continental stations.

*** Recommended for its scientific value but support from ATC in terms of protocols, data base, spare analyzer will not be ensured as long as the parameters are not mandatory.

The table shows the mandatory and recommended parameters for ICOS Class 1 and Class 2 sites.

ICOS-Norway will upgrade Zeppelin Observatory to become an ICOS Class 1 site and Birkenes Observatory to an ICOS Class 2 site, and comply with the ICOS quality assurance and quality control.

To become an ICOS site it requires that the site goes through a so-called labeling process to get a certificate as a qualified ICOS site. The labeling process evaluate the site set up, the instrumentation with its calibration set-up and data handling, as a quality certificate of the data output from the ICOS site. The labeling process is a time consuming process as the instrument (Picarro) needs to be evaluated for minimum 1 month at the central ICOS lab in France. The same lab provides calibration cylinders and it takes 4 months to produce them. After having the instrument and calibration routines established at the site, the measurements will have to go through a 6 months evaluation period before approval as an ICOS site. In total it takes about 1.5 years to get an ICOS certificate.



The three steps in the labeling process of an ICOS station.

Status of the labeling process for Birkenes and Zeppelin Observatories:

Both stations have their analyzers (Picarro) installed and run continuous measurements of CH₄ and CO₂ at both sites and CO at Zeppelin.

Mandatory meteorological parameters are measured with the upgraded equipment to meet the ICOS precision criteria at both sites.

Plans for 2017:

- Both analyzers sent to ICOS central lab for evaluation.
- Implement ICOS calibration tanks and routines.
- Establish automatic data flow to the ICOS Atmospheric Thematic Centre (ATC) and Carbon Portal.
- Implement ICOS data quality control procedures
- At Zeppelin, start sampling of ¹⁴C radiocarbon.
- At Birkenes, start the process with landowner and local authority to get permission to install a tall sampling tower (up to 100m) at Birkenes.

At class 1 sites an automatic flask sampler is mandatory, but as this is under development by one of the German partners in ICOS, it is not clear when the sampler will be ready for installation at Zeppelin.

AIR INLET AT ZEPPELIN

In 2011 the air inlet for the GHG measurements at Zeppelin were improved to reduce possible influence from the station and visitors at the station. The inlet was moved away from the station and installed in a 15 m tower nearby for the following components:

- N₂O
- CH₄
- CO₂
- CO
- Halogenated compounds
- NOAA flasks sampling program
- Isotope flask sampling of CO₂ and CH₄



DETERMINATION OF BACKGROUND DATA

Based on the daily mean concentrations an algorithm is selected to find the values assumed as clean background air. If at least 75% of the trajectories within +/- 12 hours of the sampling day are arriving from a so-called clean sector, defined below, one can assume the air for that specific day to be non-polluted. The remaining 25% of the trajectories from European, Russian or North-American sector are removed before calculating the background.

CALCULATION OF TRENDS FOR GREENHOUSE GASES AND VOCs

To calculate the annual trends the observations have been fitted as described in Simmonds et al. (2006) by an empirical equation of Legendre polynomials and harmonic functions with linear, quadratic, and annual and semi-annual harmonic terms:

$$f(t) = a + b \left(\frac{N}{12} \right) \cdot P_1 \left(\frac{t}{N} - 1 \right) + \frac{1}{3} \cdot d \left(\frac{N}{12} \right)^2 \cdot P_2 \left(\frac{t}{N} - 1 \right) + c_1 \cdot \cos \left(\frac{2\pi t}{12} \right) + s_1 \sin \left(\frac{2\pi t}{12} \right) + c_2 \cos \left(\frac{4\pi t}{12} \right) + s_2 \sin \left(\frac{4\pi t}{12} \right)$$

The observed f can be expressed as functions of time measures from the 2N-months interval of interest. The coefficient a defines the average mole fraction, b defines the trend in the mole fraction and d defines the acceleration in the trend. The c and s define the annual and inter-annual cycles in mole fraction. N is the mid-point of the period of investigation. P_i are the Legendre polynomials of order i .

This equation is used for the VOCs, while for the GHGs the fit between the empirical equation and observations improves if the semi-annual harmonic terms are replaced by an additional Legendre polynomial.

ON THE SURFACE IN SITU OBSERVATIONS OF AEROSOL MICROPHYSICAL AND OPTICAL PROPERTIES AT BIRKENES, ZEPPELIN AND TROLLHAUGEN OBSERVATORY

Table A 12: Overview of atmospheric aerosol parameters measured by surface in situ observations operated at which station

	Birkenes	Trollhaugen	Zeppelin
Particle Number Size Distribution (fine size range $D_p < 0.8 \mu\text{m}$)	X	X	X
Particle Number Size Distribution (coarse size range $D_p > 0.8 \mu\text{m}$)	X		
Aerosol Scattering Coefficient (spectral)	X	X	
Aerosol Absorption Coefficient (spectral)	X	X	X
Cloud Condensation Nuclei (indirect climate effect)	X		

Concerning surface in situ observations of microphysical and optical properties of atmospheric aerosol, the table on the left gives an overview over the parameters observed at Birkenes, Trollhaugen, and Zeppelin stations and operated by NILU.

To achieve high quality data with appropriate uncertainty and precisions, this requires networked instruments to participate in inter-comparisons at ACTRIS aerosol calibration centre in Leipzig, Germany, in regular

intervals. This activity has proven to be necessary in order to ensure comparable measurements within the distributed infrastructure. The frequency of these inter-comparisons, once every 2-3 years, is balanced with minimising the downtime associated with these quality assurance measures. In 2016, instruments targeting the direct aerosol climate effect were in the focus of inter-comparisons. Both the integrating nephelometer and the newer filter absorption photometer, measuring the spectral aerosol particle scattering and absorption coefficients respectively, were scheduled for being inter-compared, with satisfactory outcome in both cases.

With respect to microphysical aerosol properties, the particle number size distribution (PNSD) at surface-level is observed at all 3 stations covered in this report, at least over parts of the relevant range in particle size. The relevant particle sizes cover a range of $0.01 \mu\text{m} - 10 \mu\text{m}$ in particle diameter. The diameter range of $1.0 \mu\text{m} - 10 \mu\text{m}$ is commonly referred to as coarse mode, the range $D_p < 1.0 \mu\text{m}$ as fine mode. The fine mode is separated further into Aitken-mode ($0.01 \mu\text{m} < D_p < 0.1 \mu\text{m}$) and accumulation mode ($0.1 \mu\text{m} < D_p < 1 \mu\text{m}$). The distinction of these modes is justified by different predominant physical processes as function of particle size. In the Aitken-mode, particles grow by condensation of precursor gases from the gas-phase, and coagulate among themselves or with accumulation mode particles. Accumulation mode particles grow by taking up Aitken-mode particles or by mass uptake while being activated as cloud droplets, and they are removed by precipitation. Coarse mode particles in turn are formed by break-up of biological or crustal material, including pollen, bacteria, and fungus spores, and removed by gravitational settling and wet removal. The PNSD of an aerosol is needed for quantifying any interaction or effect of the aerosol since all of them depend strongly on particle size.

To measure the PNSD over the full relevant size range, several measurement principles need to be combined. A Differential Mobility Particle Spectrometer (DMPS) measures the particle

number size distribution, now in the range of 0.01 - 0.8 μm particle diameter after several improvements of the instruments at all three stations, i.e. almost the full fine mode. In a DMPS, the particles in the sample air stream are put into a defined state of charge by exposing them to an ionised atmosphere in thermal equilibrium. The DMPS uses a cylindrical capacitor to select a narrow size fraction of the particle phase. The particle size of the selected size fraction is determined by the voltage applied to the capacitor. The particle number concentration in the selected size fraction is then counted by a Condensation Particle Counter (CPC). A mathematical inversion that considers charge probability, diffusional losses of particles in the system, transfer function of the capacitor, and counting efficiency of the CPC is then used to calculate the particle number size distribution.

The PNSD of particles with diameters $0.25 \mu\text{m} < D_p < 30 \mu\text{m}$ is measured with an Optical Particle Spectrometer (OPS). In the OPS, the particles in the sample stream are focussed through a laser beam. The instrument registers number and amplitude of the pulses of light scattered by the particles. The particle pulses are sorted into a histogram by their amplitude, where the pulse amplitude yields the particle diameter and the pulse number the particle concentration, i.e. together the PNSD. Both, the DMPS and the OPS, yield method specific measures of the particle diameter, the electrical mobility and the optical particle diameter, respectively. When related to the spherical equivalent geometric particle diameter commonly referred to, both particle size measures depend on particle shape (causing a 5% systematic uncertainty in particle diameter), the optical particle diameter in addition on particle refractive index (causing a 20% systematic uncertainty in particle diameter). Where possible, the PNSDs provided by DMPS and OPS are joined into a common PNSD, in this report. To quality assure this process, PNSDs are accepted only if DMPS and OPS PNSD agree within 25% in particle diameter in their overlap size range. Together, both instruments provide a PNSD that spans over 3 orders of magnitude in particle diameter, and over 6 orders of magnitude in particle concentration.

Another measured microphysical property is the Cloud Condensation Nuclei (CCN) Concentration, i.e. the concentration of particles that could act as condensation nuclei for liquid-phase cloud droplets, which is a property depending on the water vapour supersaturation. The corresponding instrument, a Cloud Condensation Nucleus Counter (CCNC), exposes the aerosol sample to an “artificial cloud” of defined supersaturation, and counts the cloud activated particles optically. Observations of the CCN concentration are essential for quantifying the indirect aerosol climate effect. The CCNC at Birkenes has been in operation since 2012, but is currently not included in the monitoring programme.

Optical aerosol parameters quantify the direct aerosol climate effect. The observation programme at Birkenes includes the spectral particle scattering coefficient $\sigma_{sp}(\lambda)$ and the spectral particle absorption coefficient $\sigma_{ap}(\lambda)$. The scattering coefficient quantifies the amount of light scattered by the aerosol particle population in a sample per distance a light beam travels through the sample. The absorption coefficient is the corresponding property quantifying the amount of light absorbed by the particle population in the sample. An integrating nephelometer is used for measuring $\sigma_{sp}(\lambda)$ at 450, 550, and 700 nm wavelength. In this instrument, the optical sensors look down a blackened tube that is filled with aerosol sample. The tube is illuminated by a light source with a perfect cosine intensity characteristic perpendicularly to the viewing direction. It can be shown mathematically that this setup integrates the scattered light seen by the optical sensors over all scattering angles. The nephelometer at Birkenes has successfully undergone quality assurance by intercomparison

within the EU research infrastructure ACTRIS in 2015. In 2017 we detected drift in the older filter absorption photometer operated at Birkenes since 2009 through carefully implemented quality control within ACTRIS. The drift was detected by operating the older filter absorption photometer in parallel with a newer, more stable make and model in order to ensure a continuous, rupture-free aerosol absorption time series at Birkenes. In addition, the newer instrument was sent to an inter-comparison within the European research infrastructure for short-lived climate forcers ACTRIS. These exercises connect individual instruments to a network-wide primary standard, ensuring traceability and comparability of observations at stations in the network. The old instrument exhibiting the drift has since been decommissioned.

For the nephelometer at Trollhaugen, such intercomparisons are impossible because of the remote Antarctic location and associated logistical challenges. However, the Trollhaugen instrument undergoes the same regular on-site quality assurance as the Birkenes instrument, including regular calibration verification traceable to physical first principles (calibration with high-purity carbon dioxide, where scattering coefficient of carbon dioxide can be calculated from fundamental quantum mechanics).

The spectral particle absorption coefficient $\sigma_{ap}(\lambda)$ is measured by filter absorption photometers. A filter absorption photometer infers $\sigma_{ap}(\lambda)$ by measuring the decrease in optical transmissivity of a filter while the filter is loaded with the aerosol sample. The transmissivity time series is subsequently translated into an absorption coefficient time series by using Lambert-Beer's law, the same law also used in optical spectroscopy. The filter absorption photometers deployed at Birkenes are a custom-built 1 wavelength Particle Soot Absorption Photometer (PSAP), and a commercial 3-wavelength PSAP. The 1-wavelength PSAP received quality assurance by intercomparison within ACTRIS in 2013 discovering calibration stability issues. The 3-wavelength PSAP has undergone ACTRIS intercalibration successfully in 2015, i.e. without discovering any issues. Thus, both instruments are interpreted in combination to benefit from both, quality assurance in a research network and spectral capabilities. For 2013 and later, the data of the 3-wavelength PSAP are used, for 2010-2012, the data of the older 1-wavelength are used after being corrected by comparison with the newer instrument during the overlap period. For comparison with the nephelometer, the PSAP data has been transferred to a wavelength of 550 nm using the measured spectral dependence (3-wavelength PSAP), or by assuming an absorption Ångström coefficient α_{ap} of -1 (1-wavelength PSAP, adding 2% systematic uncertainty to the data).

For measuring $\sigma_{ap}(\lambda)$ at Zeppelin, a recently developed filter absorption photometer, an aethalometer type AE33, has been deployed in 2015. The AE33 features a larger spectral range of 370 - 950 nm as compared to other instruments, and offers a 7-wavelength resolution across this range. Previous aethalometer models suffered from high systematic uncertainties due to uncorrected dependencies on filter loading (e.g. Collaud Coen et al., 2010). Comparisons and calibrations within ACTRIS have shown that this systematic uncertainty has been reduced significantly in the AE33 model by an internal loading compensation (Drinovc et al., 2015). Due to this successful instrument evaluation, the instrument programme at Birkenes has been upgraded by an AE33 in 2017 as well.

All in situ observations of aerosol properties representing the ground-level are conducted for the aerosol at dry-state (RH < 40%) for obtaining inter-comparability across the network.

DETAILS ABOUT AEROSOL OPTICAL DEPTH MEASUREMENTS

The amount of particles in the air during sunlit conditions is continuously monitored by means of a Precision-Filter-Radiometer (PFR) sun photometer, located at the Sverdrup station in Ny-Ålesund and a Cimel instrument at Birkenes. The observations in Ny-Ålesund are performed in collaboration with PMOD/WRC (N. Kouremeti, S. Kazadzis), Davos, Switzerland. The main instrument characteristics are given below.



AERONET - Cimel C-318

- Sun (9 channels) and sky radiances
- Wavelength range: 340-1640 nm
- 15 min sampling
- No temperature stabilization
- AOD uncertainty: 0.01-0.02



PFR-GAW- Precision Filter Radiometer

- Direct sun measurements (4 channels)
- Wavelength range: 368 - 862 nm
- 1 min averages
- Temperature stabilized
- AOD uncertainty: 0.01

Figure 57: Photos and typical features of the standard instrument of the AERONET (left panel) and GAW PFR network instruments (right panel)

The sun-photometer measurements in Ny-Ålesund are part of the global network of aerosol optical depth (AOD) observations, which started in 1999 on behalf of the WMO GAW program. The instrument is located on the roof of the Sverdrup station, Ny-Ålesund, close to the EMEP station on the Zeppelin Mountain (78.9°N, 11.9°E, 474 m a.s.l.). The Precision Filter Radiometer (PFR) has been in operation since May 2002. In Ny-Ålesund, the sun is below 5° of elevation from 10 October to 4 March, limiting the period with sufficient sunlight to the spring-early autumn season. However, during the summer months it is possible to measure day and night if the weather conditions are satisfactory. The instrument measures direct solar radiation in four narrow spectral bands centred at 862 nm, 501 nm, 411 nm, and 368 nm. Data quality control includes instrumental control like detector temperature and solar pointing control as well as objective cloud screening. Measurements made at full minutes are averages of 10 samples for each channel made over a total duration of 1.25 seconds.

SCIAMACHY TOMSOMI and OMI ozone columns and meteorological data from Ny-Ålesund are used for the retrieval of aerosol optical depth (AOD).

At Birkenes Observatory, aerosol optical depth measurements started in spring 2009, utilizing an automatic sun and sky radiometer (CIMEL type CE-318) of the global Aerosol Robotic Network (AERONET) at NASA-GSFC, with spectral interference filters centred at selected wavelengths: 340 nm, 380 nm, 440 nm, 500 nm, 675 nm, 870 nm, 1020 nm, and 1640 nm. The measurement frequency is approximately 15 minutes (this depends on the air-mass and time of day). Calibration is performed about once per year, at the Atmospheric Optics Group at the University of Valladolid (GOA-UVa), Spain. GOA manages the calibration for the AERONET sun photometers of the European sub-network of AERONET. Raw data are processed and quality assured centrally by AERONET. Data reported for 2009 - 2016 are quality-assured AERONET level 2.0 data, which means they have been pre- and post-field-calibrated, automatically cloud cleared and have been manually inspected by AERONET.

OUTLOOK ON OBSERVATIONS OF AEROSOL OPTICAL DEPTH IN NY-ÅLESUND BEYOND 2016

A major obstacle to obtaining a year-round AOD climatology in the Arctic arises from the long polar night. To fill gaps in the aerosol climatology at Ny-Ålesund, it is planned to deploy a lunar photometer on a quasi-permanent basis in the frame of the SIOS infrastructure project. This is a collaborative initiative between NILU, PMOD/WRC and ISAC-CNR. Seasonal deployments of a lunar photometer owned by PMOD/WRC were already made in the winters of 2014/15 and 2016/17. A multiple-season deployment is envisaged from autumn 2018..

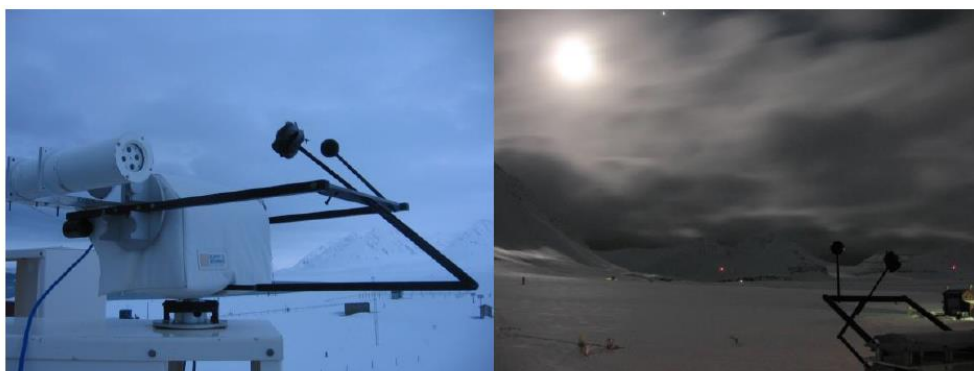


Figure 58: Moon PFR on the Kipp & Zonen tracker during the day (left, parking position) and during night-time measurements (right).

The PFR instrument modified by PMOD-WRC was installed on a tracker model Kipp & Zonen provided usually hosting a sun photometer. Figure 58 shows the instrument on the tracker during day-time and night-time. Six lunar cycles were monitored: the first during February 2014, while the other 5 during winter 2014-2015. We collected data on 66 measurement periods, from Moon-rise to Moon-set or from minimum-to-minimum elevation as in Polar Regions no set-rise events are possible. Among these, we obtained 17 distinct good measurement periods, due to the frequent occurrence of clouds. For further details see e.g. Mazzola at al., 2015.

APPENDIX III: Abbreviations

Abbreviation	Full name
ACSM-ToF	Aerosol Chemical Speciation Monitor
ACTRIS	Aerosols, Clouds, and Trace gases Research InfraStructure Network
ADS-GCMS	Adsorption-Desorption System - Gas Chromatograph Mass Spectrometer
AeroCom	Aerosol Comparisons between Observations and Models
AERONET	Aerosol Robotic Network
AGAGE	Advanced Global Atmospheric Gases Experiment
AIRS	Atmospheric Infrared Sounder
AMAP	Arctic Monitoring and Assessment
AOD	Aerosol optical depth
AWI	Alfred Wegener Institute
BC	Black carbon
CAMP	Comprehensive Atmospheric Monitoring Programme
CCN	Cloud Condensation Nuclei
CCNC	Cloud Condensation Nucleus Counter
CFC	Chlorofluorocarbons
CICERO	Center for International Climate and Environmental Research - Oslo
CIENS	Oslo Centre for Interdisciplinary Environmental and Social Research
CLTRAP	Convention on Long-range Transboundary Air Pollution
CO	Carbon monoxide
CPC	Condensation Particle Counter
DMPS	Differential Mobility Particle
EMEP	European Monitoring and Evaluation Programme
ENVR ^{plus}	Environmental Research Infrastructures Providing Shared Solutions for Science and Society
EOS	Earth Observing System
ERF	Effective radiative forcing ERF
ERFaci	ERF due to aerosol-cloud interaction
EU	European Union
EUSAAR	European Supersites for Atmospheric Aerosol Research
FLEXPART	FLEXible PARTicle dispersion model
GAW	Global Atmosphere Watch
GB	Ground based

Abbreviation	Full name
GHG	Greenhouse gas
GOA-UVA	Atmospheric Optics Group of Valladolid University
GOSAT	Greenhouse Gases Observing Satellite
GOSAT-IBUKI	Greenhouse Gases Observing Satellite "IBUKI"
GWP	Global Warming Potential
HCFC	Hydrochlorofluorocarbons
HFC	Hydrofluorocarbons
ICOS	Integrated Carbon Observation System
InGOS	Integrated non-CO2 Greenhouse gas Observing System
IPCC	Intergovernmental Panel on Climate Change
ISAC-CNR	Institute of Atmospheric Sciences and Climate (ISAC) of the Italian National Research Council
ITM	Stockholm University - Department of Applied Environmental Science
JAXA	Japan Aerospace Exploration Agency
LLGHG	Well-mixed greenhouse gases
MOCA	Methane Emissions from the Arctic Ocean to the Atmosphere: Present and Future Climate Effects
MOE	Ministry of the Environment
NARE	Norwegian Antarctic Research Expeditions
NASA	National Aeronautics and Space Administration
NEOS-ACCM	Norwegian Earth Observation Support for Atmospheric Composition and Climate Monitoring
NIES	National Institute for Environmental Studies
NOAA	<u>National Oceanic and Atmospheric Administration</u>
NRS	Norsk Romsenter
OC	Organic Carbon
ODS	Ozone-depleting substances
OH	Hydroxyl radical
OPS	Optical Particle Spectrometer
OSPAR	Convention for the Protection of the marine Environment of the North-East Atlantic
PFR	Precision filter radiometer
PMOD/WRC	Physikalisch-Meteorologisches Observatorium Davos/World Radiation Center
PNSD	Particle number size distribution

Abbreviation	Full name
ppb	Parts per billion
ppm	Parts per million
ppt	Parts per trillion
PSAP	Particle Soot Absorption Photometers
RF	Radiative forcing
RI	Research Infrastructure
RIMA	Red Ibérica de Medida fotométrica de Aerosoles
SACC	Strategic Aerosol Observation and Modelling Capacities for Northern and Polar Climate and Pollution
SCIAMACHY	SCanning Imaging Absorption spectroMeter for Atmospheric CHartography
SIS	Strategisk instituttsatsing
SMPS	Scanning Mobility Particle
TES	Tropospheric Emission Spectrometer
TOA	Top Of Atmosphere
TOMS OMI	Total Ozone Mapping Spectrometer Ozone Monitoring instrument
UN	United Nations
UNFCCC	United Nations Framework Convention on Climate Change
VOC	Volatile organic compounds
WDCA	World Data Centre for Aerosol
WDCS	World Data Centre of Aerosols
WMGHG	Well-mixed greenhouse gases
WMO	World Meteorological Organization

Norwegian Environment Agency

Telephone: +47 73 58 05 00 | **Fax:** +47 73 58 05 01

E-mail: post@miljodir.no

Web: www.environmentagency.no

Postal address: Postboks 5672 Sluppen, N-7485 Trondheim

Visiting address Trondheim: Brattørkaia 15, 7010 Trondheim

Visiting address Oslo: Grensesvingen 7, 0661 Oslo

The Norwegian Environment Agency is working for a clean and diverse environment. Our primary tasks are to reduce greenhouse gas emissions, manage Norwegian nature, and prevent pollution.

We are a government agency under the Ministry of Climate and Environment and have 700 employees at our two offices in Trondheim and Oslo and at the Norwegian Nature Inspectorate's more than sixty local offices.

We implement and give advice on the development of climate and environmental policy. We are professionally independent. This means that we act independently in the individual cases that we decide and when we communicate knowledge and information or give advice.

Our principal functions include collating and communicating environmental information, exercising regulatory authority, supervising and guiding regional and local government level, giving professional and technical advice, and participating in international environmental activities.